

UNITED STATES DEPARTMENT OF THE INTERIOR  
GEOLOGICAL SURVEY

---

REPORT ON TELEVIEWER LOG AND STRESS MEASUREMENTS  
IN HOLES USW G-3 AND UE-25p1  
YUCCA MOUNTAIN, NYE COUNTY, NEVADA

By

J. M. Stock, J. H. Healy, J. Svitek, and L. Mastin



Open-File Report 86-369

Prepared in cooperation with the  
Nevada Operations Office, U.S. Department of Energy  
(Interagency Agreement DE-AI08-78ET44802)

This report is preliminary and has not been reviewed  
for conformity with U.S. Geological Survey editorial  
standards and stratigraphic nomenclature. Any use of  
trade names is for descriptive purposes only and does  
not imply endorsement by the USGS.

Menlo Park, California  
1986

Open-File Report 86-369

Open-File Report 86-369

UNITED STATES  
DEPARTMENT OF THE INTERIOR  
GEOLOGICAL SURVEY

REPORT ON TELEVIEWER LOG AND STRESS MEASUREMENTS  
IN HOLES USW G-3 AND UE-25p1  
YUCCA MOUNTAIN, NYE COUNTY, NEVADA

By

J. M. Stock, J. H. Healy, J. Svitek, and L. Mastin

## CONTENTS

	Page
Abstract.....	1
Acknowledgements.....	2
Introduction.....	2
Geologic Setting.....	2
Borehole Televiewer - Method.....	4
Borehole Televiewer - Results	
i. Throughgoing Fractures.....	6
ii. Drilling-induced Hydrofractures.....	11
iii. Borehole Breakouts.....	13
iv. Sedimentary Features.....	13
Hydraulic Fracturing Stress Measurements - Method	
i. Horizontal Stress Values .....	16
ii. Effect of Borehole Deviation .....	17
iii. Vertical Stress Values .....	20
Hydraulic Fracturing Stress Measurements -	
Equipment and Test Chronology .....	21
Hydraulic Fracturing Stress Measurements - Results	
i. Stress Measurements in USW G-3 .....	26
ii. Stress Measurements in Ue-25p1 .....	26
iii. Impressions of Fractured Intervals.....	29
Discussion.....	
i. General Features of the Yucca Mountain Stress Field.....	30
ii. Fault Stability.....	33
iii. Extrapolation of Results to Shallower Levels.....	35
iv. Relationship to the Regional Stress Field.....	35
Summary.....	36
References.....	37
Appendix I: USW G-3 Televiewer Photos.....	48
Appendix II: Ue-25p1 Televiewer Photos.....	63

## ILLUSTRATIONS

Figure 1. Simplified geologic map of Yucca Mountain showing locations of holes USW G-3 and Ue-25p1, as well as other holes mentioned in text.....	3
2. Sketch of borehole televiewer and determination of strike and dip of planar features seen in the televiewer log.....	5
3. Plot of azimuth of dip (relative to geographic north) and dip, as a function of depth, of fractures seen in the televiewer log of USW G-3.....	7
4. Plot of azimuth of dip (relative to geographic north) and dip, as a function of depth, of fractures seen in the televiewer log of Ue-25p1.....	8

	Page
<b>Figure 5.</b> Lower hemisphere, equal area projection of poles to throughgoing fractures seen in the televiewer log of USW G-3.....	9
6. Lower hemisphere, equal area projection of poles to throughgoing fractures seen in the televiewer log of Ue-25p1.....	10
7. Tracing of USW G-3 televiewer log showing principal features visible in the upper 700 m.....	12
8. Example of a borehole breakout, Ue-25p1.....	14
9. Compilation of center azimuths of breakouts seen in the televiewer log of Ue-25p1.....	15
10. Map view of deviation log of USW G-3.....	18
11. Map view of deviation log of Ue-25p1.....	19
12. Pressure-time records of three successful hydraulic fracturing stress measurements in USW G-3.....	23
13. Pressure-time records of three successful hydraulic fracturing stress measurements in Ue-25p1.....	25
14. Steady pumping pressure as a function of flow rate for two tests in Ue-25p1.....	28
15. Horizontal stresses plotted as a function of vertical stress, $S_V$ , for USW G-1, USW G-2, USW G-3 and Ue-25p1...	31
16. Results of stress measurements in USW G-3 and Ue-25p1, showing values of the least horizontal stress $S_h$ , the greatest horizontal stress $S_H$ , and the vertical stress $S_V$ .....	32
17. Results of stress measurements in USW G-3 and Ue-25p1, showing the critical values of $S_h$ for which slip might take place on preexisting faults of optimal orientation, for values of the coefficient of friction between 0.6 and 1.0.....	34

#### TABLES

Table 1. Vertical stress profile for hole Ue-25p1.....	40
2a. Vertical stress profile for the upper part of USW G-3...	42

	Page
<b>Table 2b. Vertical stress profile for the lower part of USW G-3...</b>	<b>43</b>
<b>3. Summary of stress measurements, USW G-3 and Ue-25p1.....</b>	<b>44</b>
<b>4. Lower limits on <math>S_h</math> from tests in the upper part of Ue-25p1.....</b>	<b>45</b>
<b>5. Constraints on hydraulic fracturing tensile strength in the volcanic units at Yucca Mountain.....</b>	<b>46</b>
<b>6. Influence of borehole deviations on results of hydrofrac tests.....</b>	<b>47</b>

UNITED STATES  
DEPARTMENT OF THE INTERIOR  
GEOLOGICAL SURVEY

REPORT ON TELEVIEWER LOG AND STRESS MEASUREMENTS  
IN HOLES USW G-3 AND UE-25P1,  
YUCCA MOUNTAIN, NYE COUNTY, NEVADA

By

J. M. Stock, J. H. Healy, J. Svitek, and L. Mastin

---

ABSTRACT

Hydraulic fracturing stress measurements and televiewer observations were made in drill holes USW G-3 and Ue-25p1 on Yucca Mountain, Nevada, as part of a continuing investigation of the tectonic stress field in the vicinity of a proposed site for the disposal of nuclear waste. The results from USW G-3 are similar to the results reported previously from USW G-1 and USW G-2 with a low least horizontal principal stress in a direction approximately N65°W. This indicates a normal faulting stress regime consistent with the inferred regional extension in this part of the Basin and Range province.

Ue-25p1 was drilled on a basement high indicated by gravity and seismic refraction data. Initial attempts to frac this hole failed because the pressures required to fracture the rock exceeded the strength of our standard packer system. A new and stronger resettable packer system was designed, tested, and debugged during the measurement program in USW G-3 and Ue-25p1. Much of the data collected in this experiment is not used in our present interpretation because of obvious or suspected malfunction of this new packer system. Based on the experience of this experiment further modifications were made to the packer system and recent tests indicate the development of a much improved and stronger system. The results of this development effort will be reported separately.

The number of reliable hydraulic fracturing tests in Ue-25p1 is not sufficient to reliably characterize the state of stress at this site, but some definite conclusions can be drawn from these data. The pressure curves observed during many of the frac tests are significantly different from the curves observed in USW G-1, USW G-2, and USW G-3. The breakdown pressures are higher, suggesting a higher least horizontal principal stress and/or a substantially higher apparent tensile strength for the rocks in this hole. The instantaneous shut-in pressure does not clearly reveal the least horizontal principal stress in most of the frac tests, but two pressure versus volume pumping tests in the Paleozoic rocks show a fracture opening pressure close to the vertical stress, suggesting that the least horizontal principal stress could possibly be as high as the vertical stress. One good hydraulic

fracturing test reveals a least horizontal stress much less than the vertical stress, with a greatest horizontal principal stress close to but less than the vertical stress. No drilling-induced hydraulic fractures were observed in this hole, in contrast to the three USW G holes which had drilling-induced hydraulic fractures in the upper portions of the televIEWER logs. This suggests that the  $S_h$  values are higher than the hydrostatic pressure in Ue-25p1. Borehole breakouts in the lower part of Ue-25p1 indicate an extension direction of N60-65°W, consistent with that observed in the other holes. These observations suggest that the stresses at Ue-25p1 may still correspond to a normal faulting stress regime, although it may be close to the transition between normal and strike-slip faulting stress regimes. Ue-25p1 may have more stable stresses than the other three holes, with  $S_h$  values closer to  $S_v$  and further from the frictional sliding criterion defined by Byerlee's law.

#### ACKNOWLEDGEMENTS

We thank Jim Springer, Gretchen Zwart, and Keith Brown for assistance with instrumentation and field operations, Rob Harris for analysis of density and breakout data, and Dennis Styles, Tom Denham, Jackie Hennagan, and Rick Ludlum for assistance with packer operation and televIEWER logging. Mark Zoback helped with a valuable discussion of the results. We also thank the DOE and Fenix and Scission personnel at the Nevada Test Site, especially Wallace Hammer and Ray Escobedo, for their support during the field operations.

#### INTRODUCTION

The Nevada Nuclear Waste Storage Investigations Project has devoted substantial effort to the evaluation of a prospective site for a nuclear waste repository at Yucca Mountain, Nevada. As part of these studies, USGS personnel have performed borehole televIEWER logs and hydraulic fracturing stress measurements in four holes at Yucca Mountain to determine the magnitudes and orientations of the horizontal principal stresses. This information is important to the evaluation of the seismic stability of the repository site and to the safe design and construction of the repository facility. This report describes the results of measurements in holes USW G-3 and Ue-25p1 collected during February, March, November, and December 1983, and January 1984. Previous measurements in holes USW G-1 and USW G-2 have been described by Healy et al. (1984) and Stock et al. (1984, 1985).

#### GEOLOGIC SETTING

Yucca Mountain is in southern Nevada at the western edge of the Nevada Test Site (NTS) (figure 1), and is bounded by Crater Flat to the west, Jackass Flats to the east, and Highway 95 to the south. Yucca Wash forms its northern boundary with the Calico Hills. Yucca Mountain comprises a thick sequence of Miocene volcanic tuff and flow units, ranging from the Tiva Canyon member of the Paintbrush Tuff at the surface to the Tuff of Lithic Ridge and older tuffs at depth. These units have been tilted gently eastward in a series of fault blocks bounded by high-angle, west-dipping, normal faults that are generally NNW- to N-striking (Scott and Bonk, 1984). The tuffs extend to at least 3 km

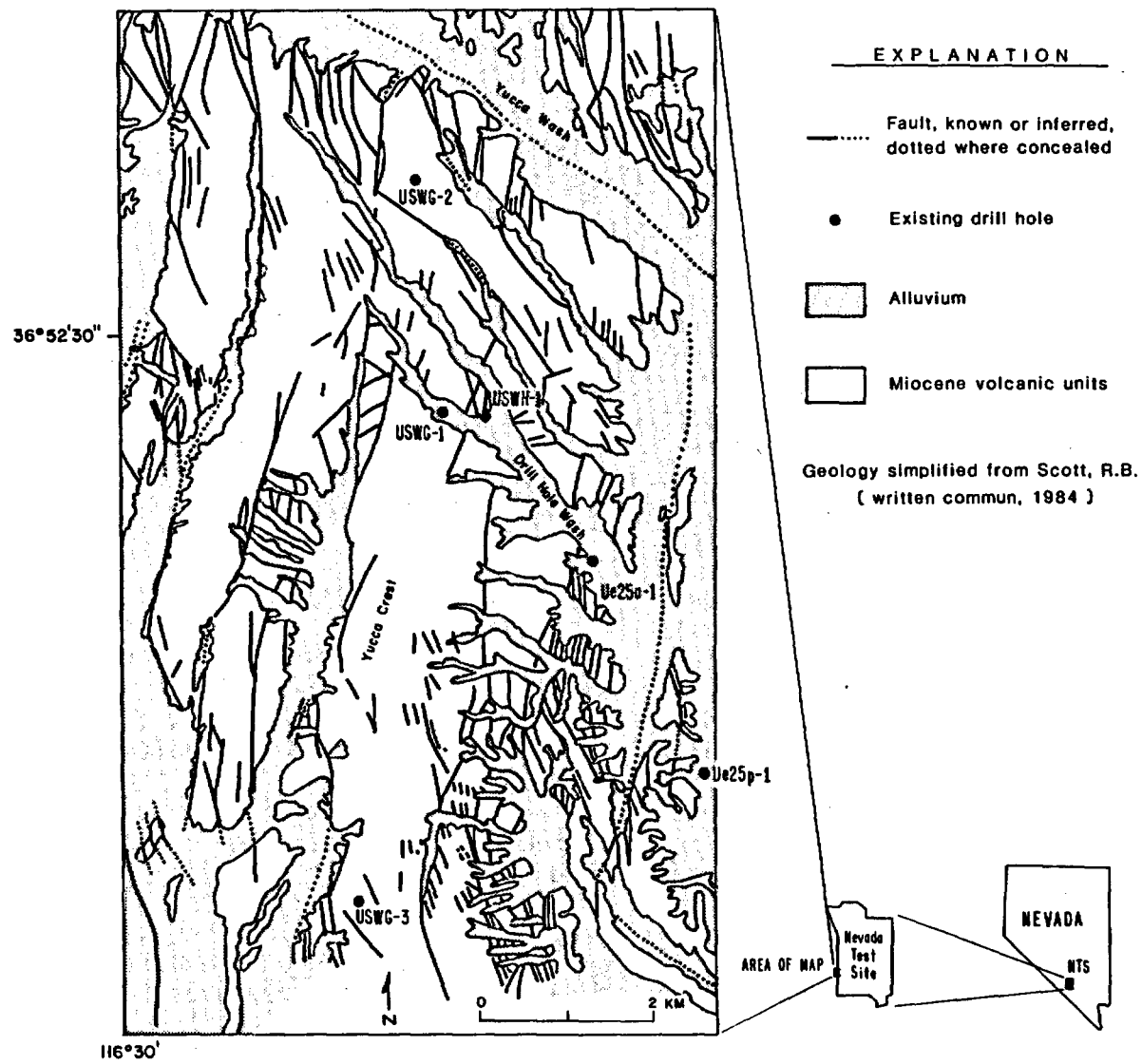


**Figure 1.** Simplified geologic map of Yucca Mountain showing locations of holes USW G-3 and Ue-25p1, as well as other holes mentioned in the text. Stippled area represents alluvium; white outcrop is Tertiary volcanic units.

depth under the main part of Yucca Mountain (location of holes USW G-1, G-2, and G-3). The interpretation of gravity (Snyder and Carr, 1982) and seismic refraction data (Hoffman and Mooney, 1983) indicates a structural high in the Paleozoic subsurface beneath part of the eastern side of Yucca Mountain. This is also indicated at hole Ue-25p1 and adjacent holes where Silurian and Ordovician carbonate units were drilled at 1,244 m depth.

USW G-3 was drilled on the crest of Yucca Mountain, completely within the Miocene volcanic units, at coordinates  $36^{\circ} 49' 04.90''$  N,  $116^{\circ} 28' 00.71''$  W. Its surface elevation is 1,480 m, and it has an unusually low water table, 752 m below the surface. The hole is approximately vertical from the surface to the bottom of the casing at 792 m depth, then deviates to the west at a gradually increasing angle, up to 25° from vertical at the bottom of the hole. A detailed stratigraphy and description of core is given by Scott and Castellanos (1984).

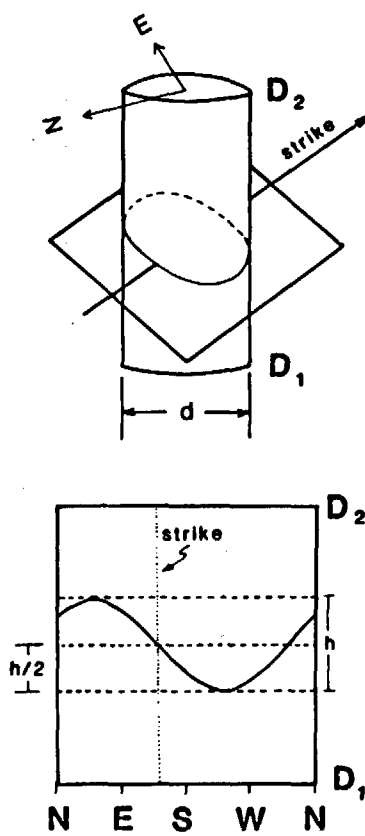
Drill hole Ue-25p1, at coordinates  $36^{\circ} 49' 38.13''$  N,  $116^{\circ} 25' 20.70''$  W, has a surface elevation of approximately 1,120 m, and one of the shallowest water levels seen at Yucca Mountain, 385 m. Its maximum deviation from vertical is 8.75° at the bottom of the hole. It penetrates relatively unfractured Miocene volcanics to 1,244 m depth, where a fault brings them into contact with Paleozoic carbonates that continue to the bottom of the hole at 1,805 m depth. Stratigraphy and core descriptions are reported by Carr et al. (1986).

#### BOREHOLE TELEVIEWER - METHOD

The acoustic borehole televiwer is a logging tool designed to map the smoothness of the borehole wall (Zemanek et al., 1969, 1970). It contains a 2-MHz transducer that pulses 1,800 times per second and rotates three times per second, emitting a signal which is reflected off the borehole wall, then transmitted uphole by wireline to be recorded at the surface. A fluxgate magnetometer is used to orient the signal with respect to magnetic north. The tool is pulled upward at a constant speed of 2.5 cm/s. The reflected signal is displayed on an oscilloscope with depth on the vertical axis, azimuth on the horizontal axis, and brightness as a function of amplitude of the reflected signal. Photographs of the oscilloscope display, taken at regular intervals, are taped together to form a continuous log of the hole. The signal is also recorded on magnetic tape to facilitate reprocessing.

The final image is an "unwrapped" view of the inside surface of the wellbore. Strong reflected signals appear as bright areas on the televiwer log, while zones of roughness such as fractures or breakouts disperse the reflected signals and can be seen as dark areas. A planar fracture inclined to the borehole axis will have a sinusoidal trace on the televiwer log, from which its strike and dip can be determined (figure 2). Other features visible on the televiwer logs include borehole breakouts, large lithophysal cavities, cobbles of contrasting lithology in conglomerate beds, occasional bedding, and drill bit- and pipe-produced wear and scuffing.

G1



#### BOREHOLE TELEVIEWER LOG

Strike: orientation of midpoint  
between peak and trough

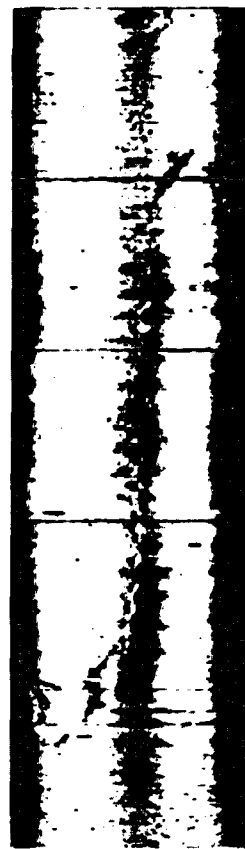
Dip:  $\tan^{-1}(h/d)$

**USWG-3**

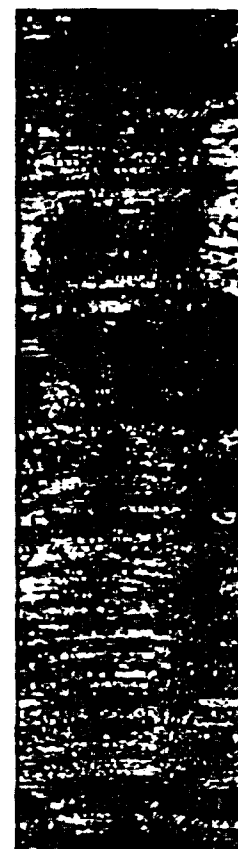
**Ue- 25P1**

**946.4 m**

**1770.9 m**



**954.0 m**



**1778.5 m**

**steeply dipping  
fracture**

**shallowly dipping  
bedding  
and  
bedding- parallel  
fractures**

Figure 2. Sketch of borehole televiwer and determination of strike and dip of planar features seen in the televiwer log. Representative portions of the televiwer logs from USW G-3 and Ue-25P1 are shown to illustrate steeply dipping fractures, shallowly dipping fractures, and bedding.

Because televIEWer logs are plotted at a constant vertical scale, the distortion of borehole features depends on hole diameter. USW G-3 was 10 cm in diameter, while Ue-25p1 was 20 to 28 cm in diameter; thus, the horizontal exaggerations of these two logs are 3.4:1 and 6.8:1 to 10:1, respectively. This strong horizontal exaggeration makes detection of shallowly dipping features very difficult, so identification of planar features (e.g., fractures, bedding) on this log is somewhat biased toward those of steeper dip.

Ideally, the televIEWer should be centered in the hole during the logging, so that the reflected signal returns directly back to the televIEWer. The televIEWer log of USW G-3 was obtained in an interval which deviated from vertical 7° to 21° toward the west, which was too pronounced a deviation for the centralizers to keep the tool centered. As the tool was frequently closer to the eastern side of the hole, good signal return was obtained from the azimuths close to east and west. However, poor signal return at azimuths close to north and south gave rise to the vertical black bands present at these azimuths below 907 m (2,975'). This problem was not as pronounced in hole Ue-25p1 as it was much closer to vertical.

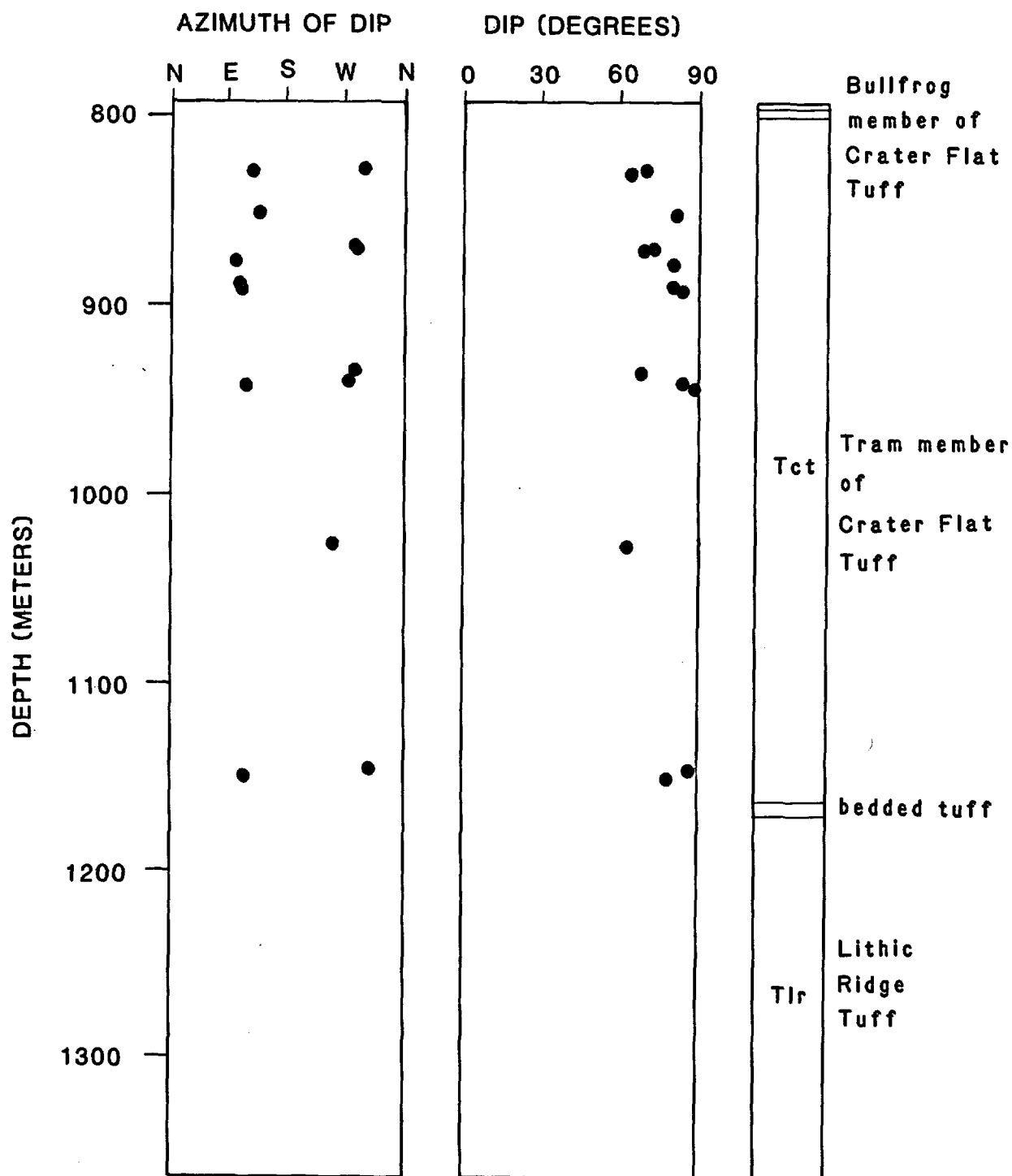
Tool problems also may have caused the pattern of regularly spaced slanted black lines, giving the appearance of a spiral fabric in USW G-3, at 890-919 m, (2,920'-3,015'), 632-946 m (2,075'-3,105'), and 968-1,013 m (3,175'-3,325'). Amplitudes of the televIEWer signal and travel time cross sections show that this pattern may be caused by lateral oscillation of the body of the tool as it is pulled upward at a constant rate and the cable passes through exceptionally crooked parts of the hole. In repeat sections of the log in zones showing this pattern, the black lines occurred with the same frequency, but in a slightly different position relative to identifiable features of the borehole wall such as fractures. This pattern has not been observed by us in Ue-25p1, USW G-1, or USW G-2.

#### BOREHOLE TELEVIEWER - RESULTS

TelevIEWer logs were obtained from 792-1,364 m in USW G-3, and in two separate intervals in Ue-25p1: 480-1,202 m (Tertiary volcanic units and fanglomerate) and 1,297-1,798 m (Paleozoic carbonate units). The complete logs are reproduced in the appendices. Preexisting fractures, drilling-induced hydraulic fractures, borehole breakouts, bedding, and conglomerate cobbles are all visible in portions of these logs; their appearance and identification are discussed below. Study of the breakouts and drilling-induced hydraulic fractures, which are stress-related, shows differences in the response of the two boreholes to drilling and coring activities, possibly due to differences in the stress regime between the two sites (discussed further below).

#### Throughgoing fractures

In this work, a fracture is defined as throughgoing if both updip and downdip intersections with the borehole wall can be seen in the televIEWer log. The appendices and Figures 3 to 6 show that the distribution and orientation of throughgoing fractures differs considerably between these two holes. The USW G-3 televIEWer log does not show many throughgoing fractures;



THROUGHGOING FRACTURES SEEN IN TELEVIEWER LOG,  
USW G-3

Figure 3. Plot of azimuth of dip (relative to geographic north) and dip, as a function of meters depth, of fractures seen in the televiewer log of USW G-3. A simplified lithologic column is shown at the right for reference. Orientations are corrected for hole deviation.

THROUGHGOING FRACTURES OBSERVED IN TELEVIEWER LOG

Ue-25p#1

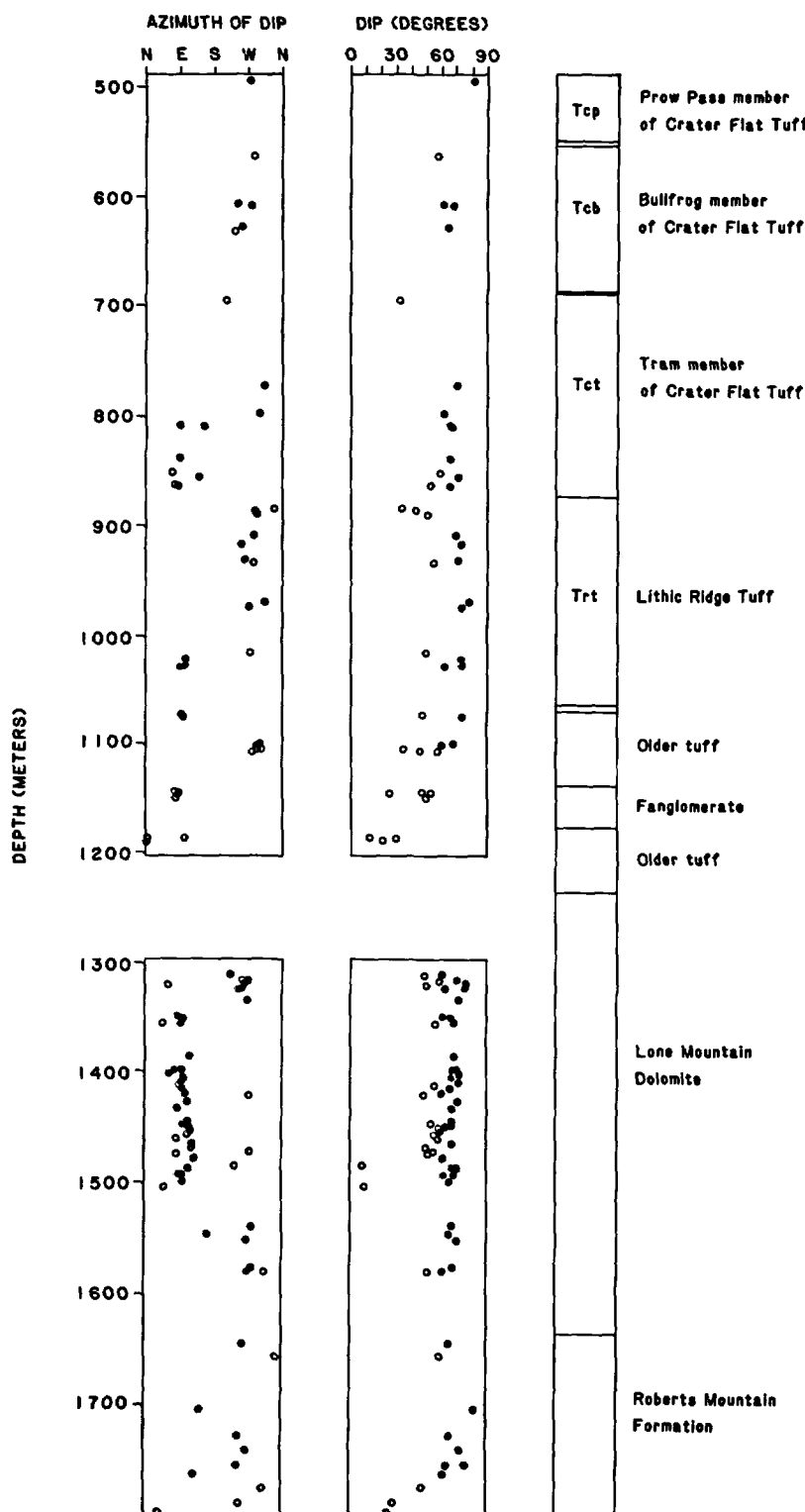
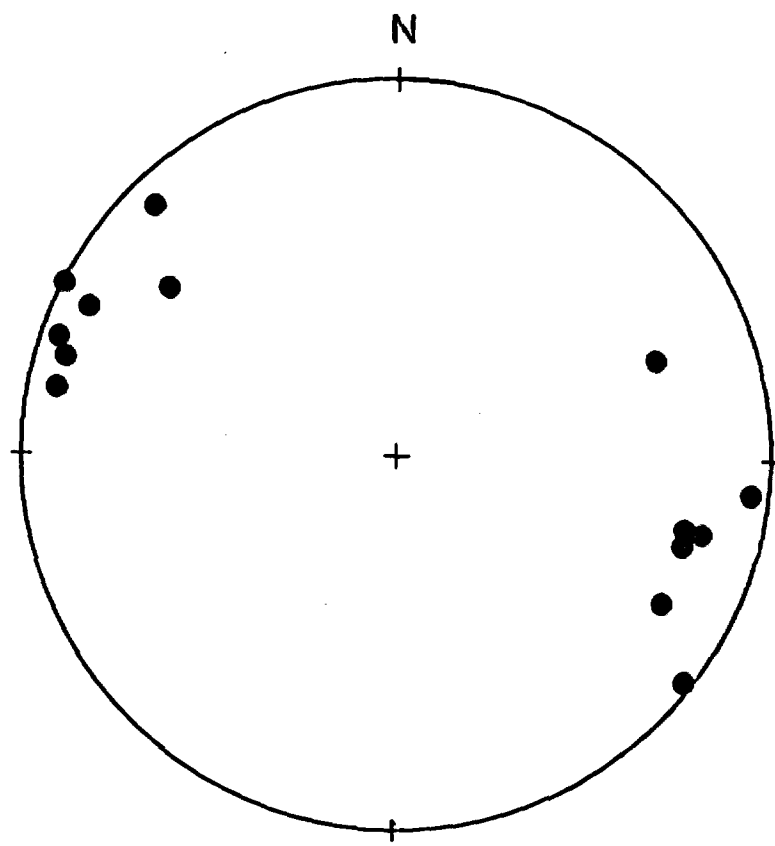


Figure 4. Plot of azimuth of dip (relative to geographic north) and dip, as a function of meters depth, of fractures seen in the televiewer log of Ue-25p1. Fractures with dips less than 60° are represented by open circles; fractures with dips greater than 60° are represented by filled circles. Lithologic column is shown for reference. The two sections of the log were collected separately. The section of hole from 1,202 to 1,297 m was never accessible for televiewer logging.

**NEVADA TEST SITE USW G-3**  
**Poles to fractures seen in televIEWER log**  
**Lower hemisphere, equal area projection**



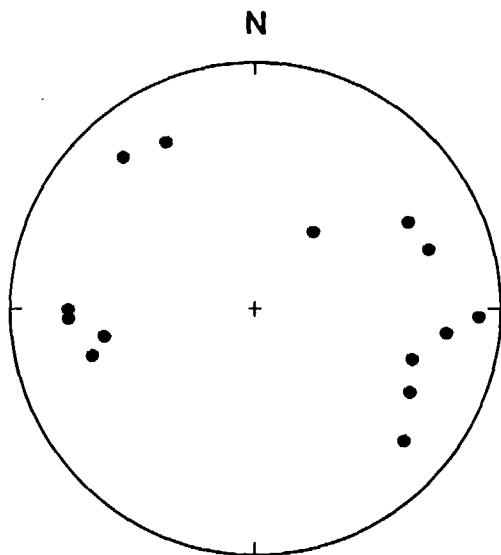
**792 - 1364 m**  
**CRATER FLAT TUFF**  
**(BULLFROG MEMBER, TRAM MEMBER)**  
**AND LITHIC RIDGE TUFF**

Figure 5. Lower hemisphere equal area projection of poles to the through-going fractures seen in the televIEWER log of USW G-3. Fracture orientations have been corrected for hole deviation.

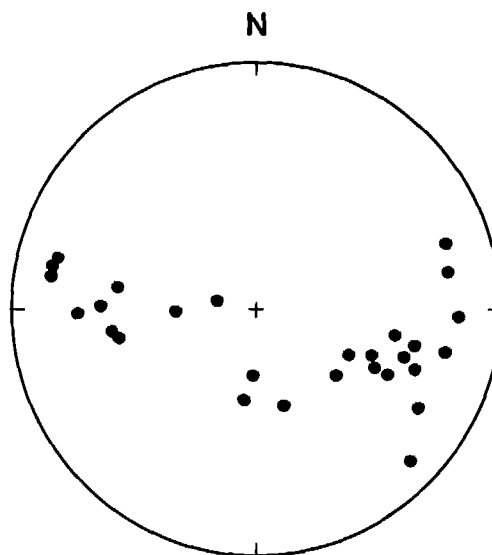
## NEVADA TEST SITE Ue-25p#1

Poles to fractures seen in televiewer log

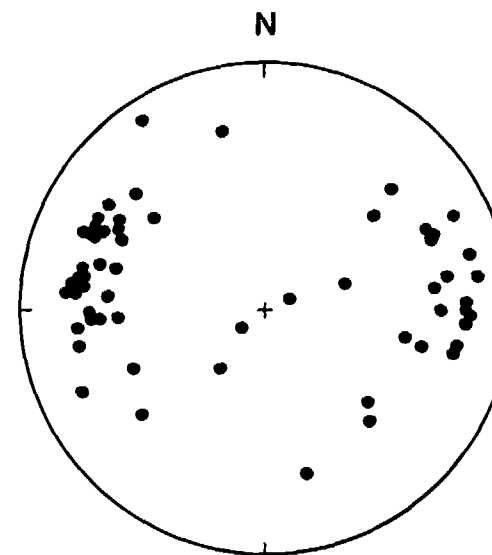
Lower hemisphere, equal area projection



488 - 873 m  
CRATER FLAT TUFF  
(PROW PASS MEMBER,  
BULLFROG MEMBER,  
TRAM MEMBER)



873 - 1202 m  
LITHIC RIDGE TUFF  
FANGLOMERATE  
AND OLDER TUFFS



1298 - 1798 m  
LONE MOUNTAIN DOLOMITE  
AND  
ROBERTS MOUNTAIN FORMATION

Figure 6. Lower hemisphere equal area projection of poles to the throughgoing fractures seen in the televiewer log of Ue-25p1.

we believe that this may be due to the very thick mud coating the walls of the hole, which may have filled and smoothed all except the largest fractures. The few visible fractures are all steeply dipping and have an average strike of N20°E, with dips to both east and west. There are more fractures visible in the Ue-25p1 televiewer log; these have fairly scattered orientations and both steep and shallow dips. The Lone Mountain dolomite has a higher concentration of fractures than the other units in the hole; most of the fractures seen in this unit have an average strike of N-S and dips from 50° to 70°, predominantly to the east.

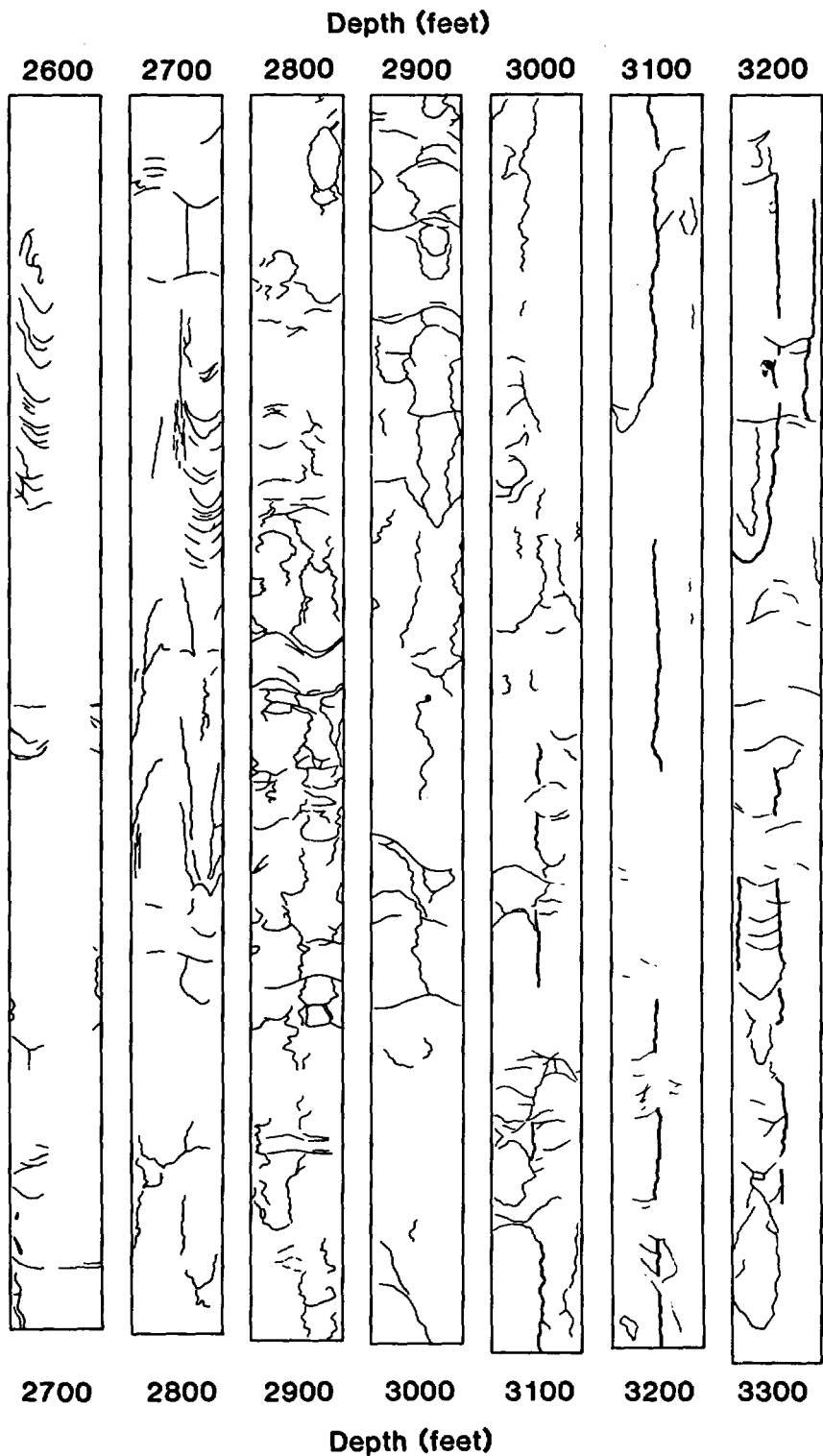
Although the Ue-25p1 log shows more fractures than the USW G-3 log, it should be noted that neither of these holes have as many visible fractures as USW G-1 and USW G-2.

#### Drilling-induced hydraulic fractures

The USW G-3 televiewer log shows long fractures which are parallel to the borehole axis for many meters, along an average azimuth of N25°E (figure 7). Some of these are very jagged, being connected to or interrupted by through-going fractures; e.g., 882-899 m (2,825'-2,950'). In other places these fractures are fairly straight and have no throughgoing fractures associated with them; e.g., 975-986 m (3,200'-3,235') and 1,006-1,018 m (3,300'-3,340'). Such fractures may be present elsewhere in the hole if they are within the black bands of poor signal return resulting from the tool being off center in the hole. These fractures, and similar ones observed in holes USW G-1 (Healy et al., 1984) and USW G-2 (Stock et al., 1984, 1985), are believed to be drilling-induced hydrofractures. In USW G-2, these fractures are present in intervals of the hole where the corresponding core was unfractured, indicating that the fractures formed after that interval of the hole was drilled. Also, these fractures, where encountered, appear to follow the axis of the hole. The orientations of the straight and continuous portions indicate that the fractures are well-centered on the hole, suggesting that their orientation is strongly controlled by the presence of the borehole and that they were formed at a later stage in the drilling process.

Drilling-induced hydrofractures are likely to form in holes where the least horizontal stress is low relative to the vertical stress, and where the water table is fairly far below the surface. In the presence of a low equilibrium water table, raising the borehole fluid level to the surface causes a large increase in the borehole pressure above the equilibrium pore pressure in the rock. If  $S_h$  is low, and this borehole pressure exceeds the least horizontal stress on the rock, a hydraulic fracture may initiate and propagate. Results of the hydraulic fracturing stress measurements in USW G-3, discussed below, are consistent with this mechanism for formation of these fractures.

Because hydraulic fractures theoretically should form perpendicular to the least horizontal principal stress,  $S_h$ , their orientation is frequently used as an indicator of stress direction. In a borehole that is oblique to the principal stress directions, these fractures would be expected to initiate at the azimuth of the least compressive stress in the borehole wall. This



**FEATURES SEEN IN TELEVIEWER LOG, USW G-3  
(UPPER PORTION)**

**Figure 7.** Tracing of USW G-3 televiewer log showing principal features visible in the upper 700 m. Fractures drawn in heavier line between 3,000 and 3,300 ft are inferred to be drilling-induced.

azimuth departs from the  $S_H$  direction as  $S_H$  approaches  $S_h$  and as the borehole axis approaches the  $S_h$  direction (Richardson, 1983). However, with the observed Yucca Mountain stress field, for the deviation of USW G-3 at the position of the drilling-induced hydraulic fractures, no more than a few degrees of rotation of the apparent principal stress direction would be expected. (See the discussion of deviated holes in the following section on hydraulic fracturing theory.) Thus, the orientation of these fractures in USW G-3 is sufficiently close to  $S_H$  that it can be taken to imply a N65°W orientation of  $S_h$ . No drilling-induced hydraulic fractures are seen in Ue-25p1, so no directional information for that hole can be inferred by this method.

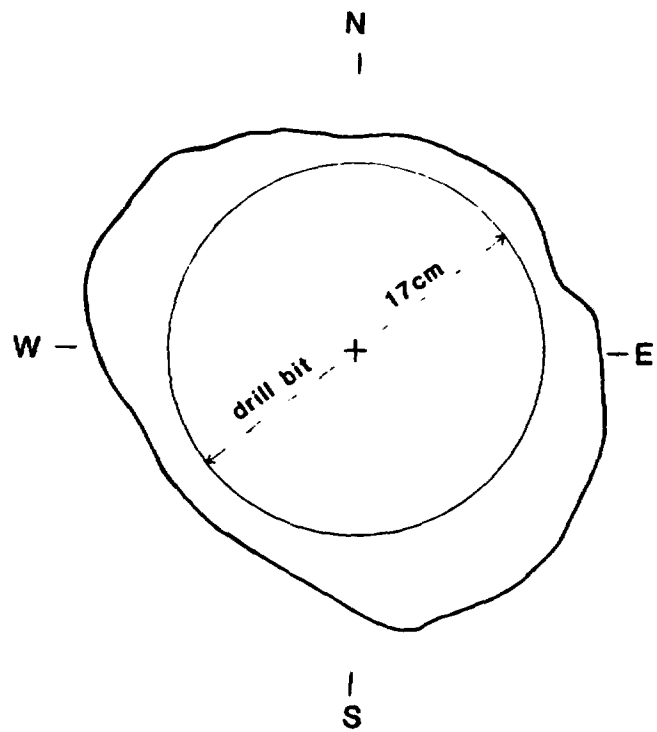
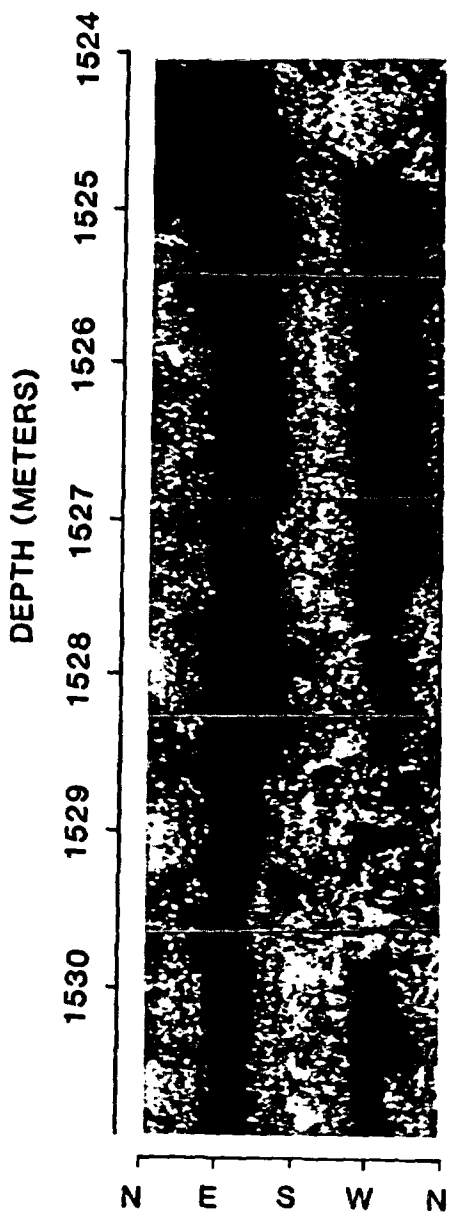
### Borehole breakouts

Breakouts are spalled portions of the borehole wall which often appear in the televIEWER log as paired, vertical, black bands, centered approximately 180° apart, with jagged edges. When the televIEWER signal is replotted with travel time as a function of azimuth, these zones correspond to azimuths along which the hole is enlarged, resulting in a roughly elliptical cross section (figure 8). They can also be identified on downhole television pictures and oriented caliper logs. It has long been known that their orientations are useful indicators of the  $S_h$  direction (e.g., Gough and Bell, 1982; Bell and Gough, 1983). Recent laboratory studies confirm that breakouts form by a combination of shear and tensile failure of the borehole wall at the azimuth of concentrated high compressive stresses, centered on the  $S_h$  direction (Mastin, 1984).

In Ue-25p1, borehole breakouts are present only in the Paleozoic units, at depths from 1,524-1,542 m (5,000'-5,060'), 1,585-1,588 m (5,200'-5,210'), 1,608-1,609 m (5,275'-5,280'), 1,631-1,640 m (5,350'-5,380'), and 1,649-1,676 m (5,410'-5,500'). Although the orientations of the centers of the breakouts do show some scatter, the average azimuth of the breakouts is N60°W (figure 9). No borehole breakouts are visible on the televIEWER log of USW G-3. The black bands at N and S azimuths in the USW G-3 log are caused by the televIEWER being off center in the hole (as discussed above). Cross sections made by reprocessing the televIEWER signal at several depths show this eccentricity clearly but provide no evidence of breakouts.

### Sedimentary features

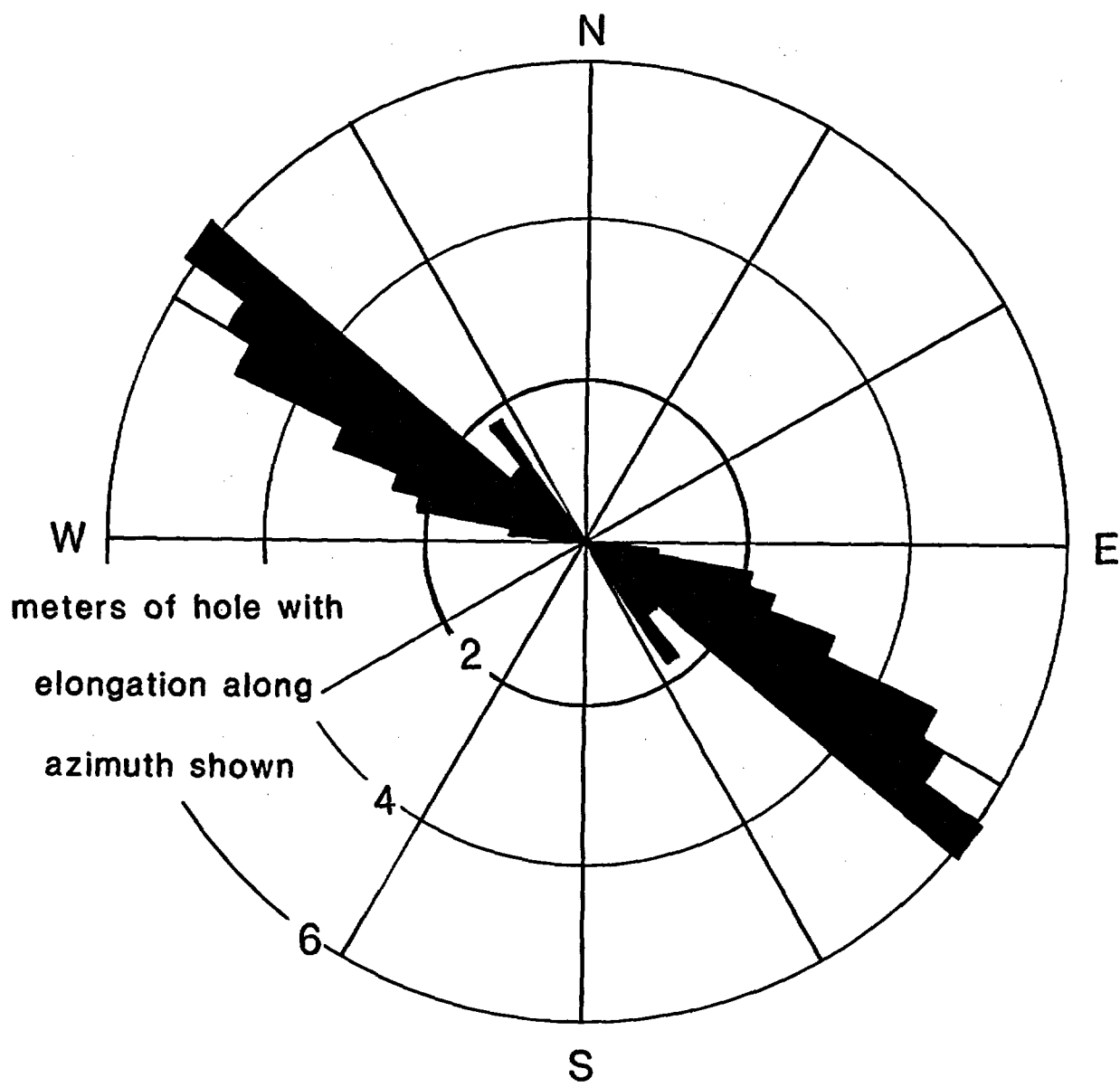
Some sedimentary features are visible on the Ue-25p1 televIEWER log. Among these are irregular light patches occurring from 1,158-1,172 m (3,800'-3,846'), with the largest at 1,168 m and 1,172 m (3,831' and 3,846') depth. These are believed to correspond to cobbles in the conglomerate unit. From 1,158-1,172 m (3,800'-3,844') this unit consists of clasts of carbonate rocks, argillite, sandstone/siltstone, and tuff, in a claystone matrix (Carr et al., 1986). Some of the clasts are also visible in the downhole television log of the hole in this interval; their large size (exceeding 30 cm in diameter) explains their visibility on the televIEWER log.



**NEVADA TEST SITE  
UE25P#1**

**Cross section of borehole  
1527 meters**

Figure 8. Example of a borehole breakout, Ue-25p1. When the televiewer log is reprocessed to yield a cross section of the hole, the dark paired bands in the televiewer log are found to correspond to the azimuths of large hole diameter.



### AZIMUTHS OF BREAKOUTS, NTS Ue-25p#1

1218 - 1524 m DEPTH

Figure 9. Compilation of center azimuths of breakouts seen in the televiewer log of Ue-25p1. The average azimuth of breakouts is N60°W.

Bedding is generally not visible in the televIEWer log of the volcanic sections of Ue-25p1 and USW G-3. In the core, many of the tuff units are massive or poorly bedded; although clear bedding is present in some parts of the core ("bedded tuff units"), it may be too fine or too shallowly dipping to show up on the televIEWer log. Fine laminations in parts of the Paleozoic units in Ue-25p1 (Carr et al., 1986) are also not visible in the televIEWer log; however, more massive bedding can be seen in the Lone Mountain Dolomite from 1,544-1,550 m (5,065'-5,085'), and in the Roberts Mountain Formation from 1,771-1,779 m (5,810'-5,836'), and below 1,783 m (5,850') (figure 2). The beds below 1,768 m (5,800') have an averaged apparent dip of 30° toward the NNW, which, when corrected for probable hole deviation, yields a true dip of 38° toward N15°W. (This dip vector may be in error by up to 10° because the deviation for this interval was estimated by extrapolation downward from the last measurement at 1,707 m.) Bedding between 1,542 m and 1,550 m (5,060' and 5,085') is less distinct, but appears to be steeper, with a strike of N25°E and a dip of 68° NW when corrected for magnetic declination and measured deviation of the borehole at this depth.

#### HYDRAULIC FRACTURING STRESS MEASUREMENTS - METHOD

##### Horizontal Stress Values

The hydraulic fracturing method (Hubbert and Willis, 1957; Haimson and Fairhurst, 1967) directly measures the magnitude of the least horizontal principal stress,  $S_h$ , and indirectly yields the magnitude of the greatest horizontal principal stress,  $S_H$ . The method involves the creation of a fracture in an isolated region of the borehole, and observation of its pressure-time behavior during repeated borehole pressurization cycles. A one-to two-meter interval of the borehole is sealed off between two inflatable rubber packers, and connected to the surface by a tubing string. Pressure is measured downhole in the tubing at the depth of the packers by a pressure transmitter attached to a wireline, which sends signals uphole to be recorded on chart paper and on computer disk. A self-contained mechanical pressure gauge is attached below the housing of the electronic gauge to provide an additional pressure record. A wireline lubricator at the top of the tubing prevents fluid leaks at the surface.

Fluid is pumped into the tubing from the surface to raise the pressure in the interval between the packers until a fracture is created in the borehole wall. Once a fracture forms, pumping is stopped, the interval is "shut in" (sealed off at the surface), and the pressure decays by flow into the fracture and/or permeation into the borehole wall. The pressure at which the fracture closes is often visible as an inflection on a plot of interval fluid pressure against time, and is referred to as the "instantaneous shut-in pressure" or ISIP. After shut-in, the pressure normally is bled back to its pre-test value. Several more of these pressurization cycles are conducted to observe fracture reopening and shut-in pressures. Ideally, these cycles are all conducted at the same flow rate so that comparison can be made between the behavior of the fracture during different cycles (Hickman and Zoback, 1983).

After several constant-rate pumping cycles have been conducted, and fracture pumping pressure has stabilized, pumping pressures are recorded for one or two cycles of stepwise decreasing flow rates, to further constrain the pressure at which the fracture closes (e.g., Earlougher, 1977; Hickman et al., 1985). The resulting plot of pumping pressure as a function of flow rate should be bilinear with a change in slope due to the change in apparent permeability of the interval as the fracture closes.

This method is based on an analytic solution for stress around a cylindrical hole in an elastic, isotropic medium. If the borehole is drilled parallel to a principal stress direction in homogeneous rock, theoretical calculations indicate that a hydrofracture should initiate at the azimuth of least tangential compressive stress at the borehole wall, that is, at the azimuth of the maximum horizontal principal stress,  $S_h$  (Hubbert and Willis, 1957). After the fracture propagates away from the zone near the borehole, the normal stress across the fracture should be equal to  $S_h$ . The borehole pressure  $P_b$  required to initiate this fracture is given by Haimson and Fairhurst (1967):

$$P_b = 3S_h - S_H + T - P_p \quad (1)$$

where  $T$  is the tensile strength of the rock and  $P_p$  is the equilibrium pore pressure in the formation. If  $T$  and  $P_p$  are known, the observed normal stress on the fracture can be used in equation (1) to determine  $S_H$ . However,  $T$  is observed to vary greatly with sample size and testing method (e.g., Ratigan, 1983). Values of  $T$  obtained by hydraulic fracturing tensile tests in the lab must usually be extrapolated upwards to the in situ borehole size in order to be used in equation (1). To avoid this uncertainty in  $T$ , Bredehoeft et al. (1976) developed a modified form of equation (1), using the fracture reopening pressure on later cycles,  $P_b$  ( $T=0$ ):

$$P_b (T=0) = 3S_h - S_H - P_p \quad (2)$$

Equation (2) can be rewritten to solve for  $S_H$  if the borehole pressure has been returned to its original value by bleeding back excess pressure after each cycle.

#### Effect of Borehole Deviation

In any hydraulic fracturing test, it is assumed that the orientation of the fracture at the borehole is the same as that in the far-field, that is, the rock is isotropic and the (vertical) borehole is parallel to a (vertical) principal stress direction. Under these circumstances, the hydraulic fracture forms perpendicular to the  $S_h$  direction. Even for vertical boreholes, this assumption may not always be correct because local topography and/or local structural irregularities can influence the principal stress directions. However, in USW G-3 there is the additional complication of strong borehole deviation (figures 10 and 11), so that the basic assumptions of the method must be more carefully evaluated.

## HORIZONTAL PROJECTION OF HOLE DEVIATION, USW G-3

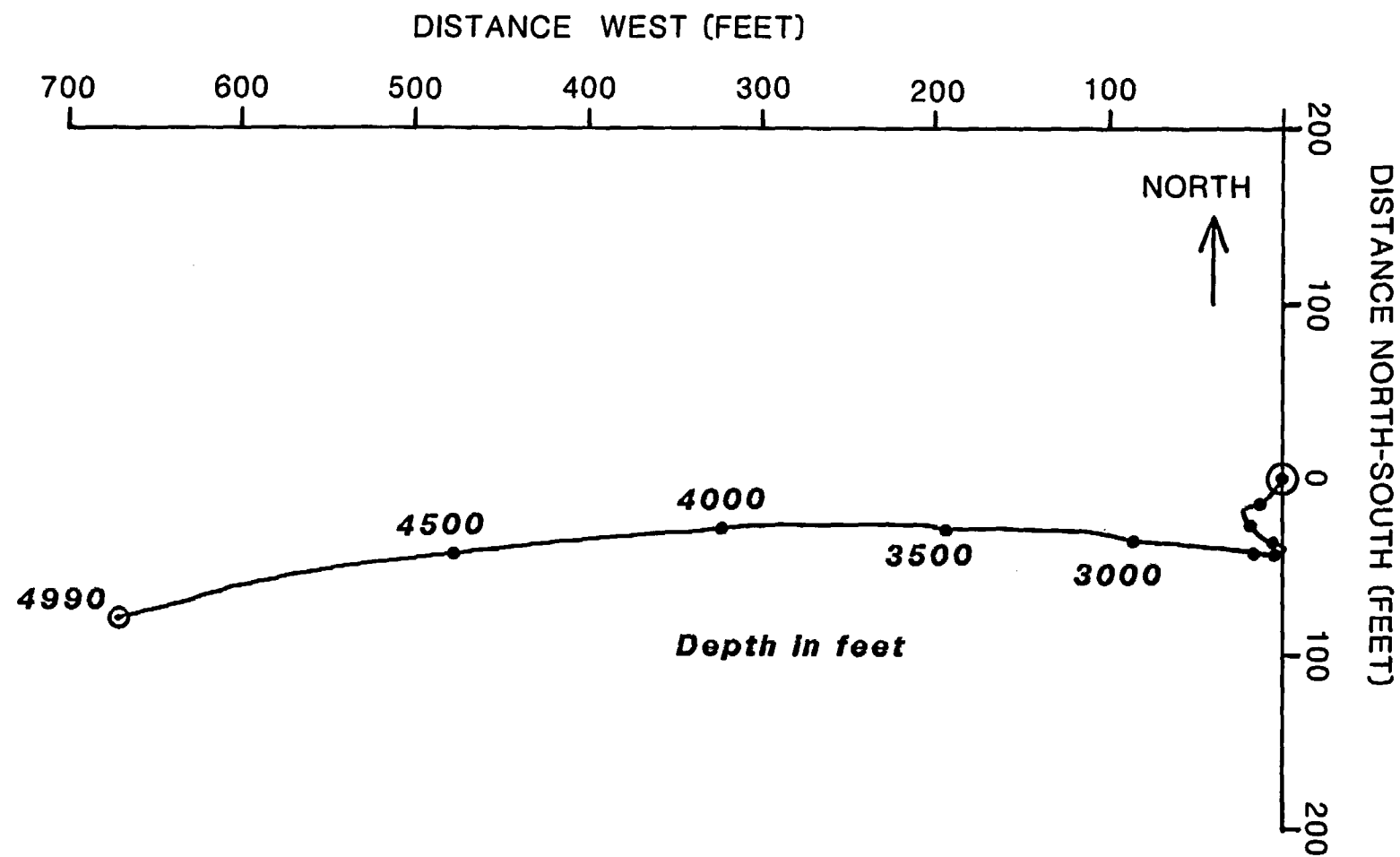


Figure 10. Map view of deviation log of USW G-3.

## HORIZONTAL PROJECTION OF HOLE DEVIATION, Ue-25p#1

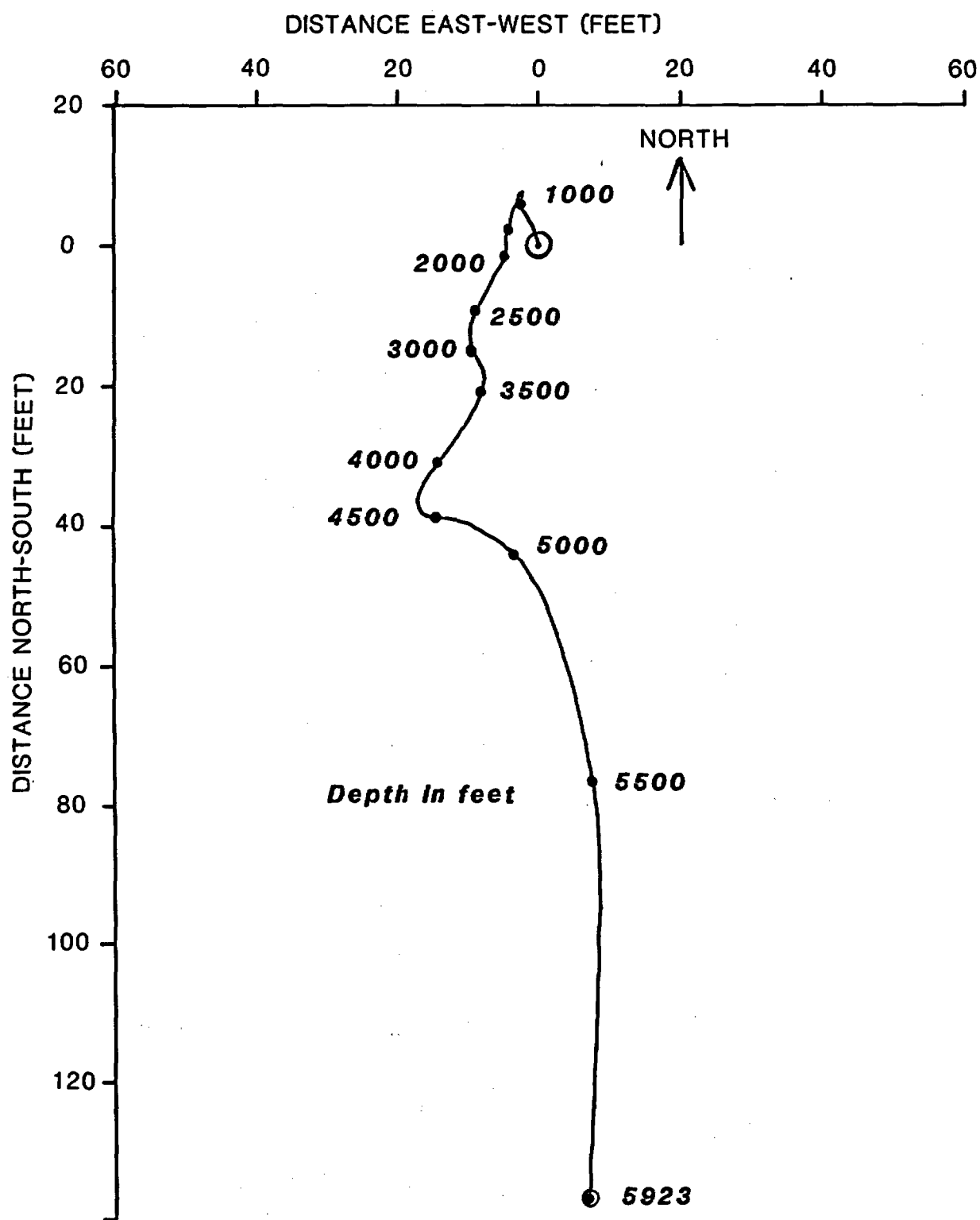


Figure 11. Map view of deviation log of Ue-25p1.

Regardless of the obliquity of the borehole to the stress field, the hydraulic fracture should initiate at the azimuth of least compressive tangential stress in the borehole, at a breakdown pressure equal to this stress plus  $P_p - T$ . As the fracture propagates, it should always follow a trajectory perpendicular to the least principal stress. For an oblique borehole, this means that the orientation of the fracture will change away from the borehole. The far field normal stress on the fracture should be equal to  $S_3$  and should be the pressure corresponding to the inflection on the pressure record when the fracture closes (ISIP).

It is possible to predict the breakdown pressures and hydraulic fracture orientations that might be expected for a borehole with the deviation observed in USW G-3 and Ue-25p1. When the observed Yucca Mountain stress field is applied to holes of the observed deviation (Table 6), it is found that the apparent azimuths of hydraulic fractures do not differ significantly from the true  $S_H$  azimuth. This is because the magnitudes of  $S_h$  and  $S_H$  are very different; as  $\phi$  goes to zero ( $S_h > S_H$ ), large deviations of apparent  $S_h$  are possible. Even with the uncertainties in the stress magnitude values used for the calculations in Table 6, the azimuth of the drilling-induced hydraulic fractures seen in USW G-3 should be very close to the true  $S_H$  direction. For tests in more severely deviated boreholes, or in regions with horizontal stresses that are closer in magnitude, the possibility of erroneous directional information would be higher.

Hole deviation might influence the  $S_H$  result if the actual breakdown pressure was not equal to that given in equation (1) for an ideally oriented hole. Calculations of expected breakdown pressures, when compared with breakdown pressures for an ideally oriented borehole (Table 6), show that the small deviation of Ue-25p1 should not have affected the breakdown pressures. However, observed  $P_b$  ( $T=0$ ) pressures in USW G-3 may be 10 to 15 bars less than would be predicted by equations (1) and (2). Thus, use of the observed  $P_b$  values to compute  $S_H$  might result in a calculated  $S_H$  value that was 10-15 bars higher than actually present.

#### Vertical Stress Values

Once values of  $S_h$  and  $S_H$  are obtained by hydraulic fracturing stress measurements, the vertical stress,  $S_v$ , is still needed to characterize the complete stress field. In the absence of topography,  $S_v$  is equivalent to the weight of the overburden and can be calculated if the densities of the rock units are known.  $S_v$  values for both holes (Tables 1 and 2) were calculated using borehole compensated (BHC) density logs, and average densities of equivalent units from nearby holes in zones where no BHC log was obtained. In addition,  $S_v$  in USW G-3 was corrected for borehole deviation and drift towards regions of lower surface elevation (Table 2), and corrected for topographic effects as discussed below.

If the topography is irregular, small wavelength variations should be averaged out prior to calculation of  $S_v$  at depth. Such corrections are most important for USW G-3. For instance, the elevation at the surface of USW G-3 is 1,480 m; however, the average surface elevation within a circle of 700-m

radius centered on the top of the hole is approximately 1,390 m. For USW G-3 topographic corrections, the average elevation of the ground surface above each test was obtained by integration over a diameter equal to the depth of the test. The contribution to  $S_y$  from the rock in the drill hole above this average elevation was subtracted from the values listed in Table 2 to provide a rough estimate of the magnitude of  $S_y$  at the depths of the test (Table 3). Maximum uncertainty limits of these values are the uncorrected value of  $S_y$  as an upper bound, and the average topography in the absence of the excess height of the ridge as a lower bound; this gives an uncertainty of  $\pm 20\text{-}25$  bars for the USW G-3  $S_y$  values. An estimate for the  $S_y$  correction can also be derived analytically if surface topography can be approximated as a smooth function, and density and elastic constants are assumed uniform (e.g., Swolfs and Savage, 1985).

In hole USW H-1, a hydrology hole several km northwest of Ue-25p1 (figure 1), BHC density values and downhole gravimetry measurements agree very closely (Snyder and Carr, 1982), indicating that the BHC density values for this hole are representative of the region around the borehole and can be considered an accurate source for  $S_y$ . Borehole gravity measurements, yielding average densities and interval densities, were also obtained in USW G-3 and Ue-25p1 (Healey et al., 1984).  $S_y$  values based on these results are listed in Tables 1 and 2. These show that below 200 m depth in Ue-25p1, the densities calculated by these two methods agree within 5 percent or less, and are within 3 percent at the depths of our hydraulic fracturing measurements. The densities listed by Healey et al. (1984) for USW G-3 are more difficult to interpret, since there is some uncertainty regarding the free air gravity gradient needed for calculation of absolute densities (Healey et al., 1984). Because borehole gravity measurements were only made in the higher part of USW G-3, they are not useful for calculation of  $S_y$  at the depths of the hydraulic fracturing tests; however, we reproduce them in Table 2 for comparison.

#### HYDRAULIC FRACTURING STRESS MEASUREMENTS - EQUIPMENT AND TEST CHRONOLOGY

Measurements in USW G-3 and Ue-25p1 were conducted in three separate field operations: February-March 1983 (volcanic section of Ue-25p1), November and December 1983 (USW G-3), and January 1984 (Paleozoic section of Ue-25p1).

The first set of tests, in the upper part of Ue-25p1, used a Lynes single-set straddle packer system. In this system, the packers are inflated through one-way valves connected to the fluid in the tubing string, with the test interval between the packers sealed to excess pressure during packer inflation. These one-way valves keep the packers inflated even when a second valve between the tubing string and the test interval is opened to begin the hydrofrac test. During this phase of testing in Ue-25p1, four tests were conducted. The packers inflated and set successfully; however, the pressure required to fracture the formation was in all cases much higher than anticipated. In two of these tests these high pressures caused the tubing connection between the two packers to fail in tension before breakdown of the formation occurred. In the third test, the high pressure blew a shear plug in the lower packer mandrel before breakdown occurred.

The fourth test of this series is the only one that created a successful hydraulic fracture. During the first cycle, the tubing connecting the two packers parted; however, both packers remained set, and a 5-cycle test, showing good breakdown and classic steady pumping pressure, was then conducted. This test is interpreted to have induced a horizontal fracture, because the recorded shut-in pressure was almost identical to the expected vertical stress. This does not mean that the vertical stress is the least principal stress, however; creation of horizontal fractures is favored if the packers are not held together by the tubing connection (which normally acts to reduce the vertical shear across the interval). This test is, therefore, not discussed further in this report. The three failed tests provided information on lower limits for  $S_h$  (discussed below).

The many test failures in the volcanics in Ue-25p1 were primarily due to the unexpectedly high test pressures needed and the relatively large borehole size which reduced the strength of the packers. Thus, after consultation with personnel in the drilling program at the Nevada Test Site, we decided to develop a new packer system for future work, and a contract was negotiated with TAM International to design and build a new packer system. The new high-pressure resettable packer design has two advantages over the Lynes packers. First, the circulation valve that opened the tubing to the test interval and the valves to the packer elements could be reset individually downhole, making it unnecessary to pull the packers after each test and thus saving several hours per test. Second, the connections between the packers, and the packer elements, were built to withstand much higher pressures, making it possible to test in higher stress regimes. A third mechanical valve ("dump valve") at the top of the packer assembly was used to equalize the pressures between the tubing and the annulus prior to deflating the packers. The resettable valves were operated by vertical movement and rotation of the drill steel. In a vertical hole, the operator could feel the operation of the valves while turning the pipe with a pipe wrench, but in more deviated holes this required practice and considerable skill. Initially, the setting mechanism of these packers proved difficult to lock into the inflate position in impermeable rock, due to a hydraulic lock condition. This design problem with the prototype model caused most of the tests in USW G-3 and the Paleozoic units of Ue-25p1 to fail. The packer has since been modified by TAM to avoid this problem.

During the second field operation, 13 tests were attempted in USW G-3 at depths between 1,060 m and 1,356 m. Of these, only three were successful (1,074 m, 1,338 m, and 1,356 m; figure 12). Eight tests failed because the packers would not remain inflated. In the remaining two tests, the packers set properly the first time, and good breakdowns were observed, indicating that a hydraulic fracture was initiated. However, attempts to use the dump valve to return the pressure in the frac interval to its pre-test value before the second pumping cycle caused the packers to deflate, so the tests could not be completed.

In USW G-3, which had a water level of 752 m subsurface, bleeding off excess pressure at the surface would only return the borehole pressure to hydrostatic pressure, 74 bars above the equilibrium pore pressure. The borehole pressure could be returned to its equilibrium value at the end of

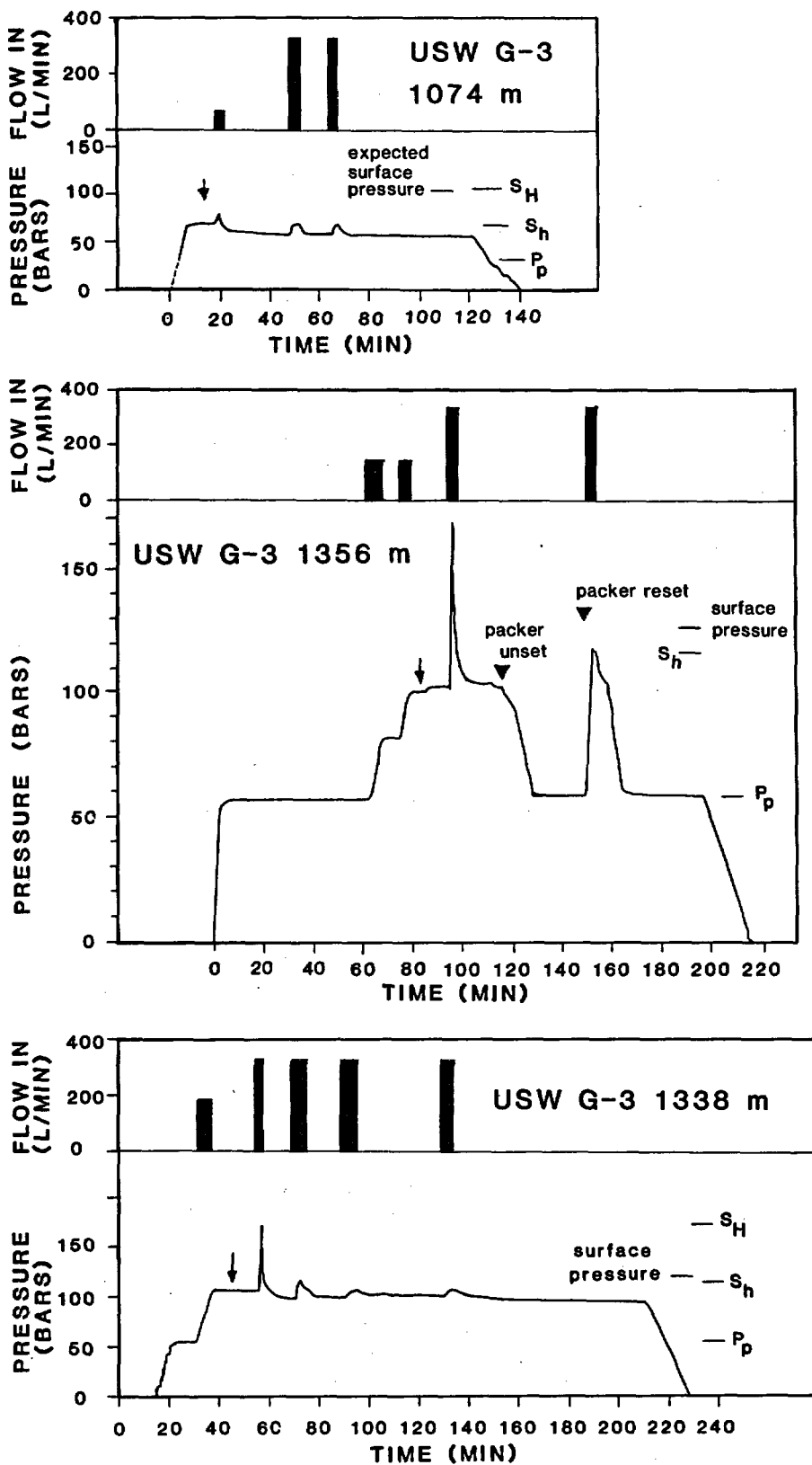


Figure 12. Pressure-time records of three successful hydraulic fracturing stress measurements in USW G-3. Lower curve in each frame is a copy of the record of the downhole mechanical pressure gauge. Arrows indicate the time when the circulation valve was opened and the hydraulic fracturing test began. The upper field for each test indicates the approximate rate of fluid flow at the surface, calculated by counting stroke rate of the drill rig mud pump used for testing.

each cycle, either by opening the dump valve or by swabbing the pipe. Swabbing was attempted several times without success. In two of the successful tests in USW G-3, the dump valve was not used, so fluid pressure was bled back to surface hydrostatic pressure and then allowed to decay slowly by permeation between cycles. In the third test, the dump valve worked properly, and the pressure returned to pore pressure in the hole between cycles.

Previous testing in USW G-1 and USW G-2 indicated that pressures close to surface hydrostatic pressure (i.e., the hydrostatic pressure of a column of water from the surface to the depth of interest) would often cause fracturing of the borehole wall due to the low magnitudes of the horizontal stresses (Healy et al., 1984; Stock et al., 1984, 1985). The presence of drilling-induced hydraulic fractures in USW G-3 suggested that the horizontal stresses were likely to be low there as well, so packer inflation pressures for the tests in USW G-3 were set to be lower than surface hydrostatic pressure.

In the third field operation, ten tests were attempted in the Paleozoic units of Ue-25p1. Because of the previous problems with manipulation of the dump valve, and difficulties with the pressure seals, the dump valve was omitted from the packer assembly for these tests. The same difficulty with the packer setting mechanism, however, caused five of these tests to fail. In two other tests the packers set properly, but the test intervals leaked. In the three remaining tests, discussed below, the packers set properly and borehole pressure was bled back to surface pressure between cycles (figure 13). No swabbing was attempted. We used packer inflation pressures higher than surface pressure in all the tests in Ue-25p1 because our earlier tests in the upper part of this hole suggested that the horizontal stresses and breakdown pressures were generally higher than observed in USW G-1 and USW G-2.

The tests in the volcanics in Ue-25p1 were done with a Racine C-11 pump with a pumping capacity of 0 to 50 L/min. This pump has pressure and volume characteristics best suited to most of our hydraulic fracturing operations. For the tests in USW G-3, the drill rig mud pump was used for all the tests because flow rates higher than 50 L/min were desired. Flow rates were calculated by counting piston strokes; the uncertainty in these flow rates is estimated to be within about 10%. Total volume pumped was recorded on a digital flow meter and reset after each cycle.

Tests in the Paleozoic section of Ue-25p1 were begun using the Racine C-11 hydrofrac truck pump. This pump failed, and two air-driven pumps that were tried next also failed, so a Halliburton service truck was brought in to finish the testing. High flow rates were used for the remainder of these tests, and the actual flow rate at any time must be estimated from the pump speed under no load. The flow rates indicated for the fracs in Figures 12 and 13 are based on counting piston strokes and may have varied slightly from the values indicated, especially as pumping pressure increased.

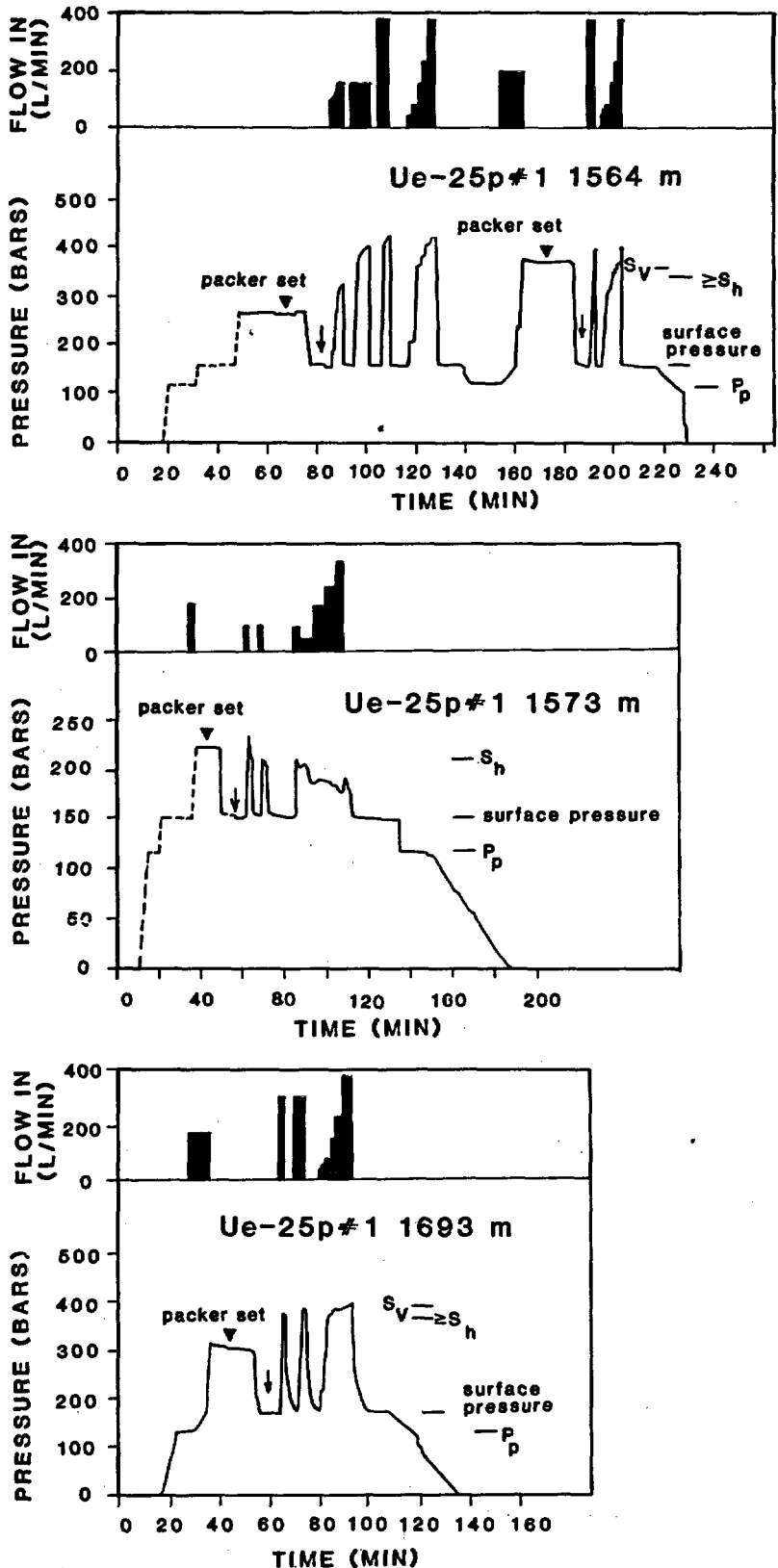


Figure 13. Pressure-time records of three successful hydraulic fracturing stress measurements in Ue-25p1. Symbols and sources of data are the same as in Figure 11.

## HYDRAULIC FRACTURING STRESS MEASUREMENTS - RESULTS

### Stress Measurements in USW G-3

The three tests in USW G-3 (figures 11 and 13, and Table 3) showed very consistent values of the least horizontal principal stress  $S_h$ . For the test, at 1,074 m, in the Tram member of the Crater Flat Tuff,  $S_h$  was determined from the behavior of the fracture during all three cycles. Cycle 1 showed a good (although surprisingly low) breakdown pressure, and cycles 2 and 3 showed repeatable fracture reopening and pumping pressures. The similarity of the pressure records from these two cycles shows that the fracture stabilized sufficiently, so this is a good value of  $S_h$ .

During the test at 1,356 m, in the Lithic Ridge Tuff, the packers deflated so only two pressurization cycles were obtained. Cycle 1 shows a sharp breakdown pressure, and cycle 2 a clear fracture reopening pressure. The value of  $S_h$  is taken from cycle 2, but if more cycles had been conducted, this value might have decreased slightly as fracture behavior stabilized. Thus, although 115 bars is probably close to the  $S_h$  value for this depth, it may be a few bars too high.

In the test at 1,338 m in the Lithic Ridge Tuff, the first cycle shows a good breakdown, and the second cycle has a clear fracture reopening pressure. However, halfway through cycle 2 the pressure dropped dramatically, and the fracture pressurization during reopening on cycles 3 and 4 is much slower than on cycle 2, even though the same high pumping rates were used, possibly indicating that the fracture broke around the packers during cycle 2, so that cycles 3 and 4 are pumping tests communicating with the open hole. The  $S_h$  value of 114 bars from this test is thus based on cycles 1 and 2. As discussed above, the fracture behavior may not have completely stabilized by this time, so this value of  $S_h$  may be slightly high.

Values of the greatest horizontal stress,  $S_h$ , were computed using equation (2) and the fracture reopening pressures on the second cycle (Table 3). These values are believed to be reasonable in spite of the borehole deviation (see discussion of equation 1). For the tests at 1,074 m and 1,338 m, even though the excess pressure was not completely bled back between cycles, the short time elapsed between cycles and the very thick mud cake on the bore-hole wall probably prevented significant increase in  $P_p$  of the surrounding rock between cycles 1 and 2. Thus, equilibrium values of  $P_p$  are used in the computations. For all three tests, the  $S_h$  values are considerably less than  $S_y$ , corresponding to a normal faulting stress regime with  $\phi = 0.5$ , where  $\phi = (S_2 - S_3)/(S_1 - S_3)$  (Angelier, 1979), with  $S_1 = S_y$  and  $S_3 = S_h$  for a normal faulting stress regime.

### Stress Measurements in Ue-25p1

The test at 1,564 m in the Lone Mountain Dolomite consisted of two cycles run at a flow rate of 150 L/min, one cycle at a flow rate of 400 L/min, and one cycle with rates from 40 to 400 L/min to measure the normal stress on the fracture (figure 13). Pressurization rates were similar on the first three

cycles, and no breakdown pressure was seen, suggesting that a preexisting fracture was probably being tested. Because the test pressures approached values equal to twice the packer inflation pressure, the packers were unset and inflated again at a higher pressure. Two more cycles were conducted showing very similar behavior to the previous cycles. Plots of pumping pressure as a function of flow rate indicate that the normal stress on the fracture is  $337 \pm 11$  bars (figure 14). Because this test may have opened a preexisting fracture of unknown orientation, the normal stress on the fracture is only used as an upper bound on  $S_h$  (figure 13). This stress is close to the vertical stress  $S_v$ . Although no fractures were identified on the televiewer log of this interval prior to hydrofrac testing, bedding parallel fractures, which are nearly horizontal, are present elsewhere in the televiewer log of the Lone Mountain Dolomite.

The second test in the Lone Mountain Dolomite, at 1,573 m depth, had a breakdown of 236 bars on the first cycle, and a fracture reopening pressure of about  $195 \pm 5$  bars on the second and third cycles. Several different pumping rates were used on the third cycle in an attempt to obtain steady pumping pressures and further constrain  $S_h$ . The lower pressure observed at very high flow rates at the end of the third cycle suggest that the fracture broke around the packers and was then connected to the open hole. The  $S_h$  value of 207 bars from this test is thus based only on observation of the shut-in curves from cycles 1 and 2 and the beginning of cycle 3.

The third test, at 1,693 m in the Roberts Mountain Formation, was similar to the test at 1,564 m in that no distinct breakdown was observed. The first and second cycles look very similar except that all pressures are slightly higher during cycle 2. This may be due to a slight increase in flow rate during cycle 2. The value of 365 bars given for the normal stress on the fracture is based on the steady pumping pressures and flow rates recorded during cycle 3 (figure 14). Because this test may have reopened a preexisting fracture, this value is used as an upper bound for  $S_3$ . (We assume, based on the other tests in Ue-25p1 and USW G-3, that  $S_h = S_3$ .) The normal stress on the tested fracture is close to  $S_v$ . Again, no fractures were observed in the televiewer log of this interval, taken prior to testing.

Because of the unusual character of the tests at 1,564 m and 1,693 m, we are not confident in estimating  $S_h$ .  $S_h$  for the test at 1,573 m was computed using equation (2) and the fracture reopening pressure on cycle 2 (figure 13). This value of  $S_h$  may be a few bars too high because  $P_p$  may have increased slightly between cycles 1 and 2, due to the previously-noted effect of excess pressure remaining in the borehole between cycles. No mud coated the borehole wall in Ue-25p1 to retard permeation of excess pressure into the formation; however, since only a short time elapsed between cycles 1 and 3, there would be only a slight effect on the magnitude of  $P_p$ . We prefer to use equation (2) with its associated uncertainty rather than equation (1), because we have no tensile strength information on the Lone Mountain Dolomite. This results in a value of  $310 \pm 11$  bars for the test at 1,573 m depth, lower than the predicted  $S_v$  value of 356 bars. These stresses are close to the transition between normal and strike-slip stress regimes, with  $S_h < S_h \leq S_v$ .

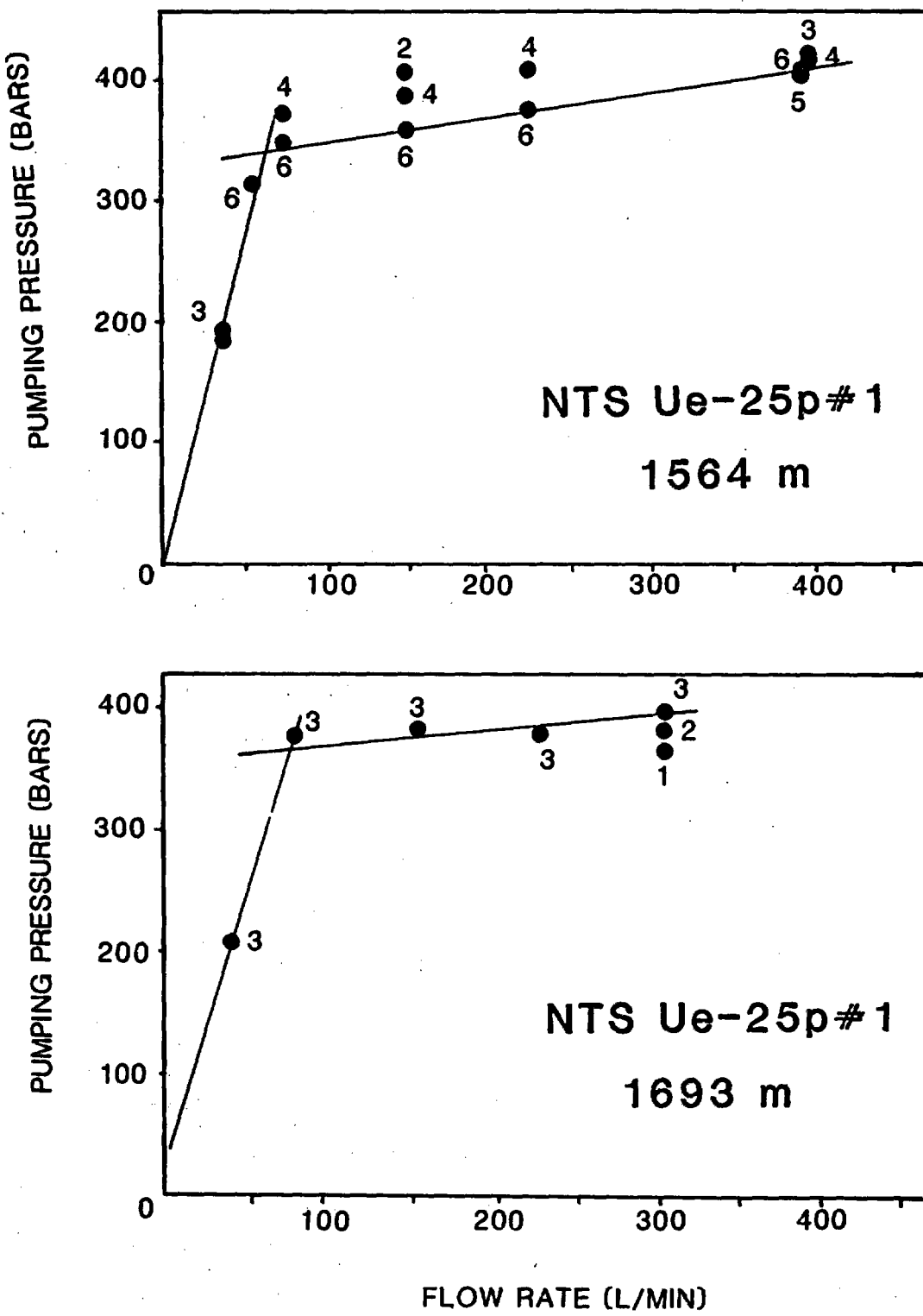


Figure 14. Steady pumping pressure as a function of flow rate for two tests in Ue-25p1. Numbers next to the points indicate the pumping cycle during which the data were obtained. The change in slope of the line indicates the change in apparent permeability of the interval as the fracture closes. The normal stress on the fracture is determined by extrapolation of the open-fracture gradient back to zero flow rate.

The three tests in the volcanics in the upper part of Ue-25p1, in which the packer system failed prior to breakdown of the formation, can be used to place lower bounds on the magnitude of  $S_h$  (Table 4). From equation (1) and the inequalities  $P_{failure} < P_b$  and  $S_h \leq S_H$ , the following relation can be derived:

$$S_h < \frac{P_{failure} - T + P_p}{2} \quad (3)$$

Since no laboratory values of  $T$  are available, an average value for  $T$  of  $54 \pm 10$  bars has been used in equation (3). This number is based on all available values of  $T$  derived from hydraulic fracturing tests in the volcanics at Yucca Mountain (Table 5), using the equation

$$T_{hydrofrac} = P_b - P_b(T=0)$$

after Bredehoeft et al. (1976).

The calculated lower bounds on  $S_h$  (Table 4) unfortunately do not provide significant new constraints on the  $S_h$  magnitude at these depths. These lower bounds are very low, falling close to the frictional stability lines of  $\mu = 0.6$  and  $\mu = 1.0$ .  $S_h$  values at these depths, if close to these lower bounds, would be close to the frictional stability line, consistent with the good  $S_h$  value obtained at 1,573 m in the hole. In this case, the stress state in the upper part of Ue-25p1 may not have been very different from that encountered in the equivalent units in the three USW G holes. The higher breakdown pressures in Ue-25p1 could have resulted from a slightly higher value of  $S_h$  and slightly lower value of  $S_H$ , which would considerably increase the required breakdown pressure and at the same time make the stress state slightly more stable. Alternatively,  $S_h$  values could be much higher than the lower bounds; the uncertainties do not allow this to be resolved.

#### Impressions of Fractured Intervals

Normally, at the end of hydraulic fracturing stress measurements, oriented impression packers are used to determine the orientation of the hydraulic fractures and hence the  $S_h$  direction. Due to time constraints, impressions were taken in only two intervals in USW G-3: at 1,059 and 1,338 m. Both of these impressions showed high angle fractures with apparent dips (in the borehole reference frame) of  $86^\circ$  and  $84^\circ$ , respectively. The observed orientations of these fractures, when corrected for deviation of the borehole, yield fracture dips of  $73^\circ$  toward  $S74^\circ W$  (at 1,059 m) and  $69^\circ$  toward  $N60^\circ W$  (at 1,338 m). This implies  $S_h$  directions of  $S75^\circ W \pm 10^\circ$  and  $N60^\circ W \pm 10^\circ$ , respectively. The latter direction is reasonably consistent with the orientations derived from breakouts and drilling-induced hydrofractures discussed above. The  $S75^\circ W$  direction is anomalous, especially in view of the fact that it is the shallower of the two. The  $20^\circ$  dip of both of these fractures toward the west is opposite to the direction of rotation that might be predicted from topographic rotation of the principal stress directions. There is some loss of accuracy in the instrument orientations due to the borehole deviations of  $14^\circ$  and  $19^\circ$  in these intervals, which exceed the  $10^\circ$  range of the Kuster single shot PeeWee magnetic survey instrument used. The

excess borehole deviation requires interpolation of the instrument's readings beyond scale, and some interference between the compass and its housing may have occurred.

Only one impression was taken at site Ue-25p1 due to time limitations. The impression was damaged by material which fell in on the packer and scrubbed over the impression material as the tool was brought out of the hole, so that no usable impression was obtained.

## DISCUSSION

### General Features of the Yucca Mountain Stress Field

The results from USW G-3 agree with previous measurements from USW G-1 and USW G-2, in which the magnitudes of both the least horizontal stress  $S_h$  and the greatest horizontal stress  $S_H$  are less than the vertical stress  $S_v$ , corresponding to a normal faulting stress regime ( $S_h < S_H < S_v$ ) (figure 15). One good test from Paleozoic rocks in Ue-25p1 is also in agreement with this general pattern. Two other tests above and below this good test constrain  $S_h$  to be less than  $S_v$ . The  $S_h$  direction of  $N65^\circ W \pm 10^\circ$  (obtained from the orientation of drilling-induced hydraulic fractures in USW G-3) and  $N60^\circ W$  (from the borehole breakouts in Ue-25p1) agrees very closely with the  $S_h$  orientation of  $N65^\circ W \pm 10^\circ$  obtained from similar features in USW G-1 (Healy et al., 1984) and USW G-2 (Stock et al., 1984). Thus, WNW-directed extensional stress is consistently observed in the drill holes we have tested at Yucca Mountain.

Within this general pattern, there are apparent, individual differences among the drill holes. In the three USW G holes,  $S_H$  was approximately halfway between  $S_h$  and  $S_v$  in magnitude ( $\phi = 0.5$ ).  $S_h$  was very low relative to  $S_v$ , so that if the borehole pressure was raised by filling the hole to the surface with fluid, the borehole pressure would exceed  $S_h$  and hydraulic fractures would be likely to extend and propagate (figure 16). In the Paleozoic section of Ue-25p1, however,  $S_H$  was almost as high as  $S_v$  ( $\phi = 1.0$ ), so that the stress regime was close to the transition between normal and strike slip ( $S_h < S_H < S_v$ ). Because  $S_h$  is higher relative to  $S_v$  in Ue-25p1 than it is in the three USW G holes, filling the borehole to the surface with fluid would not cause the borehole pressure to exceed  $S_h$ . Therefore it is not surprising that drilling-induced hydrofractures are not seen in the Paleozoic section of Ue-25p1.

Lower bounds on the least horizontal principal stress can be calculated from tests in the volcanics in Ue-25p1 where the packers failed before breakdown. These lower bounds show that the stress regime there may have been one of normal faulting, similar to the stress state in the three USW G holes, with slightly more stable stresses. The lack of drilling-induced hydraulic fractures and breakouts in the volcanic units of Ue-25p1 also suggest that the horizontal stresses are closer in magnitude there, and with  $S_h$  closer to  $S_v$ . It is possible, although unlikely, that these differences between the volcanic units in Ue-25p1 and in the USW G holes may be enhanced by the different drilling techniques used. The three USW G holes were drilled with

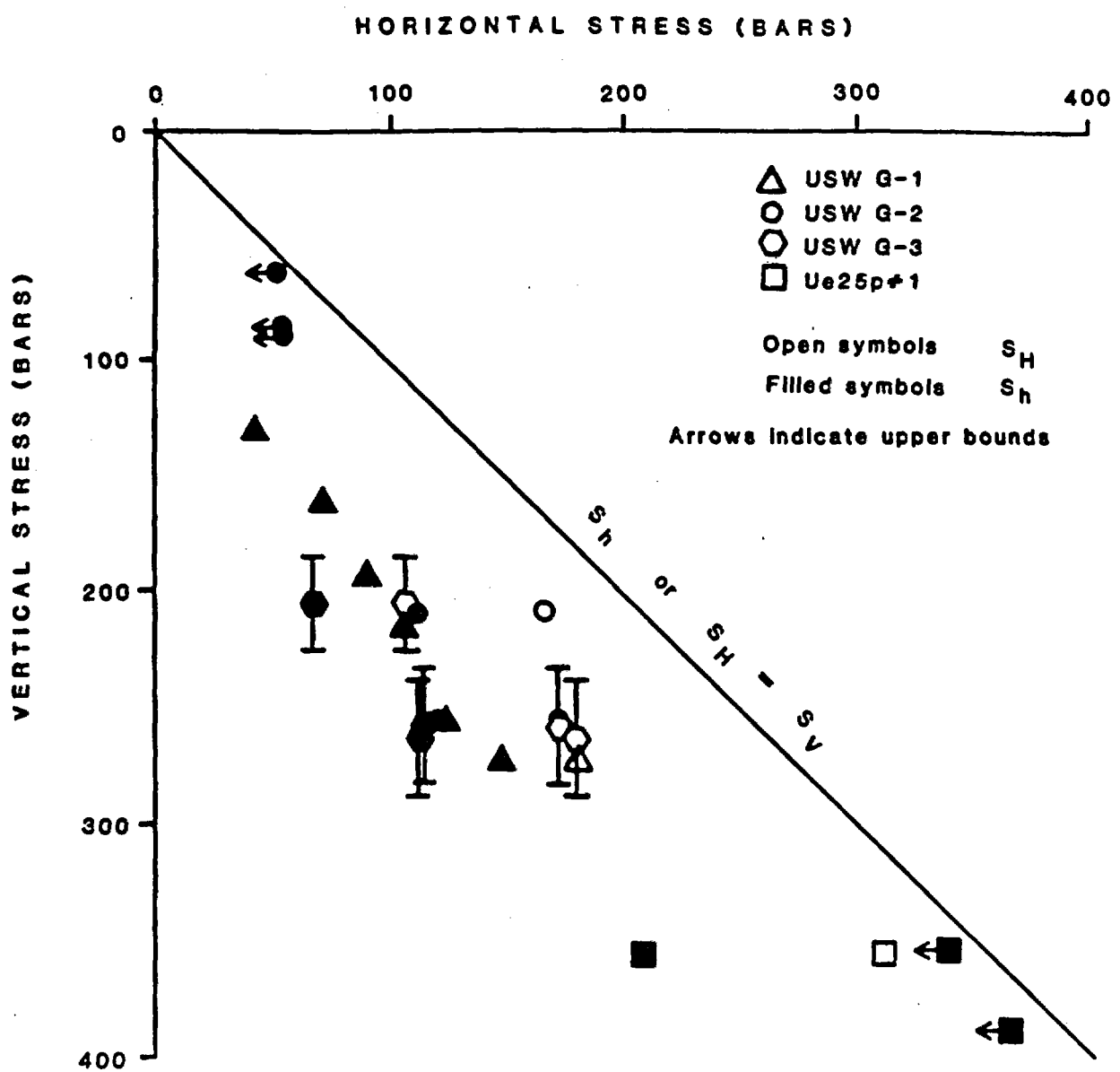


Figure 15. Horizontal stresses plotted as a function of vertical stress,  $S_v$ , for USW G-1, USW G-2, USW G-3, and Ue-25p1. Open symbols are  $S_h$  values, and filled symbols are  $S_h$  values. Dashed lines show the critical values of  $S_h$  for which slip might take place on preexisting faults of optimal orientation for values of the coefficient of friction between 0.6 and 1.0. Bars on USW G-3 values are uncertainty limits on  $S_v$  values.

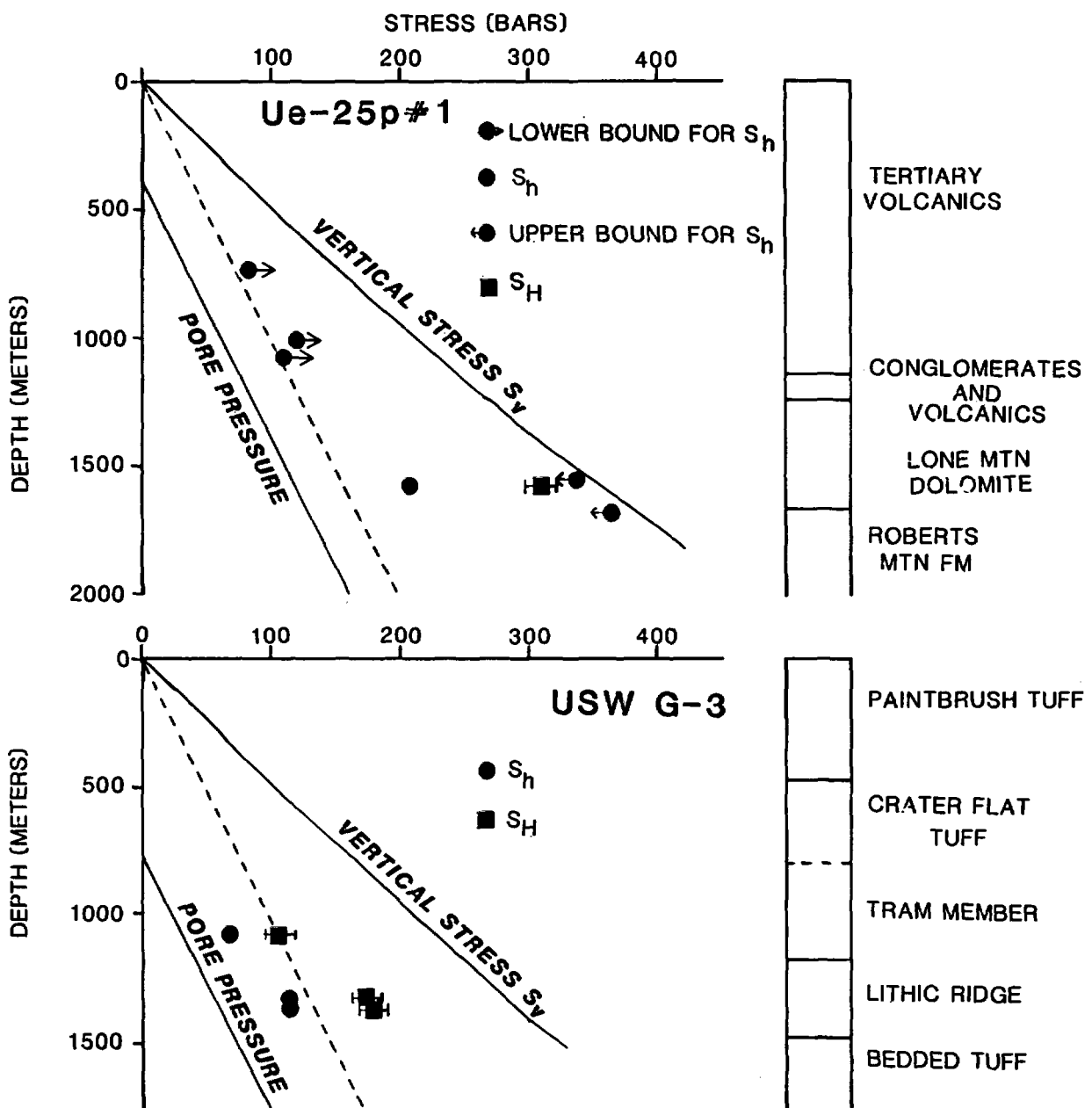


Figure 16. Results of stress measurements in USW G-3 and Ue-25p1 showing values of the least horizontal stress  $S_h$ , the greatest horizontal stress  $S_H$ , and the vertical stress  $S_v$ . Bars indicate the uncertainty in the  $S_H$  values. Two tests in Ue-25p1 have arrows to indicate that the values are upper limits on  $S_h$  (see discussion in text). Dashed line indicates the pore pressure that would result if the boreholes were filled to the surface with fluid during drilling.

mud and continuously cored, whereas the volcanics in Ue-25p1 were drilled mainly with air soap and not cored continuously. However, the much higher breakdown pressures required to fracture the volcanics in Ue-25p1 are a clear indication that the stress state must be slightly different there.

### Fault Stability

In a given normal faulting stress field, the preexisting fault most likely to slip ("favorably oriented preexisting fault") is one striking along the  $S_h$  direction, and having a dip  $\epsilon$ , where  $2\epsilon = (\tan^{-1}\mu + 90^\circ)$ , and  $\mu$  is the coefficient of friction of the fault plane. For such a fault, the slip condition can be written in the form

$$(S_v - P_p)/(S_h - P_p) = [(\mu^2 + 1)^{1/2} + \mu]^2 \quad (4)$$

(e.g., Zoback et al., 1978; McGarr et al., 1982). If the ratio of  $(S_v - P_p)/(S_h - P_p)$  is less than this function of  $\mu$ , the fault will be stable and no frictional sliding should occur; however, if the stress ratio exceeds this value, the fault can be expected to slip.

Because favorably oriented preexisting faults (strike N25°E, dip 60-67°) exist at Yucca Mountain (figure 1 and Scott and Bonk, 1984), we use equation (4) to obtain critical values of  $S_h$  as a function of  $S_v$  and  $\mu$ . The lines plotted in Figure 17 show that for USW G-3, the measured  $S_h$  values are close to those at which slip might be expected to occur on favorably oriented preexisting faults for reasonable values of  $\mu$ . The  $S_h$  value measured in Ue-25p1 is not quite as close to the critical value at which slip would be expected to occur. This is consistent with evidence from the occurrence of breakouts and drilling-induced hydraulic fractures that it may be experiencing somewhat higher horizontal stresses which result in a more stable stress regime. Bounds on  $S_h$  from tests in the volcanics in the upper part of Ue-25p1 also suggest that favorably oriented preexisting faults may be less likely to slip at this part of Yucca Mountain. However, since no successful measurements were obtained in this part of Ue-25p1, it would be advisable to make measurements in other holes nearby rather than rely on extrapolation of these results from the lower portion of the hole.

An alternative model that frequently has been used to predict stress distribution with depth is one of gravitational loading. If a laterally confined, homogeneous rock mass is subject to a vertical gravitational force, then  $S_v$  will be equal to the weight of the overlying rock. Plane strain analysis predicts that the horizontal stresses will be equal, with a magnitude of  $[\nu/(1-\nu)]S_v$ , where  $\nu$  is Poisson's ratio (e.g., Jaeger and Cook, 1979). Such a model is in reasonable agreement with the  $S_h$  values obtained from the USW G holes (Swolfs and Savage, 1985). However, this model does not successfully explain the  $S_h$  result from Ue-25p1, nor the high values of  $S_h$  with respect to  $S_h$  that are observed throughout the area, from both our stress measurements and other regional stress indicators. We feel that there are difficulties in applying this model to the NTS area for the following reasons.

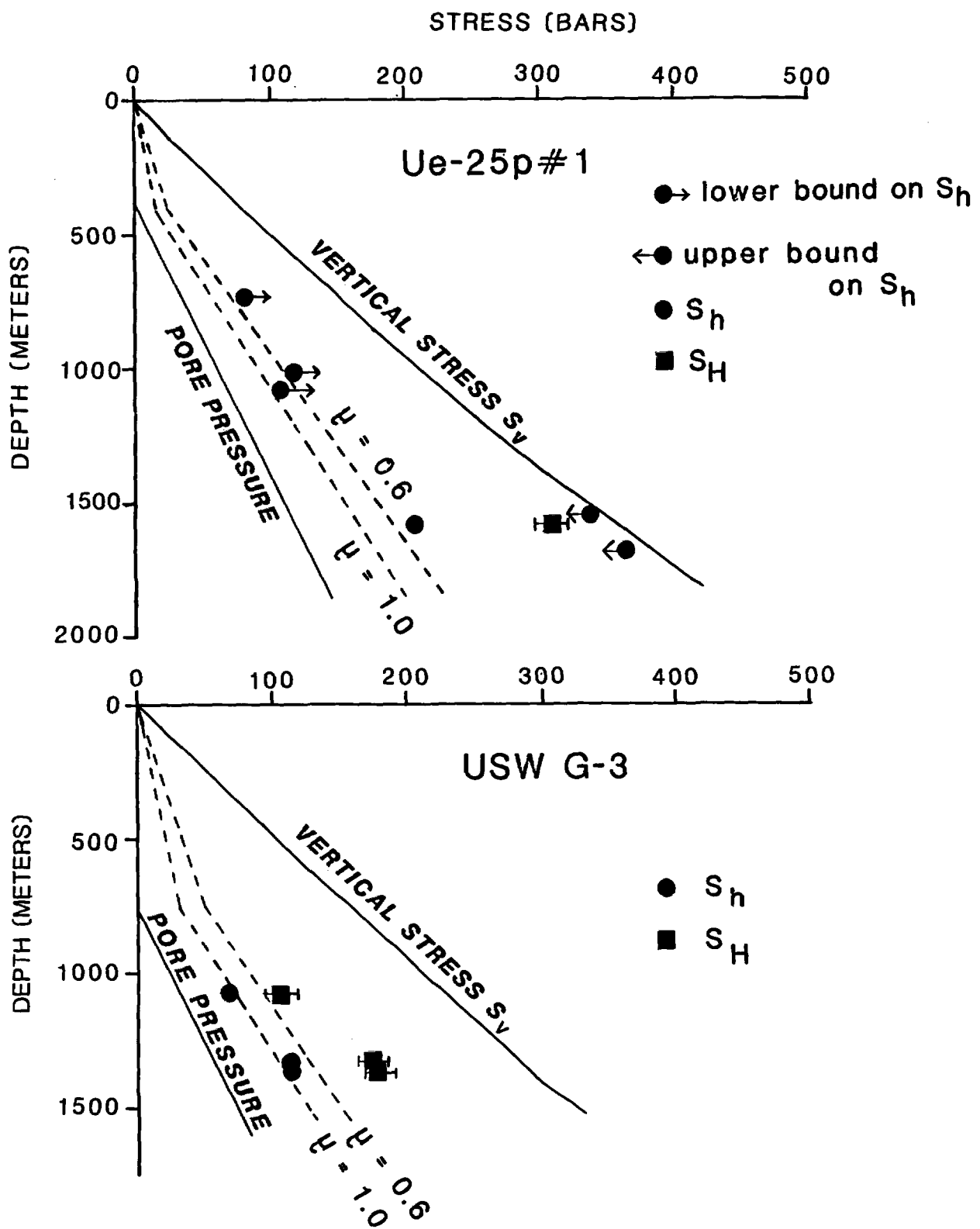


Figure 17. Stress values plotted against depth in USW G-3 and Ue-25p1 showing values of the least horizontal principal stress  $S_h$  and the greatest horizontal principal stress  $S_H$ . Dashed lines indicate the critical values of  $S_h$  for which slip might take place on preexisting faults of optimal orientation for values of the coefficient of friction between 0.6 and 1.0. Lithostatic curve  $S_V$  in USW G-3 is not corrected for topographic effects.

(1) Such a model predicts that the two principal horizontal stresses will be equal in magnitude (i.e.,  $\phi=0$ ). This implies considerable scatter in the  $S_h$  and  $S_H$  directions. Such scatter has been observed in other tectonic areas, but not in the NTS area. Swolfs and Savage (1985) suggest that strong fracture anisotropy may control topography and contribute to higher  $S_H$  values. However, consistent  $S_h$  directions are obtained from regional stress data from a variety of depths in the region, including areas lacking the topographic grain and strong fracture anisotropy present at shallow depths at Yucca Mountain.

(2) The assumption of lateral confinement as a far field boundary condition may not be realistic for the Yucca Mountain area, as the region is seismically active and undergoing measurable geodetic strain.

(3) A gravitational-loading model in a region with a surface water table is consistent with fault stability at all depths. However, in a region of very low water table, it predicts slip on preexisting faults at depth, where the  $[v/(1-v)]S_y = S_h$  line crosses the Byerlee's law stability line given by equation (4). The instability of these faults would increase with depth. Microseismicity suggests that Yucca Mountain is relatively stable, so stresses due to pure gravitational loading at depth seem unlikely.

#### Extrapolation of Results to Shallower Levels

All of the successful hydraulic fracturing stress measurements obtained at Yucca Mountain were at depths below that of the repository block. These results are of use in evaluating the regional stress field, but may not be directly extrapolated to shallower levels, because of the increased importance of local topographic variation near the surface. It seems vital to perform shallower stress measurements (both hydraulic fracturing and overcoring), as well as examine all available borehole data that may be pertinent to the stress field. In particular, televiewer logs, downhole television, geophysical logs, and cores may reveal useful information on fracture density, fracture orientation, and the presence and orientation of drilling-induced hydraulic fractures and breakouts at shallower levels of Yucca Mountain.

Swolfs and Savage (1985) present an analytic solution for the near-surface stress distribution at Yucca Mountain by approximating the topography as a symmetric ridge. The ridge shape results in high lateral stresses and consequent increased fault stability within the first few hundred meters of the surface, which do not strongly depend on the boundary conditions of the model at depth. Our stress measurements are too deep to provide a check on these predicted high near-surface stresses. This model merits further investigation by shallower stress measurements, as it would have important implications on the stress field at repository depths.

#### Relationship to the Regional Stress Field

The stress regime at Yucca Mountain fits the pattern observed elsewhere in regions of active faulting, where the magnitudes of the principal stresses appear to be controlled by the frictional strength of preexisting faults, as

described by equation (4) above (Brace and Kohlstedt, 1980; Zoback and Healy, 1984). Although recent active faulting has not been documented at Yucca Mountain itself, it is present in the surrounding area. Recent earthquake focal mechanisms from the NTS area are generally strike-slip with minor components of normal motion (Rogers et al., 1983). The observed focal mechanisms would not be inconsistent with slip on N- to E-striking preexisting faults, due to a stress regime similar to that observed at Yucca Mountain ( $S_h < S_H < S_v$ , with  $S_h$  oriented N65°W and  $\phi = 0.5$  to 0.7). However, these focal mechanisms can also be fit by a stress field with similar horizontal stress orientations but with  $S_H > S_v$ . Thus, it is possible that the  $S_H$  values from Yucca Mountain are slightly lower than those expected elsewhere in southern Nevada.

#### SUMMARY

Hydraulic fracturing stress measurements in drill holes USW G-3 and Ue-25p1 at Yucca Mountain demonstrate that the stress regime is generally one of normal faulting, with  $S_h < S_H < S_v$ . The least principal stress ( $S_h$ ) direction is N60°W - N70°W, as determined from the orientation of drilling-induced hydraulic fractures visible in the USW G-3 televiewer log, and from borehole breakouts visible in the Ue-25p1 televiewer log. In USW G-3,  $S_h$  values are much lower than  $S_v$  values, and are close to values for which frictional sliding might occur on favorably oriented preexisting faults, for values of the coefficient of friction between 0.6 and 1.0.  $S_H$  in USW G-3 is roughly intermediate in magnitude between  $S_h$  and  $S_v$ . In Ue-25p1, one good test indicates that  $S_h$  is less than  $S_v$ , and  $S_H$  is closer in magnitude to  $S_v$ , so that the stresses are near the transition between normal and strike-slip stress regimes. Two other tests constrain  $S_h$  to be less than or equal to  $S_v$ . This difference in stress regimes between the two holes may explain the observed variation in occurrence of stress-related features such as borehole breakouts (seen only in the lower part of Ue-25p1) and drilling-induced hydraulic fractures (seen in much of USW G-3).

Stress results from USW G-3 are very similar to results from previous work in holes USW G-1 and USW G-2 at Yucca Mountain. Considered together, the stress measurements from the four Yucca Mountain holes present a consistent picture of WNW-directed extension, with stresses that generally form a normal faulting stress regime but in some areas, such as near Ue-25p1, may approach the transition between normal and strike-slip regimes. These stresses are not inconsistent with observed focal mechanisms from the Nevada Test Site area, suggesting that they could be regionally representative.

## REFERENCES

- Angelier, J., 1979, Determination of the mean principal directions of stresses for a given fault population: *Tectonophysics*, v. 56, p. T17-T26.
- Bell, J. S. and D. I. Gough, 1983, The use of borehole breakouts in the study of crustal stress, in *Hydraulic Fracturing Stress Measurements*, National Academy Press, Washington, D.C., M. D. Zoback and B. C. Haimson, eds., p. 201-209.
- Brace, W. F. and D. L. Kohlstedt, 1980, Limits on lithospheric stress imposed by laboratory experiments, *Journal of Geophysical Research*, v. 85, p. 6248-6252.
- Bredehoeft, J. D., R. G. Wolff, W. S. Keys, and E. Shuter, 1976, Hydraulic fracturing to determine the regional in-situ stress field, Piceance Basin, Colorado: *Geological Society of America Bulletin*, v. 87, p. 250-258.
- Carr, M. D. et al., 1986, Geology of drill hole UE-25p1: A pre-Tertiary test hole at Yucca Mountain, southern Nye County, Nevada: U.S. Geological Survey Open-File Report, in preparation.
- Earlougher, R. C., Jr., 1977, Advances in well test analysis: AIME Monograph 5, American Institute of Mining, Metallurgical, and Petroleum Engineers, Dallas, Texas.
- Gough, D. I. and J. S. Bell, 1982, Stress orientation from borehole wall fractures with examples from Colorado, East Texas, and northern Canada: *Canadian Journal of Earth Sciences*, v. 19, p. 1358-1370.
- Haimson, B. C. and C. Fairhurst, 1967, Initiation and extension of hydraulic fractures in rock: *Society of Petroleum Engineers Journal*, v. 7, p. 310-318.
- Healey, D. L., F. G. Clutsom, and D. A. Glover, 1984, Borehole gravity meter surveys in drill holes USW G-3, Ue-25p1 and Ue-25c1, Yucca Mountain area, Nevada: U.S. Geological Survey Open-File Report 84-672.
- Healy, J. H., S. H. Hickman, M. D. Zoback, and W. L. Ellis, 1984, Report on televiewer log and stress measurements in core hole USW-G1, Nevada Test Site: U.S. Geological Survey Open-File Report 84-15.
- Hickman, S. H., J. H. Healy, and M. D. Zoback, 1985, In situ stress, natural fracture distribution, and borehole elongation in the Auburn geothermal well, Auburn, New York: *Journal of Geophysical Research*, v. 90, p. 5497-5512.
- Hickman, S. H. and M. D. Zoback, 1983, The interpretation of hydraulic fracturing pressure-time data for in-situ stress determination, in *Hydraulic Fracturing Stress Measurements*, National Academy Press, Washington, D.C., M. D. Zoback and B. C. Haimson, eds., p. 44-54.

- Hoffman, L. R. and W. D. Mooney, 1983, A seismic study of Yucca Mountain and vicinity, southern Nevada: Data report and preliminary results: U. S. Geological Survey Open-File Report 83-588.
- Hubbert, M. K. and D. G. Willis, 1957, Mechanics of hydraulic fracturing: Journal of Petroleum Technology, v. 9, p. 153-168.
- Jaeger, J. C. and N. G. W. Cook, 1979, Fundamentals of Rock Mechanics: New York, Chapman Hall.
- Mastin, L. G., 1984, The development of borehole breakouts in sandstone: Masters Thesis, Stanford University, Stanford, CA.
- McGarr, A., M. D. Zoback, and T. C. Hanks, 1982, Implications of an elastic analysis of in situ stress measurements near the San Andreas fault: Journal of Geophysical Research, v. 87, p. 7797-7806.
- Ratigan, J. L., 1983, A statistical fracture mechanics determination of the apparent tensile strength in hydraulic fracture, in Hydraulic Fracturing Stress Measurements, National Academy Press, Washington, D.C., M. D. Zoback and B. C. Haimson, eds., p. 159-166.
- Richardson, R. M., 1983, Hydraulic fracture in arbitrarily oriented boreholes: an analytic approach, in Hydraulic Fracturing Stress Measurements, National Academy Press, Washington, D.C., M. D. Zoback and B. C. Haimson, eds., p. 167-175.
- Rogers, A. M., S. C. Harmsen, W. J. Carr, and W. Spence, 1983, Southern Great Basin seismological data report for 1981 and preliminary data analysis: U. S. Geological Survey Open-File Report 83-669.
- Scott, R. B. and J. Bonk, 1984, Preliminary geologic map of Yucca Mountain with geologic sections, Nye County, Nevada: U.S. Geological Survey Open-File Report 84-494.
- Scott, R. B. and M. Castellanos, 1984, Stratigraphic and structural relations of volcanic rocks in drill holes USW GU-3 and USW G-3, Yucca Mountain, Nye County, Nevada: U. S. Geological Survey Open-File Report 84-491.
- Snyder, D. B. and W. J. Carr, 1982, Preliminary results of gravity investigations at Yucca Mountain and vicinity, southern Nye County, Nevada: U.S. Geological Survey Open-File Report 82-701.
- Stock, J. M., J. H. Healy, and S. H. Hickman, 1984, Report on televiewer log and stress measurements in core hole USW G-2, Nevada Test Site, October-November, 1982: U.S. Geological Survey Open-File Report 84-172.
- Stock, J. M., J. H. Healy, S. H. Hickman, and M. D. Zoback, 1985, Hydraulic fracturing stress measurements at Yucca Mountain, Nevada, and relationship to the regional stress field: Journal of Geophysical Research, v. 90, p. 8691-8708.

Swolfs, H. S. and W. Z. Savage, 1985, Topography, stresses, and stability at Yucca Mountain, Nevada: paper presented at the U. S. Rock Mechanics Symposium, Rapid City, SD, June 1985.

Zemanek, J., R. L. Caldwell, E. E. Glenn, S. V. Holcomb, L. J. Norton, and A. J. D. Straus, 1969, The borehole televIEWer - a new logging concept for fracture location and other types of borehole inspection: Journal of Petroleum Technology, v. 21, p. 702-774.

Zemanek, J., E. E. Glenn, L. J. Norton, and R. L. Caldwell, 1970, Formation evaluation by inspection with the borehole televIEWer: Geophysics, v. 35, no. 2, p. 254-269.

Zoback, M. D. and J. H. Healy, 1984, Friction, faulting, and in-situ stress: Annales Geophysicae, v. 2, p. 689-698.

Zoback, M. D., J. H. Healy, J. C. Roller, G. S. Gohn, and B. B. Higgins, 1978, Normal faulting and in situ stress in the South Carolina coastal plain near Charleston: Geology, v. 6, p. 147-152.

TABLE 1. VERTICAL STRESS PROFILE FOR HOLE Ue-25p1

Depth interval (m)	Average density (g/cm <sup>3</sup> )	Source	S <sub>v</sub> at base1 (bars)	S <sub>v</sub> at base2 (bars)	Lithologic unit
00 - 39	1.8	1	6.88	6.25	Alluvium
39 - 55	1.9	1	9.86	9.00	Ammonia Tanks member of Timber Mountain Tuff
55 - 79	2.1	1	14.80	13.75	Tiva Canyon member of Paintbrush Tuff
79 - 101	2.12	2	19.37	18.86	
101 - 122	2.11	3	23.71	23.40	
122 - 152	1.93	3	29.38	29.60	Topopah Springs member of the Paintbrush Tuff
152 - 183	2.27	3	36.28	36.70	
183 - 213	1.94	3	41.98	43.35	
213 - 244	2.00	3	48.06	49.77	
244 - 274	2.06	3	54.12	56.22	
274 - 305	2.21	3	60.83	63.19	
305 - 335	2.31	3	67.62	70.29	
335 - 367	2.21	3	74.33	77.59	
367 - 396	1.92	3	79.79	83.41	Tuffaceous Beds of
396 - 430	1.98	3	86.39	90.12	Calico Hills
430 - 439	2.25	3	88.37	92.06	Bedded tuff
439 - 457	1.98	3	91.86	95.93	Prow Pass member of
457 - 482	2.16	3	97.15	101.55	Crater Flat Tuff
482 - 488	2.15	2	98.41	102.95	
488 - 518	2.14	4	104.70	109.63	
518 - 546	2.05	4	110.33	115.49	
546 - 551	2.04	4	111.33	116.52	Bedded tuff
551 - 579	2.16	4	116.98	122.63	Bullfrog member of
579 - 610	2.34	4	124.09	129.98	Crater Flat Tuff
610 - 640	2.34	4	130.97	136.96	
640 - 671	2.20	4	137.65	143.82	
671 - 684	2.11	4	140.34	146.62	
684 - 688	2.17	4	141.19	147.48	Bedded tuff
688 - 701	2.13	4	143.90	150.27	Tram member of Crater
701 - 732	2.17	4	150.49	157.18	Flat Tuff
732 - 762	2.24	4	157.08	164.01	
762 - 792	2.22	4	163.61	170.85	
792 - 823	2.27	4	170.51	177.92	
823 - 853	2.31	4	177.30	184.74	
853 - 872	2.28	4	181.55	189.06	

TABLE 1 (continued). VERTICAL STRESS PROFILE FOR HOLE Ue-25p1

Depth interval (m)	Average density (g/cm <sup>3</sup> )	Source	S <sub>v</sub> at base <sup>1</sup> (bars)	S <sub>v</sub> at base <sup>2</sup> (bars)	Lithologic unit
872 - 884	2.20	4	184.14	191.83	Lithic Ridge Tuff
884 - 914	2.20	4	190.61	198.51	
914 - 945	2.21	4	197.32	205.48	
945 - 975	2.26	4	203.96	212.30	
975 - 1006	2.32	4	211.01	219.49	
1006 - 1036	2.36	4	217.95	226.46	
1036 - 1064	2.25	4	224.12	232.77	
1064 - 1067	2.29	4	224.79	233.44	Bedded tuff
1067 - 1097	2.34	4	231.67	240.53	Older tuff
1097 - 1128	2.38	4	238.90	247.88	
1128 - 1137	2.46	4	241.07	250.04	
1137 - 1170	2.55	4	249.32	258.49	Fanglomerate
1170 - 1195	2.46	3	255.35	264.47	Older tuff
1195 - 1231	2.46	2	264.03	273.75	
1231 - 1298	2.74	2	282.02	291.36	Lone Mountain Dolomite
1298 - 1311	2.71	5	285.47	294.89	
1311 - 1341	2.76	5	293.58	302.95	
1341 - 1372	2.74	5	301.90	311.28	
1372 - 1402	2.72	5	309.90	319.35	
1402 - 1433	2.74	5	318.22	327.68	
1433 - 1463	2.76	5	326.33	335.75	
1463 - 1494	2.75	5	334.68	344.08	
1494 - 1524	2.75	5	342.77	350.74	
1524 - 1554	2.71	5	350.74	360.48	
1554 - 1585	2.75	5	359.09	368.97	
1585 - 1615	2.77	5	367.23	377.18	
1615 - 1634	2.77	5	372.39	382.39	
1634 - 1646	2.79	5	375.67	385.68	Roberts Mountain Formation
1646 - 1676	2.74	5	383.73	393.89	
1676 - 1707	2.78	5	392.18	402.38	
1707 - 1737	2.80	5	400.41	410.60	
1737 - 1768	2.80	5	408.92	419.09	
1768 - 1801	2.77	5	417.88	--	

Density sources: (1) Snyder and Carr, 1982  
 (2) Averages of values within this same unit, this hole  
 (3) Birdwell compensated density log, run Nov. 30, 1982  
 (4) Dresser-Atlas compensated density log, run Jan. 18, 1983  
 (5) Birdwell compensated density log, run May 3, 1983

S<sub>v</sub> at base: 1 - derived from density sources listed above  
 2 - derived from borehole gravity measurements of Healey et al. (1984)

TABLE 2a. VERTICAL STRESS PROFILE FOR THE UPPER PART OF USW G-3

Log depth interval (m)	True depth interval (m)	Average density (g/cm <sup>3</sup> )	Source	S <sub>v</sub> at base of interval (bars)		Lithologic unit
				A	B	
0 - 129	same	2.1	1	26.55	28.60	Tiva Canyon member of Paintbrush Tuff
129 - 431	same	2.12	2	89.09	91.41	Topopah Springs member of the Paintbrush Tuff
431 - 459	same	1.95	2	94.63	95.63	Ash flow tuff
459 - 476	same	2.12	2	98.16	98.54	Bedded tuff
476 - 607	same	2.10	2	125.12	122.19	Prow Pass member of the Crater Flat Tuff
607 - 611	same	2.10	2	125.94	122.94	Bedded tuff
611 - 776	same	2.23	2	162.00	--	Bullfrog member of the Crater Flat Tuff
776 - 777	same	2.23	2	162.22	--	Crater Flat Tuff
777 - 796	same	2.23	2	166.37	--	
796 - 798	same	2.05	3	166.77	--	
798 - 803	same	2.10	3	167.70	--	Bedded tuff
803 - 823	803-822	1.98	3	171.47	--	Tram member of the Crater Flat Tuff
823 - 853	822-852	2.09	3	177.61	--	
853 - 884	852-882	2.18	3	184.02	--	
884 - 914	882-912	2.32	3	190.84	--	
914 - 945	912-942	2.32	3	197.66	--	
945 - 975	942-972	2.29	3	204.39	--	
975 - 1006	972-1002	2.30	3	211.15	--	
1006 - 1036	1002-1031	2.17	3	217.32	--	
1036 - 1067	1031-1061	2.18	3	223.73	--	
1067 - 1097	1061-1090	2.22	3	230.04	--	
1097 - 1128	1090-1120	2.24	3	236.63	--	
1128 - 1158	1120-1149	2.30	3	243.17	--	
1158 - 1173	1149-1164	2.29	3	246.54	--	
1173 - 1177	1164-1168	2.27	3	247.43	--	Bedded tuff

- Sources of density information:
- (1) Snyder and Carr, 1982
  - (2) Averages of values from holes USW G-2, Ue-25p1, and USW H-1
  - (3) Dresser-Atlas compensated density log of USW G-3, run March 23, 1982

True depth intervals calculated from Eastman Whipstock gyro multishot survey of USW G-3, run on March 19, 1982. Combined run data used.

- S<sub>v</sub> at base of interval:
- (A) calculated from densities given in column 3
  - (B) calculated from borehole gravity results of Healey et al. (1984)

Table 2b. VERTICAL STRESS PROFILE FOR THE LOWER PART OF USW G-3

Log depth interval (m)	True depth interval (m)	Average density* (g/cm <sup>3</sup> )	S <sub>v</sub> at base of interval (bars)	Elevation correction (m)	S <sub>v</sub> correction (bars)	Corrected S <sub>v</sub> (bars)
1177 - 1219	1168-1208	2.22	256.13	-4.88	-1.00	255.13
1219 - 1250	1208-1238	2.18	262.54	-12.50	-2.57	259.97
1250 - 1280	1238-1267	2.22	268.85	-17.07	-3.51	265.34
1280 - 1311	1267-1296	2.19	275.07	-23.16	-4.77	270.30
1311 - 1341	1296-1324	2.26	281.27	-26.21	-5.39	275.88
1341 - 1372	1324-1353	2.28	287.75	-29.26	-6.02	281.73
1372 - 1402	1353-1381	2.26	293.95	-35.36	-7.28	286.67
1402 - 1433	1381-1409	2.29	300.23	-41.45	-8.53	291.70
1433 - 1463	1409-1437	2.29	306.51	-47.55	-9.79	296.72
1463 - 1494	1437-1465	2.24	312.66	-53.64	-11.04	301.62
1494 - 1536	1465-1507	2.25	321.92	-68.88	-14.18	307.74

\*Values from Dresser-Atlas compensated density log of USW G-3, run March 23, 1982.

S<sub>v</sub> at base of interval calculated from densities in column 3. No borehole gravity measurements were made at this depth.

Elevation correction: difference in height of surface directly above base of interval, and elevation of top of hole. This is important in this part of USW G-3 due to excessive hole drift. Hole drift used for true vertical depths are calculated from the Eastman Whipstock gyro multishot survey of USW G-3, run on March 19, 1982. Combined run data used. Elevation corrections are calculated from plotting horizontal projection of hole drift on a topographic base map. Map contour intervals are 20 feet; thus, we estimate  $\pm 3$  m uncertainty in the elevation corrections listed.

TABLE 3. SUMMARY OF STRESS MEASUREMENTS, USW G-3 AND UE-25p1

Hole	Logged depth (m)	Breakdown pressure <sup>1</sup> (bars)	Shut-in pumping pressure (bars)	Hydrostatic pressure (bars)	Pore <sup>2</sup> pressure (bars)	$S_h$ (bars)	$S_v$ <sup>3</sup> (bars)	$T^4$ (bars)	$S_H$ (bars)	Comments
G-3	1,074	79	68	105	31	<u>68+2</u>	206	13	<u>107+10</u>	
G-3	1,338	173	115	131	56	<u>115+2</u>	258	59	<u>175+9</u>	Interpretation based on first two cycles only.
G-3	1,356	168	114	133	57	<u>114+2</u>	263	64	<u>181+8</u>	
P1	1,564	none <sup>1</sup>	337	153	115	<u>337+2</u>	353			Reopening preexisting fracture
P1	1,573	236	207	154	116	<u>207+2</u>	356	41	<u>310+11</u>	
Pa1	1,693	none <sup>1</sup>	366	166	128	<u>365+10</u>	388			Reopening preexisting fracture

1. No clear breakdown pressures seen; see comments column and Figure 10.

2. Based on water table at the appropriate depth: 385 m in Ue-25p1 and 752 m in USW G-3.

3. Based on densities and calculations in Tables 1 and 2, plus topographic averaging in USW G-3 (see text).

4. T derived from observation of fracture reopening pressures on later cycles.

TABLE 4. LOWER LIMITS ON  $S_h$  FROM TESTS IN THE UPPER PART OF Ue-25p1 (VOLCANIC UNITS)

Depth (m)	Lithology	Pfailure (bars)	P <sub>p</sub> (bars)	T (bars)*	Lower limit on S <sub>h</sub> (bars)
731	Tram member: ash flow, zeolitized, partly to moderately welded	189	34	54	85
1,001	Lithic Ridge Tuff: ash flow, zeolitized, partly to moderately welded	236	61	54	122
1,131	Older tuffs: argillized, calcitized, partly welded	204	73	54	112

\* Value of T based on observations listed in Table 5.

TABLE 5. CONSTRAINTS ON HYDRAULIC FRACTURING TENSILE STRENGTH ( $T_{\text{hydrofrac}}$ ) IN THE VOLCANIC UNITS AT YUCCA MOUNTAIN

Drill hole	Depth (m)	Lithologic unit	$P_b - P_b (T=0)$ $T_{\text{hydrofrac}}$ (bars)	Borehole diameter (cm)
USW G-1	1,288	Lithic Ridge Tuff, partly welded	50	10.8
USW G-2	1,026	Bullfrog member; moderately welded	47	18
	1,209	Bedded tuff below Tram member, vitric (partly argillic)	62	19
USW G-3	1,074	Tram member: ash flow tuff, devitrified, moderately welded	13	10.8
94	1,338	Lithic Ridge: ash flow tuff, devitrified, moderately welded	59	9
	1,356	Lithic Ridge: ash flow tuff, devitrified, moderately welded	64	9
Ue-25p1	731	Tram member: ash flow tuff, welded, zeolitized	40	27.3

$T_{\text{hydrofrac}}$  is derived from the difference between the breakdown pressure,  $P_b$ , and the fracture reopening pressure on the second cycle,  $P_b (T=0)$ . Tests listed are those for which a clear breakdown was observed. Tests believed to have reopened preexisting fractures are omitted.

TABLE 6. INFLUENCE OF BOREHOLE DEVIATIONS ON RESULTS OF HYDROFRAC TESTS

Hole	Depth (m)	Borehole orientation <sup>1</sup> drift azimuth	Approximate magnitudes of principal stresses (bars) <sup>2</sup>				Predicted <sup>3</sup> hydrofrac orientation	Predicted <sup>3</sup> breakdown pressure (bars)	Ideal <sup>4</sup> breakdown pressure (bars)
USW G-3	1,074	14.5°	N85.5°W	206	-107	68	31	N25°E	87.5
	1,338	19°	S83°W	258	-175	115	56	N25°E	153
	1,356	20.5°	S82.5°W	263	-181	114	57	N25.5°E	144
UE-25p1	731	1°	S25.5°W	151	-127	73	34	N25°E	92
	1,001	1°	S2°E	211	-180	111	61	N25°E	153
	1,131	1.25°	S30°W	243	-208	129	73	N25°E	179
	1,564	3.25°	S32.5°E	353	-304	194	115	N25°E	277
	1,573	3.25°	S27°E	356	-310	207	116	N25°E	310
	1,693	7°	S3.5°E	388	-334	214	128	N25°E	308

1. Obtained from Eastman Whipstock deviation log of hole (see figure 10).

2. Values of  $S_V$  and  $P_p$  are calculated as described in text. Values of  $S_H$  are estimates obtained from hydraulic fracturing tests.  $S_H$  magnitudes are those calculated using standard hydrofrac equation (1) in text, or approximate values obtained by interpolation of average stress ratios in these two drill holes plus USW G-1 and USW G-2. These values are used for obtaining an estimate of the effect of the hole deviation and do not represent actual  $S_H$  values obtained from the tests, with the exception of the three USW G-3 values and the value at 1,573 m depth in UE-25p1.

3. Values predicted assuming a far field stress orientation of  $S_V$  vertical,  $S_H$  at N25°E, and  $S_h$  at N65°W, and a hole deviation as given by the values in column 2. Predicted breakdown pressure is  $P_b$  ( $T=0$ ), the value of the least compressive stress in the borehole wall.

4. Value of  $P_b$  ( $T=0$ ) obtained for a perfectly vertical hole under the same stress conditions, using equation (2) of the text.

A P P E N D I X   I  
USW G-3 Televiwer Photos

TELEVIEWSER LOG DATA SHEET - USW G-3 (Part I)

Date logged: November 18 and 19, 1983

Tool no.: 2

Surface panel no.: 1

Zero depth at: center of boot at top of casing      Rezero: -5.2'

Top of logged interval: 2,600' (bottom of casing)

Bottom of logged interval: 2,761' (tool would not fall below this depth)

Depth interval (ft)	Borehole gain	Blanking	TV Gain
2,600 - 2,615	5	044	230
2,615 - 2,660	4	044	230
2,660 - 2,675	5	044	230
2,675 - 2,800	4	044	230
2,800 - 2,810	4	044	257
2,810 - 2,880	3	044	257
2,880 - 3,015	4	044	214
3,015 - 3,030	3	044	214
3,030 - 3,230	4	044	214
3,230 - 3,280	5	044	214
3,280 - 3,510	5	047	234
3,510 - 3,565	4	047	245
3,565 - 3,590	4	047	230
3,590 - 3,605	4	044	230
3,605 - 3,625	4	045	244
3,625 - 3,675	5	044	244
3,675 - 3,695	5	044	221
3,695 - 3,720	5	044	234
3,720 - 3,761	5	038	264

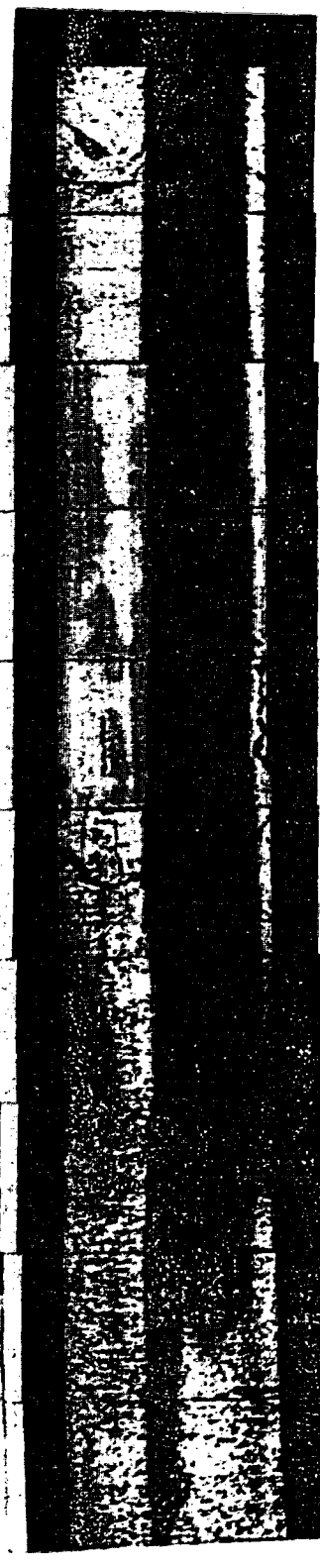
Logged by: L. Mastin, T. Denham, J. Stock



2600

2626

2650



2650

2676

2700

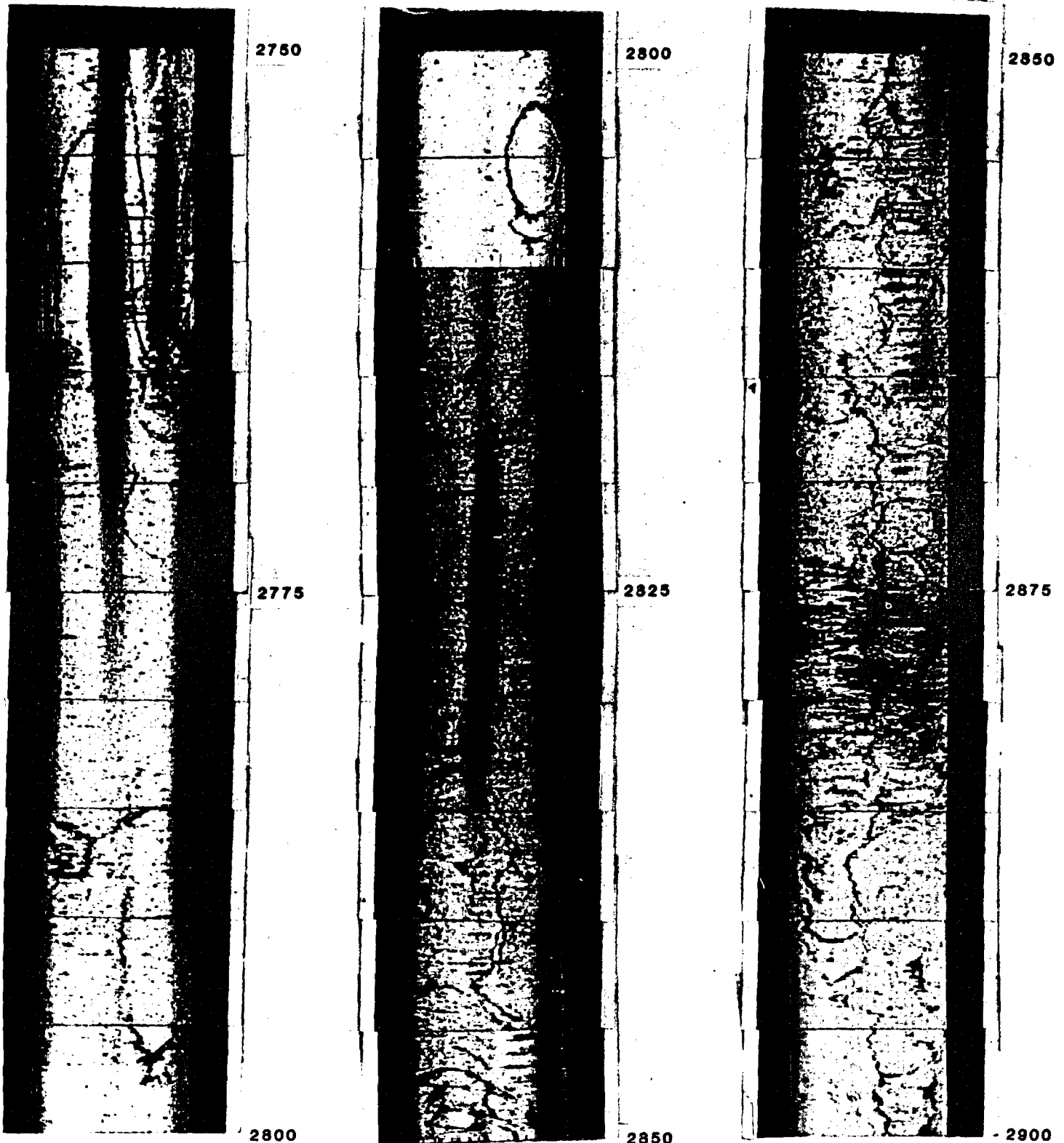


2700

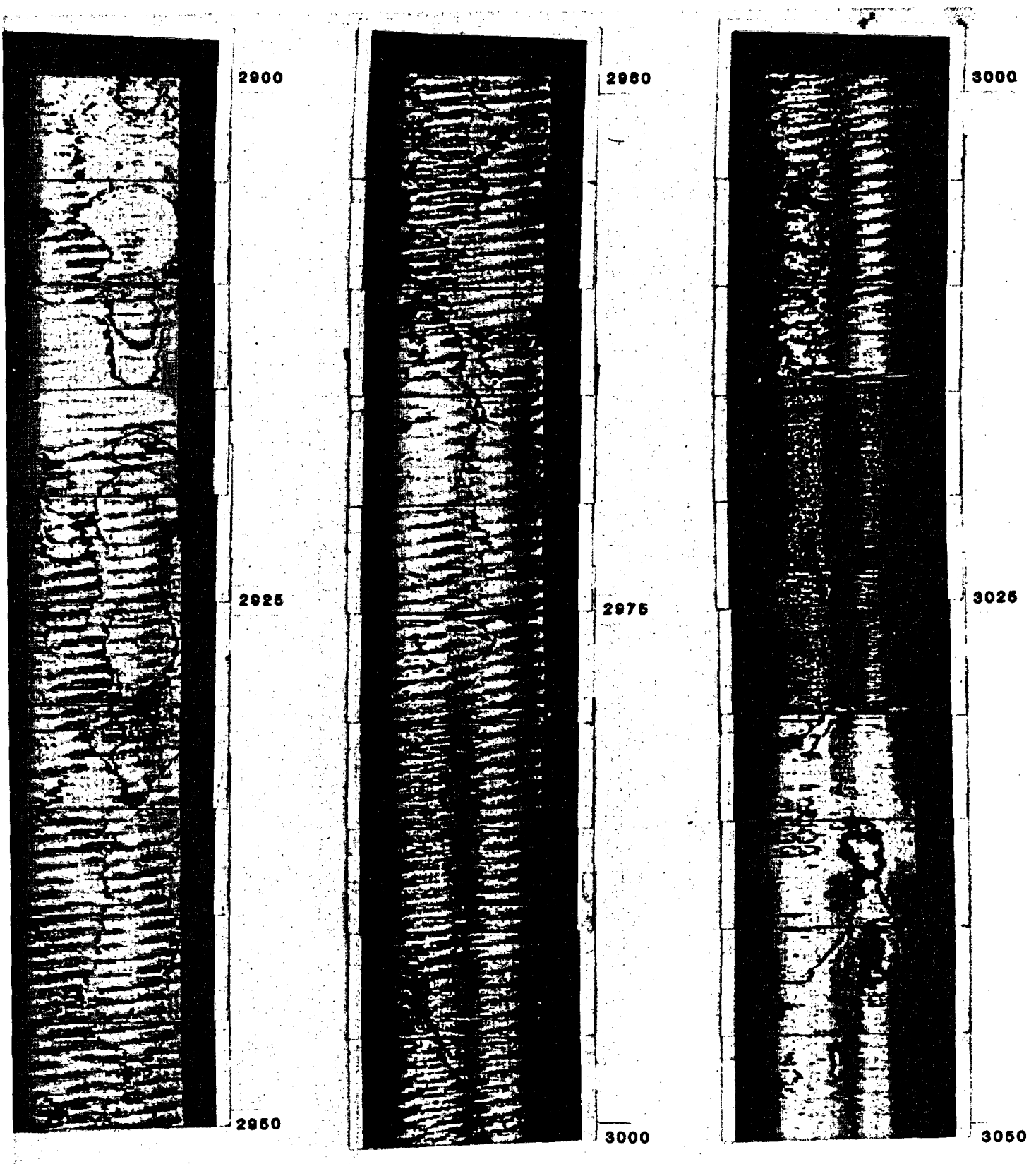
2726

2750

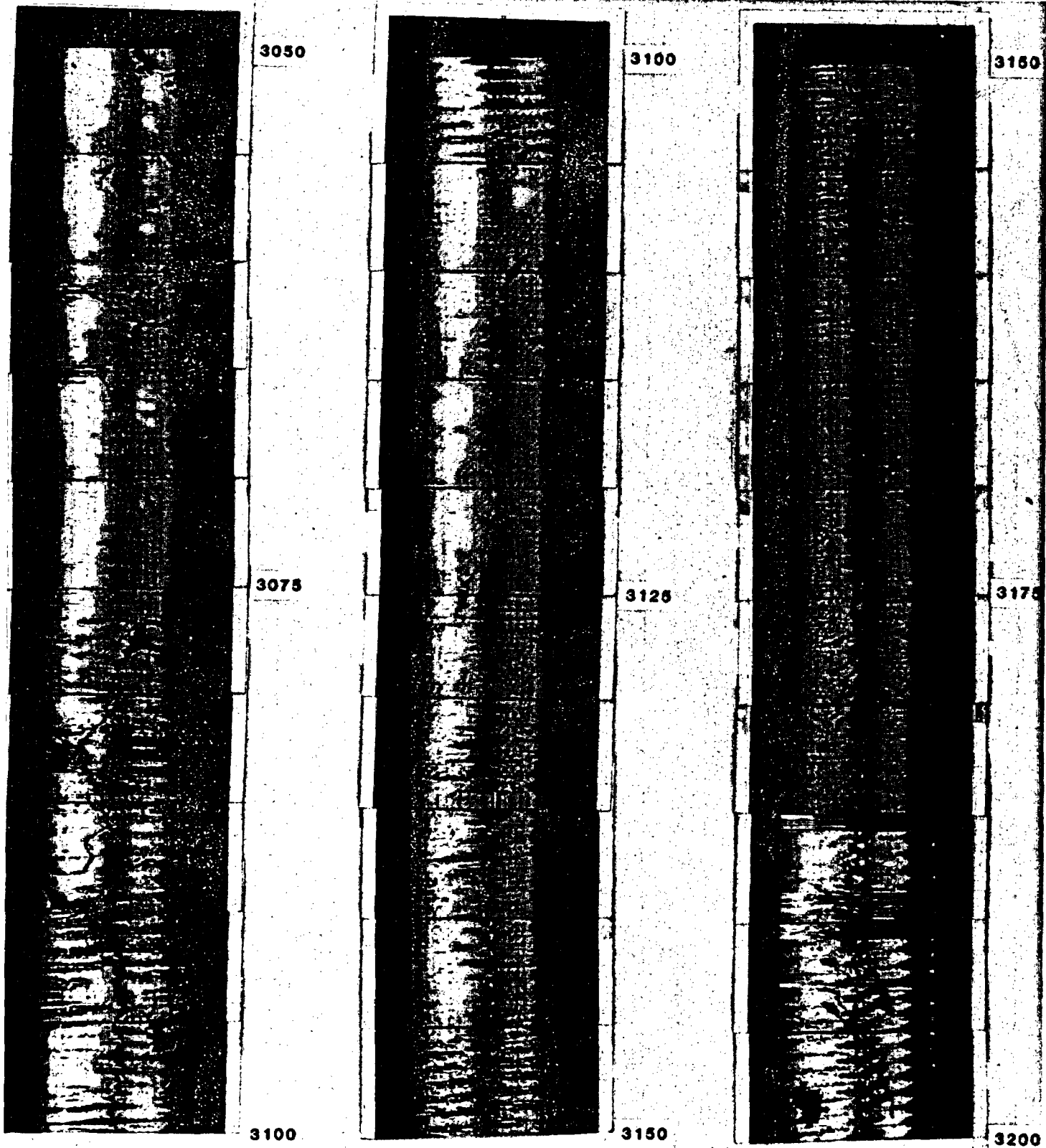
NTS USW G- 3



**NTS USW G-3**



**NTS USW G- 3**



NTS USW G- 3

TELEVIEWER LOG DATA SHEET - USW G-3 (Part II)

Date logged: December 7, 1983

Tool no.: 2

Surface panel no.: 1

Zero depth at: center of boot at top of casing Rezero: -6.4'

Top of logged interval: 3,280'

Bottom of logged interval: 4,480' (hole blocked)

Depth interval (ft)	Borehole gain	Blanking	TV Gain
3,280 - 3,310	4	047	238
3,310 - 3,335	4	047	280
3,335 - 3,341	4	047	400
3,341 - 3,760	3	047	400
3,760 - 3,880	4	047	400
3,880 - 3,895	3	047	400
3,895 - 4,200	4	047	400
4,200 - 4,410	5	047	400
4,410 - 4,480	6	047	400

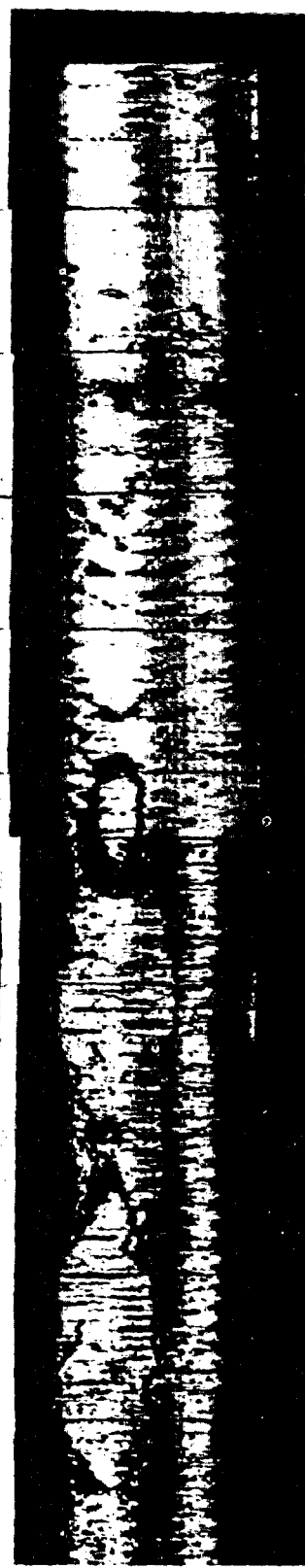
Logged by: J. Stock, L. Mastin, J. Springer



3200

3225

3250



3250

3275

3300

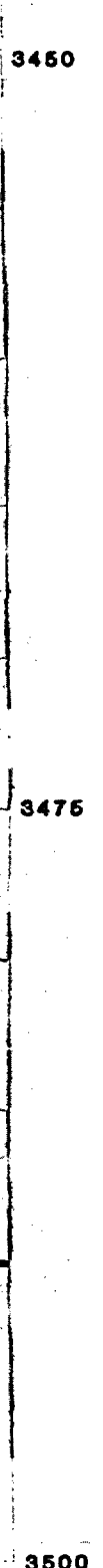
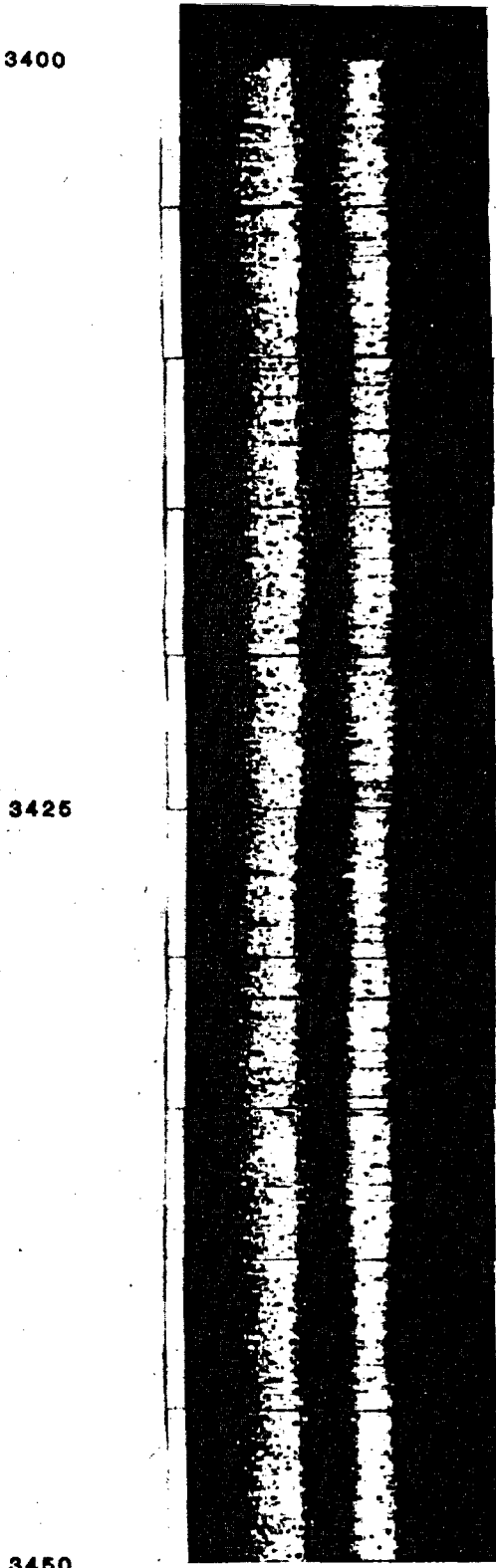
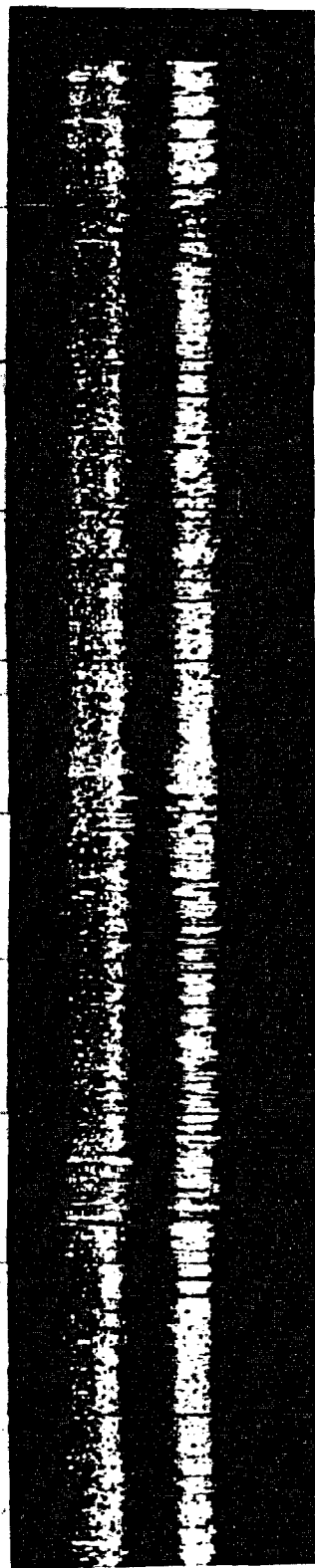


3300

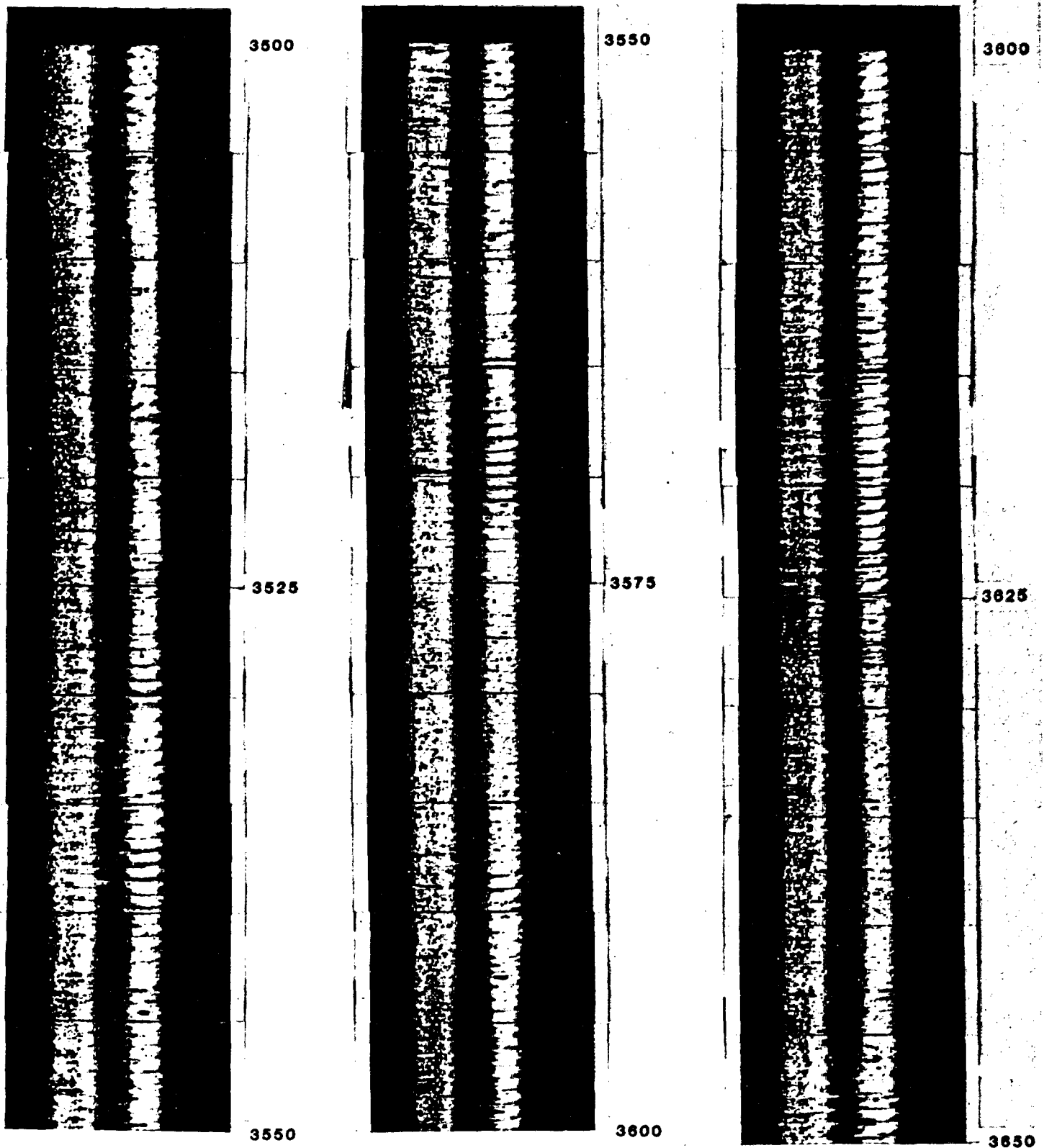
3325

3350

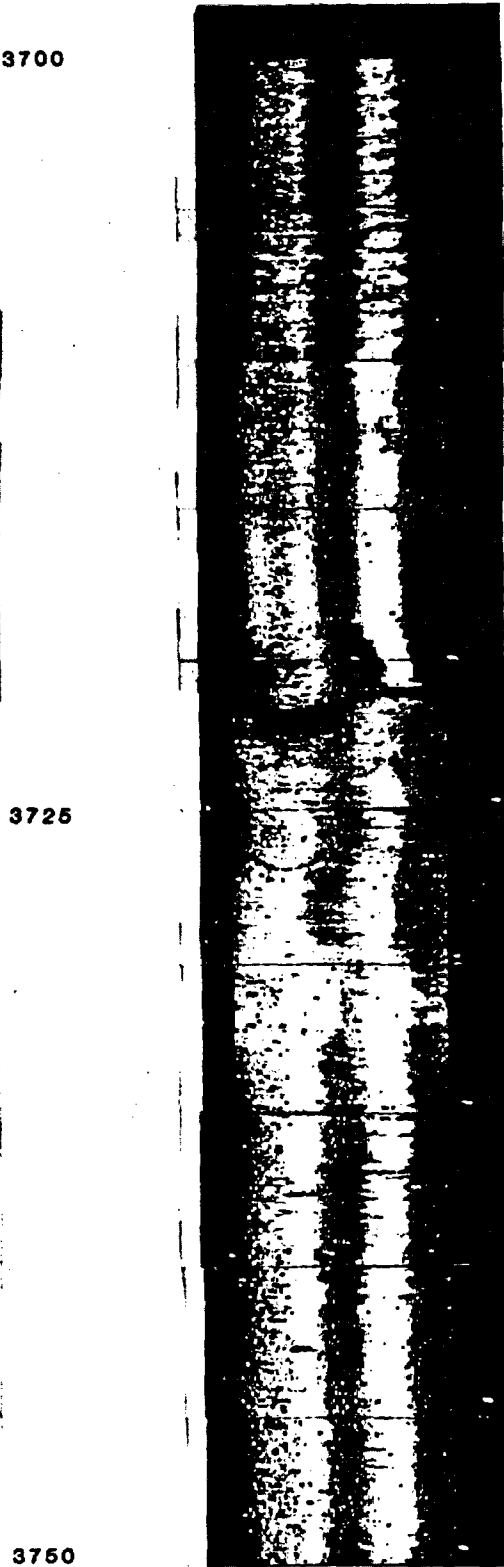
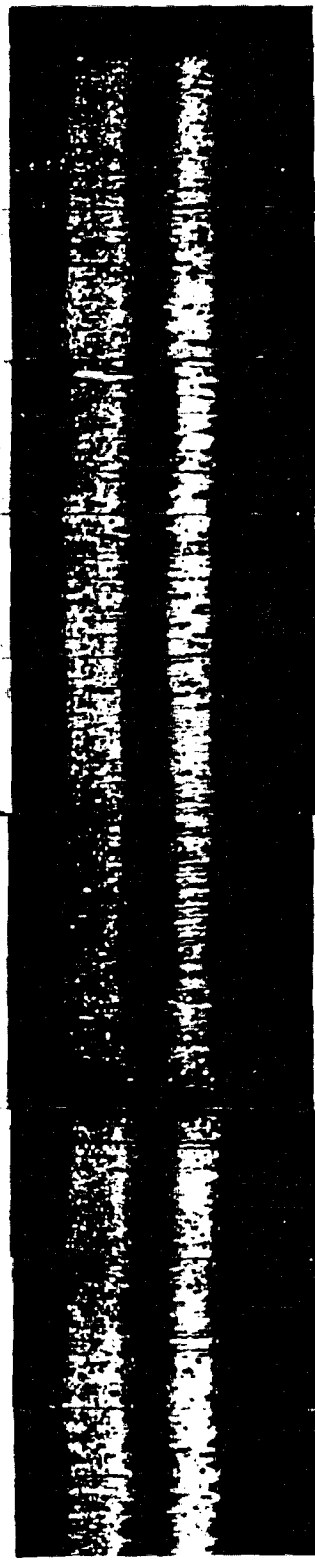
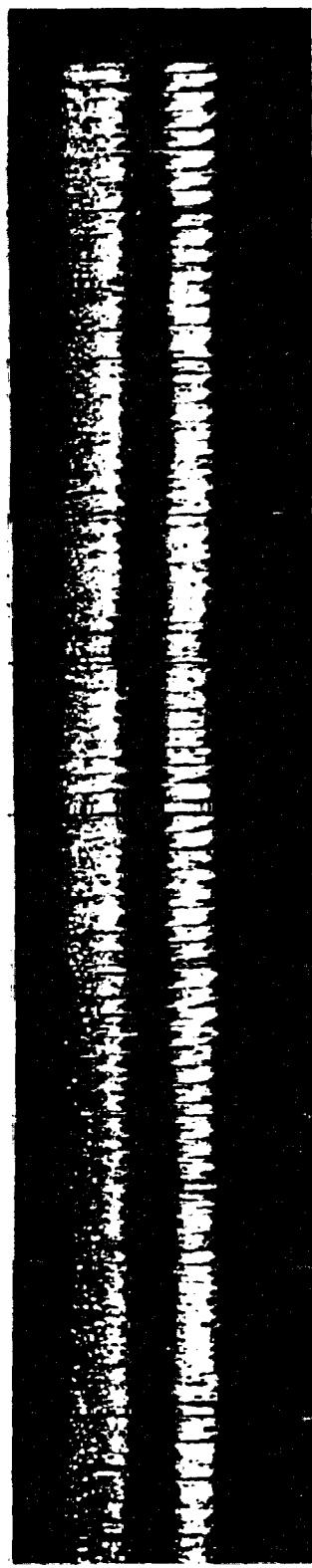
NTS USW G-3



NTS USW G - 3



NTS USW G-3



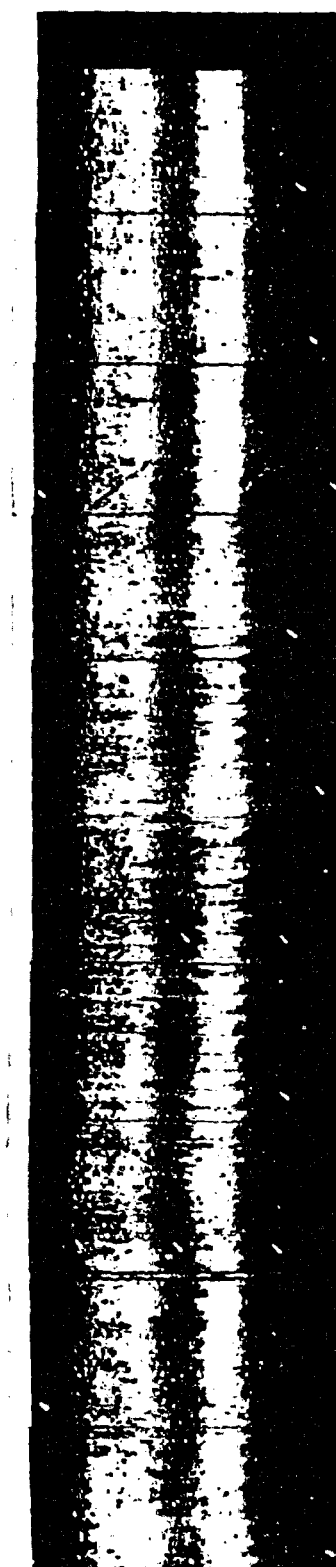
**NTS USW G - 3**



3800



3850



3900

3825

3875

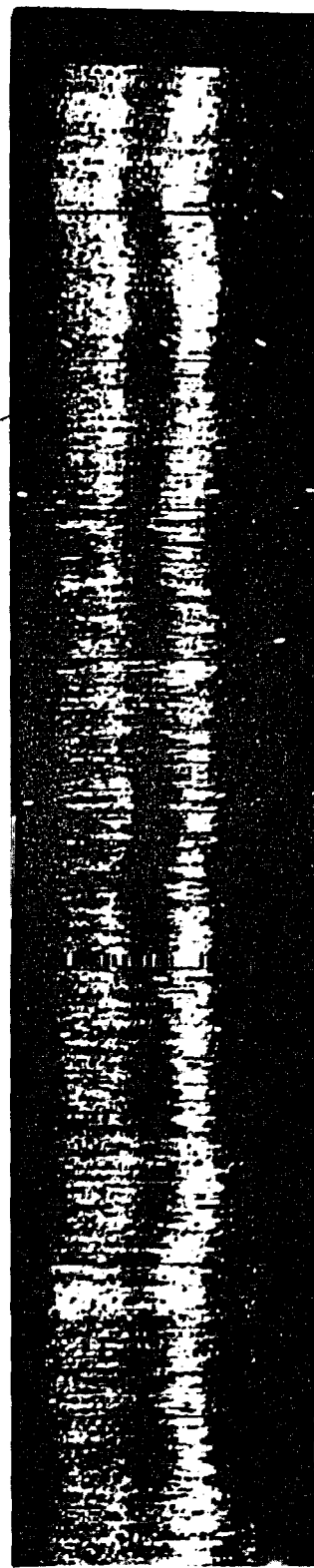
3925

3850

3900

3950

NTS USW G- 3



3950

3976

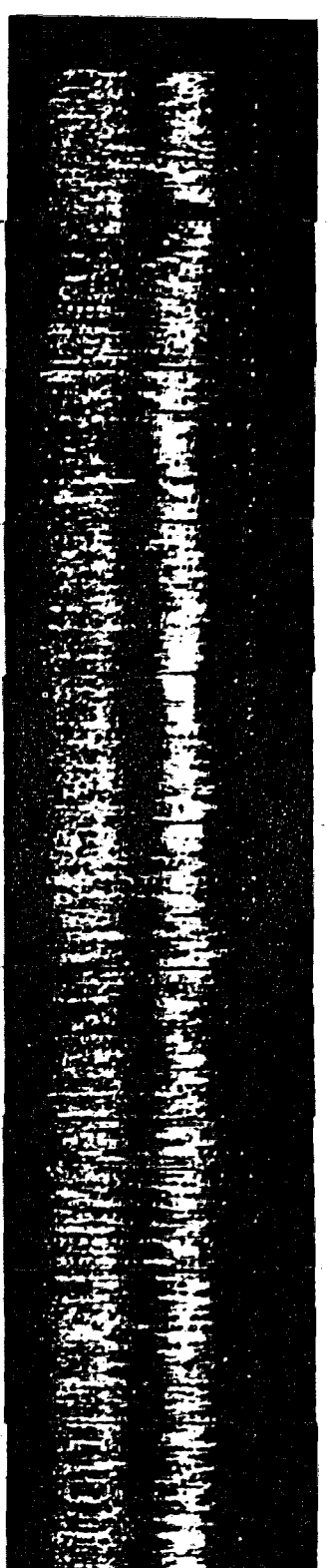
4000



4000

4026

4050

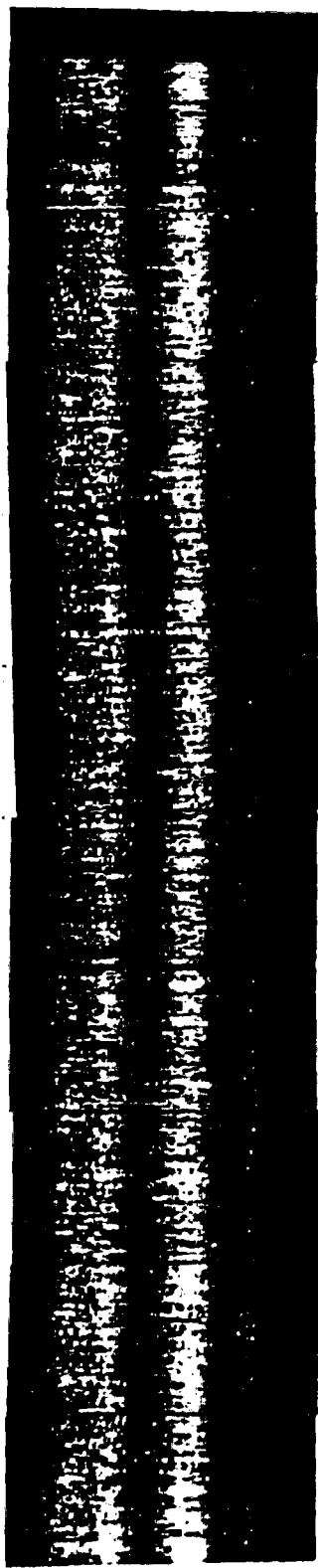


4050

4075

4100

NTS USW G- 3



4100

4125

4150



4150

4175

4200

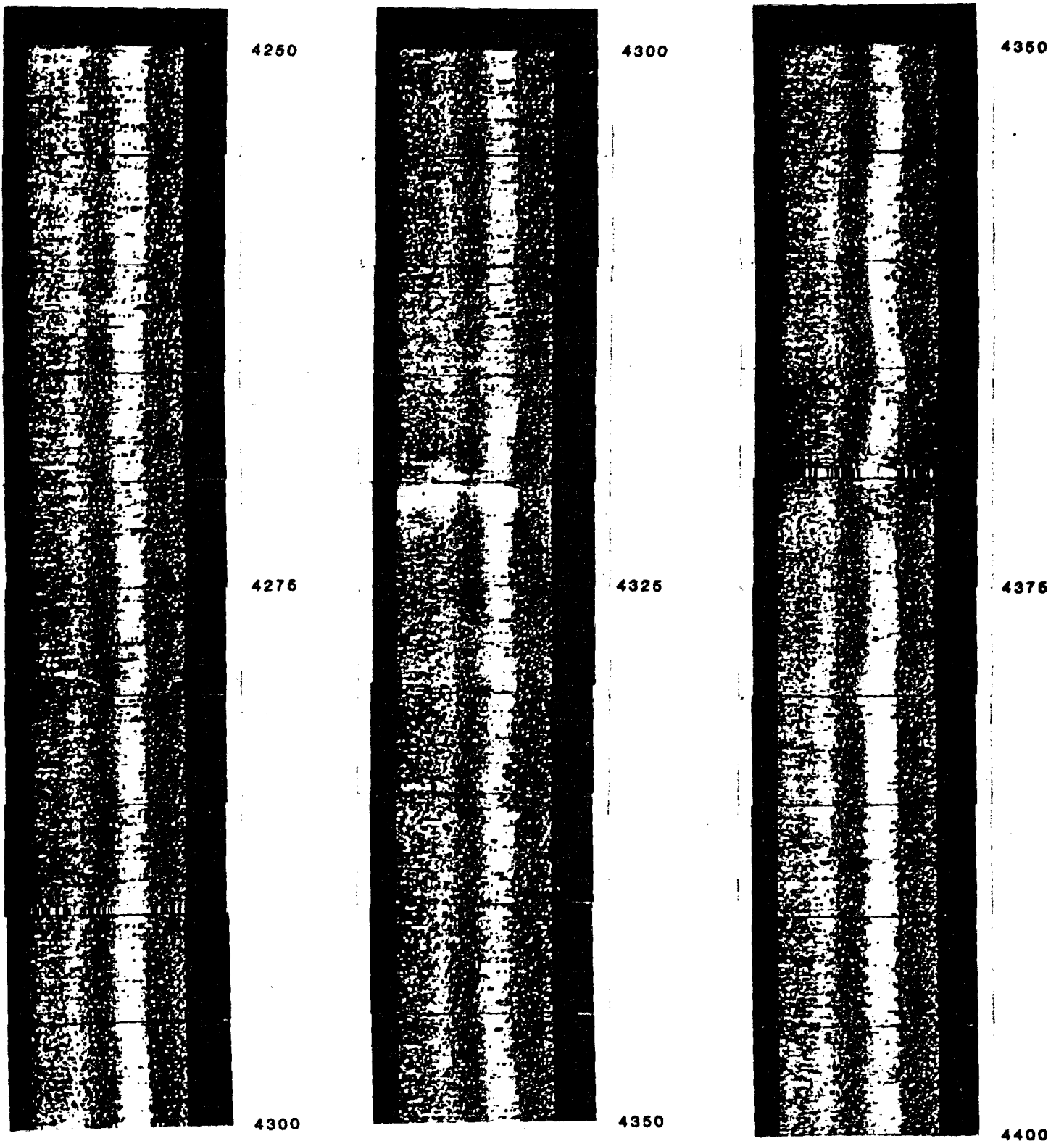


4200

4225

4250

**NTS USW G- 3**



NTS USW G- 3



4400

4425

4450



4450

4475

4480

NTS USW G-3

## A P P E N D I X    I I

### Ue-25p1 Televue Photos

#### TELEVUE LOG DATA SHEET - Ue-25p1 (Part I)

Date logged: February 28, 1983

Tool no.: 1

Surface panel no.: 1

Zero depth at: center of boot at rig floor

Top of logged interval: 1,625' (bottom of casing)

Bottom of logged interval: 3,945' (hole blocked)

Depth interval (ft)	Borehole gain	Blanking	TV Gain
1,575 - 1,600	8	059	
1,600 - 1,675	8	062	
1,675 - 1,695	10	062	
1,695 - 1,715	7	062	
1,715 - 1,860	8	062	
1,860 - 1,905	8	059	
1,905 - 1,955	7	059	
1,955 - 2,000	7	061	
2,000 - 2,030	7	049	
2,030 - 2,425	6	049	
2,425 - 2,625	8	049	
2,625 - 2,750	7	049	
2,750 - 2,920	8	049	
2,920 - 2,985	8	045	
2,985 - 3,390	8	043	
3,390 - 3,440	8	042	
3,440 - 3,455	8	045	
3,455 - 3,650	8	044	
3,650 - 3,915	8	051	
3,915 - 3,945	8	0xx	

Logged by: K. Brown, J. Healy, J. Stock, G. Zwart

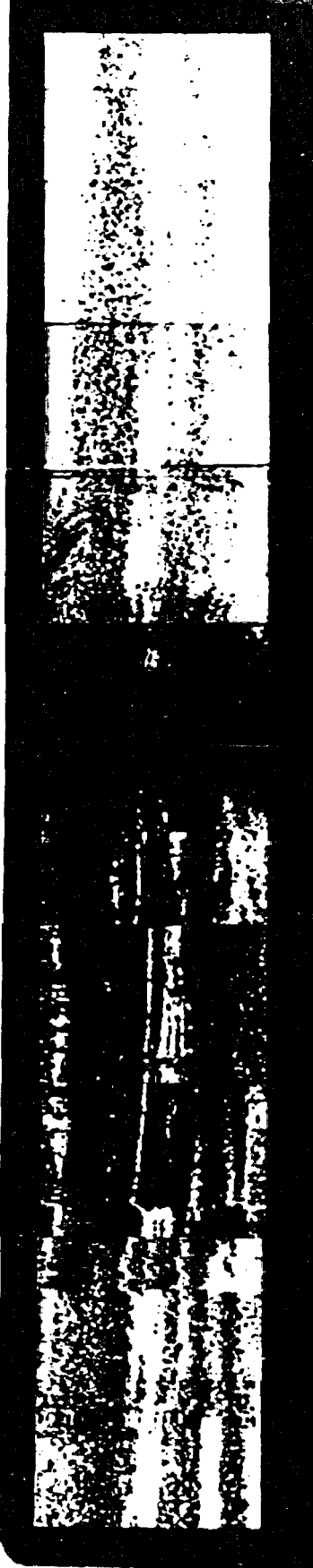
1575



1625



1675



1600

1650

1700

1675

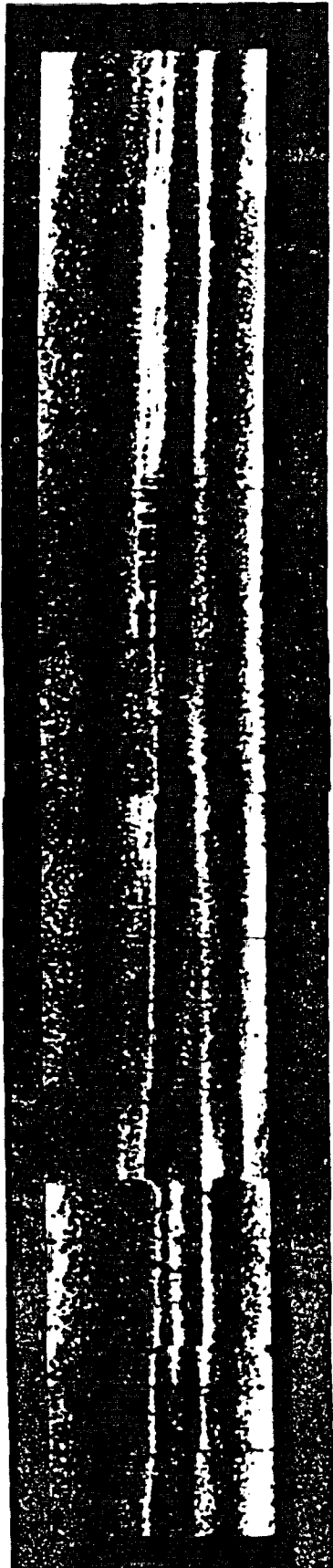
1725

1625

1725



1775



1825



1780

1800

1880

1776

1828

1875

1875

1825

1975

1988

1950

2000

1925

1975

2025

2026



2075



2081

2125



2100

2156

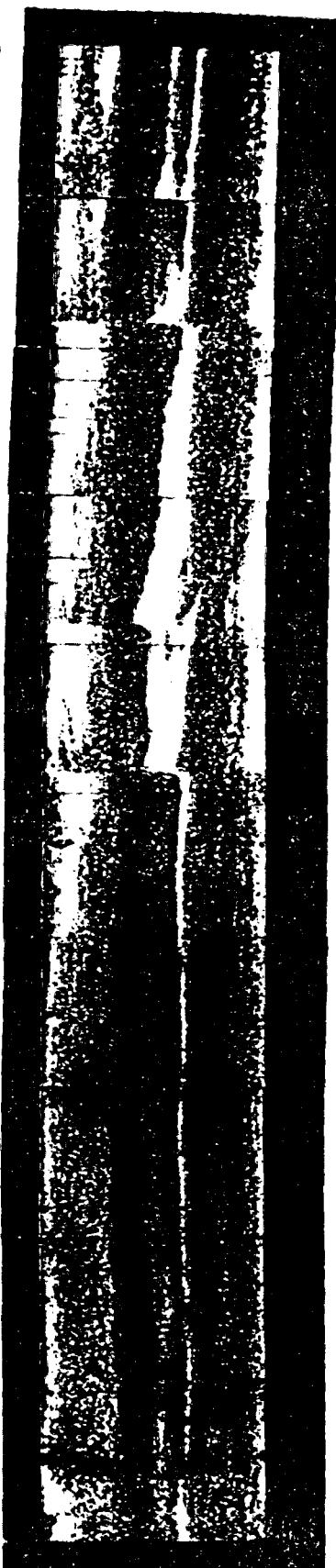
2125

2175

2175



2225



2275



2280

2280

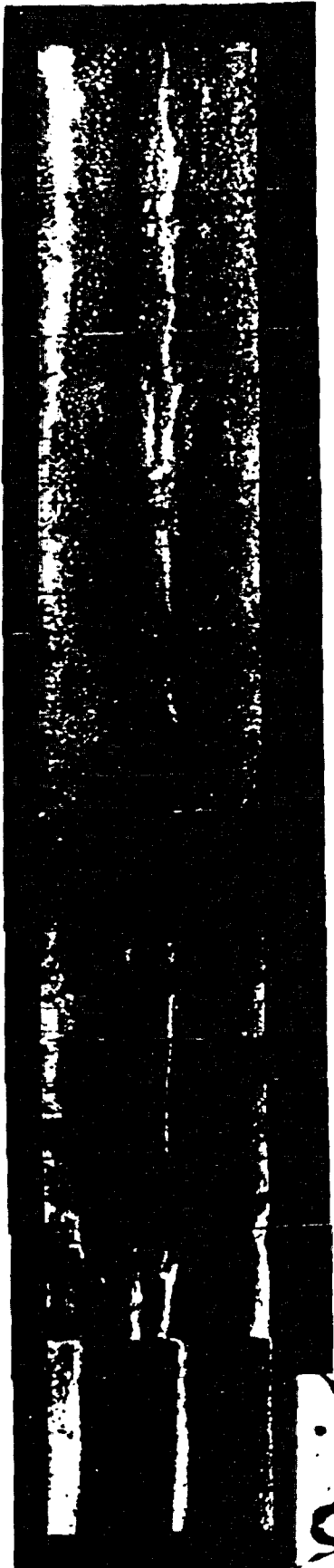
2310

2225

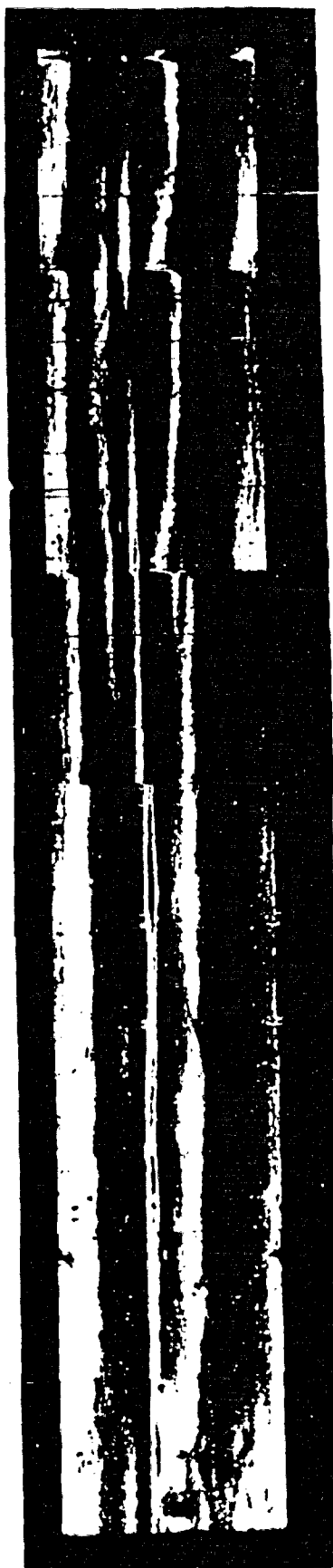
2275

2325

2325



2379



2425



2388

2488

2488

2375

2428

2475

2475



2525



2575



2580

2580

2600

2525

2575

2625

2625



2675



2725



2730

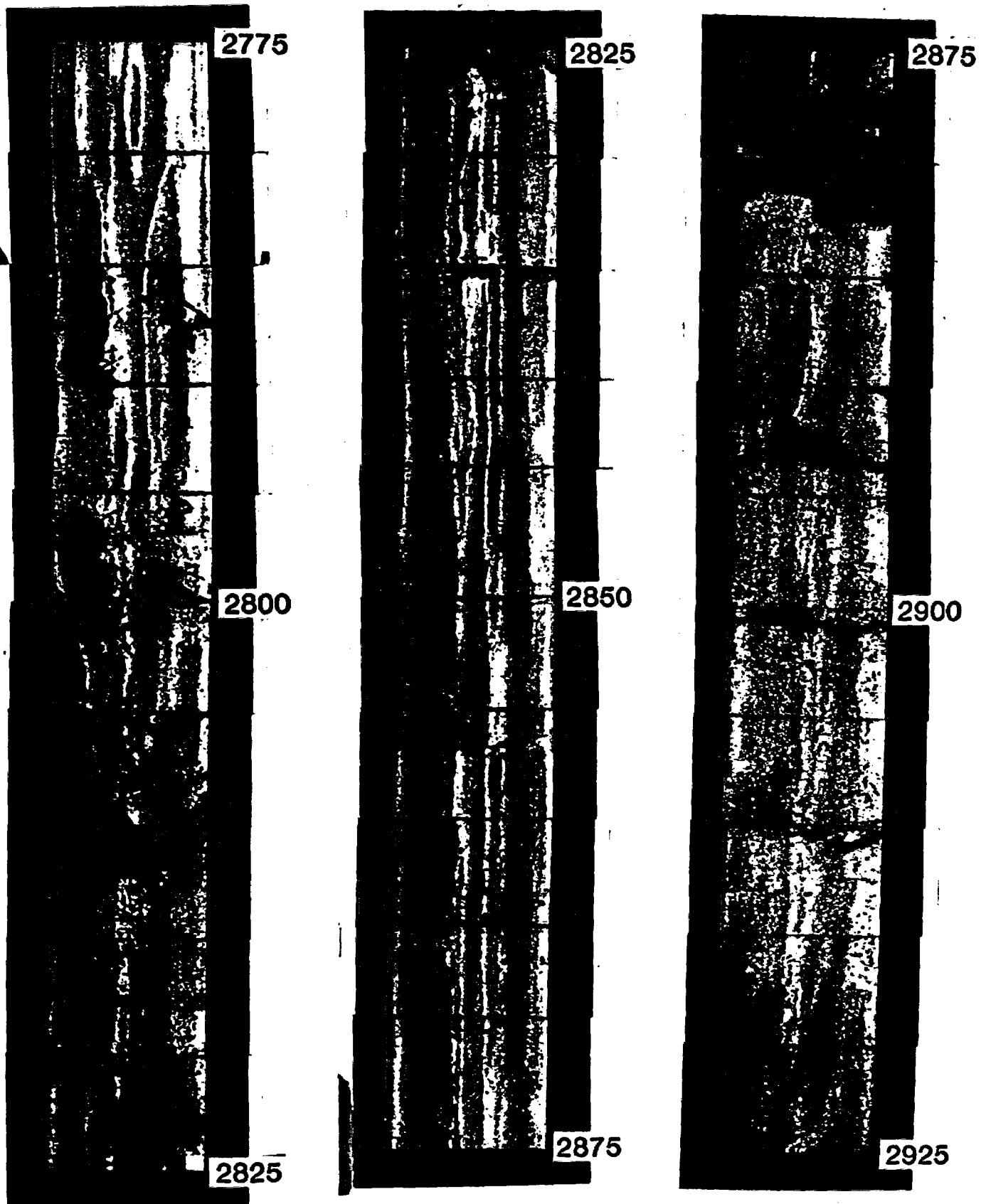
2780

2780

2875

2725

2775



**Ue25 p-1**

2925



2975



3025



2950

3000

3050

3025

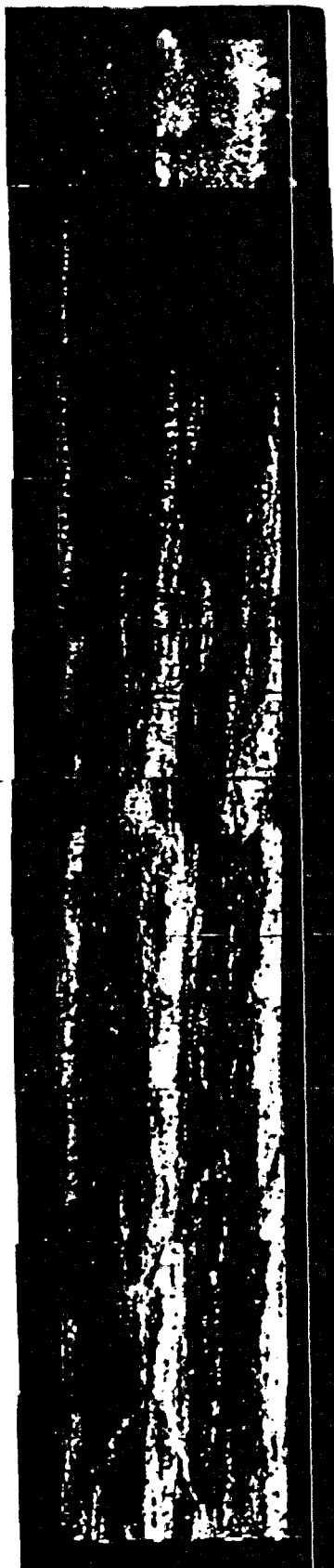
3075

2975

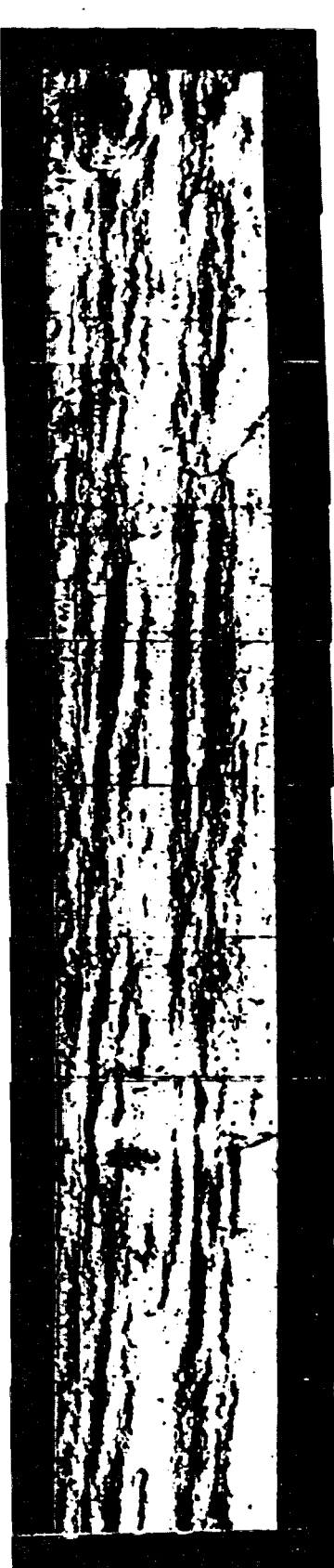
3075



3125



3175



3180

3180

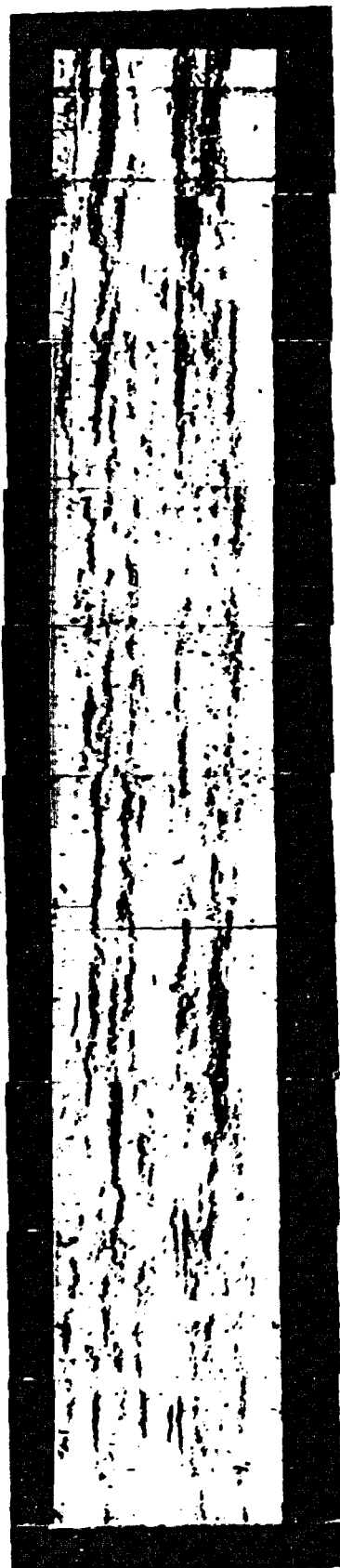
3200

3175

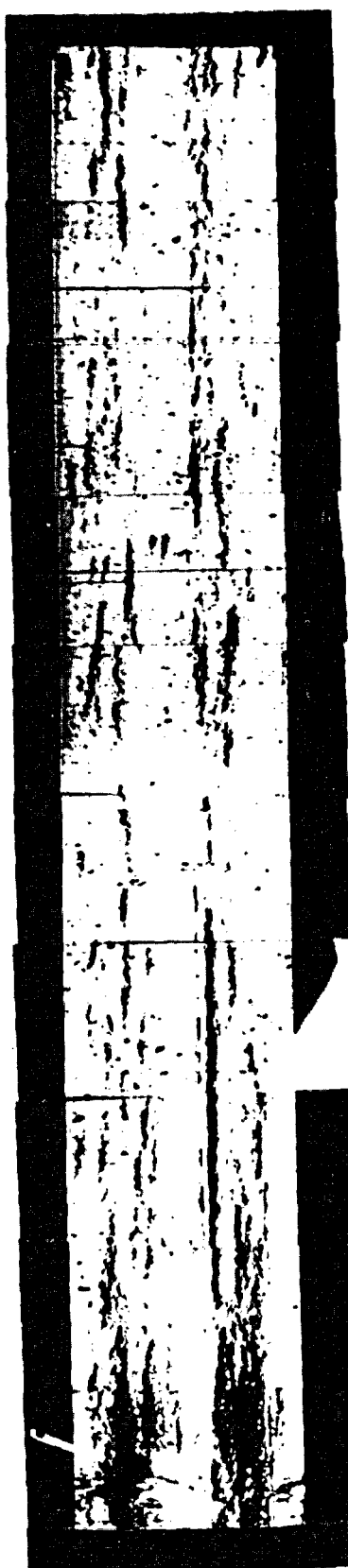
3175

3225

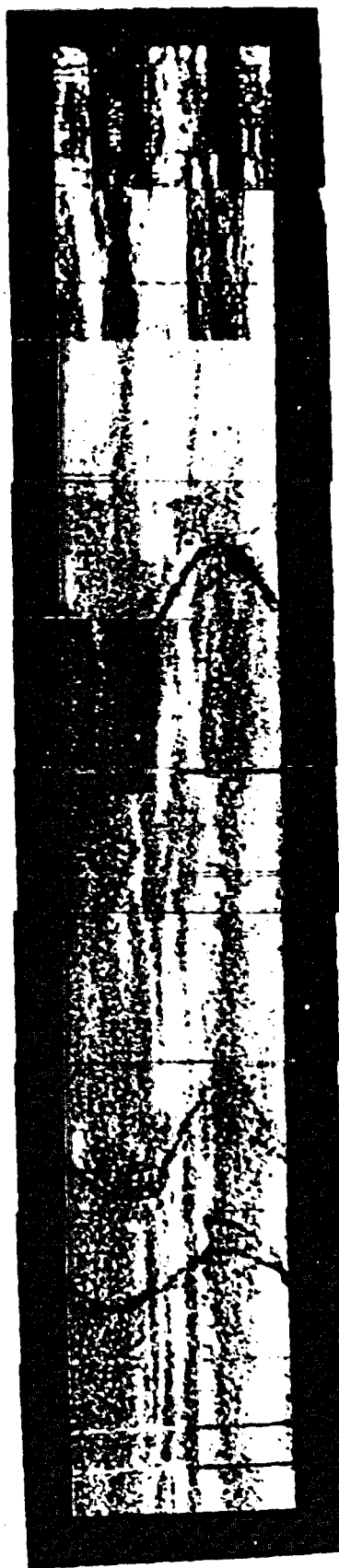
3225



3275



3325



3280

3360

3380

3275

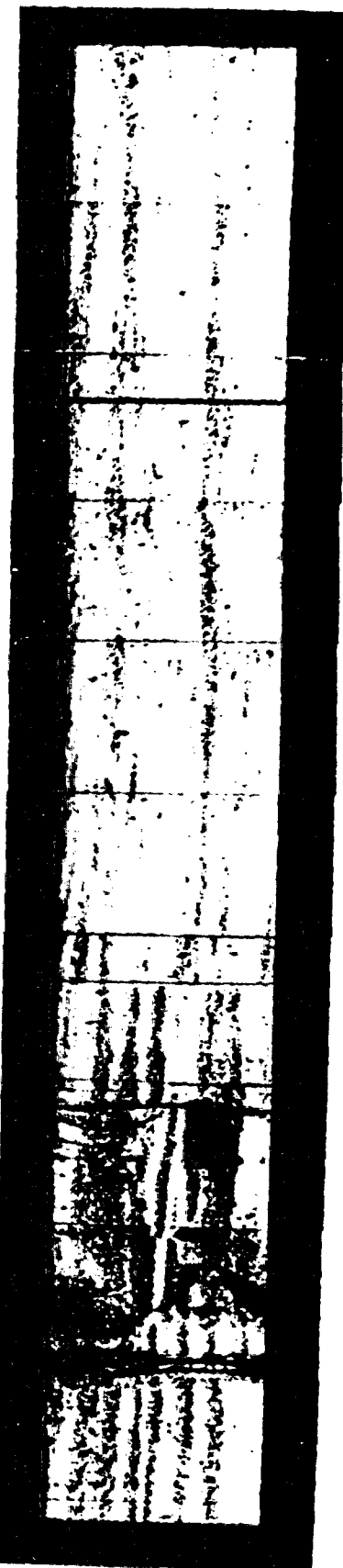
3375



3425



3475



3480

3490

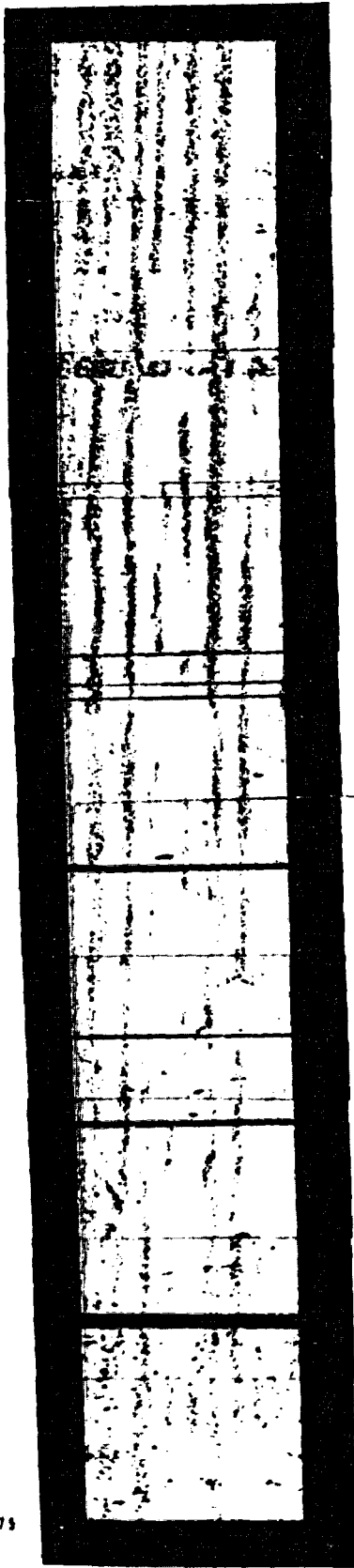
3500

3425

3475

3525

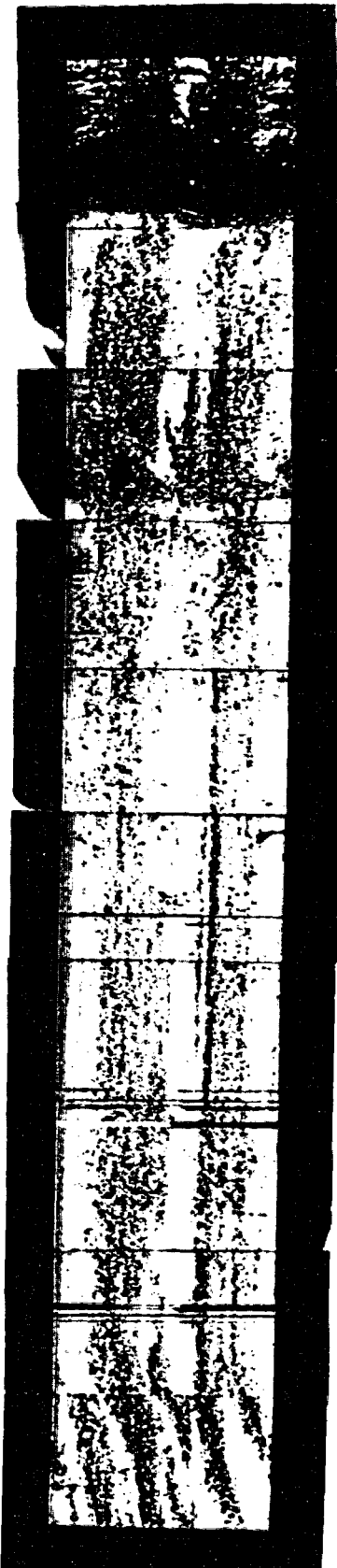
3525



3575



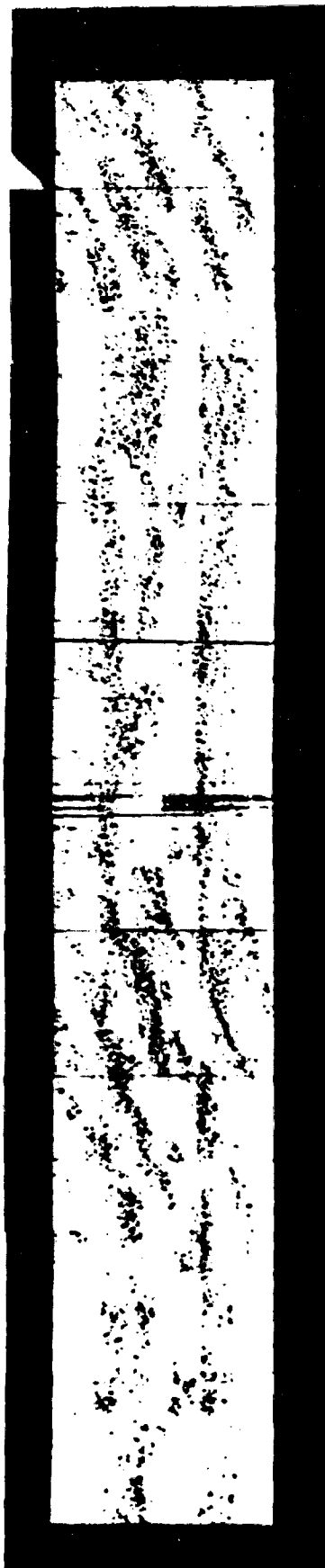
3525



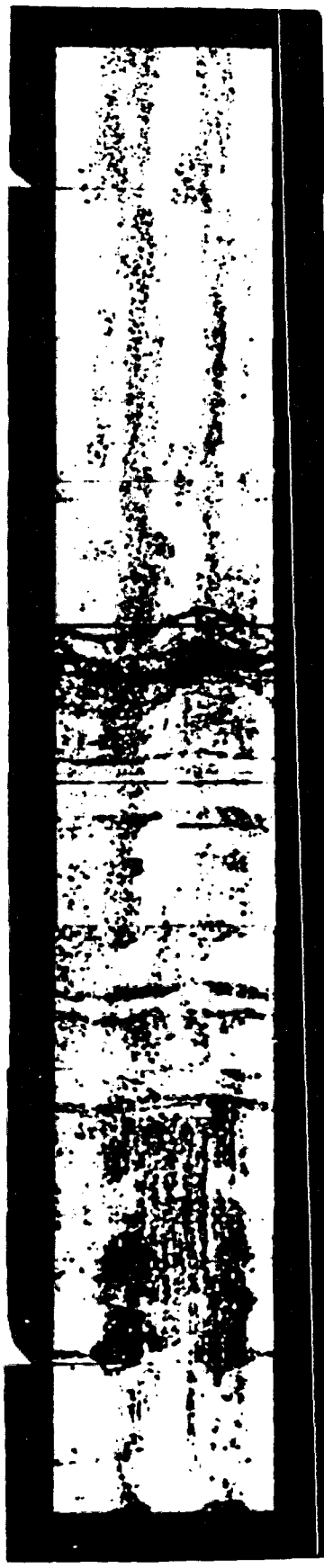
3525

3575

3675



3725



3775

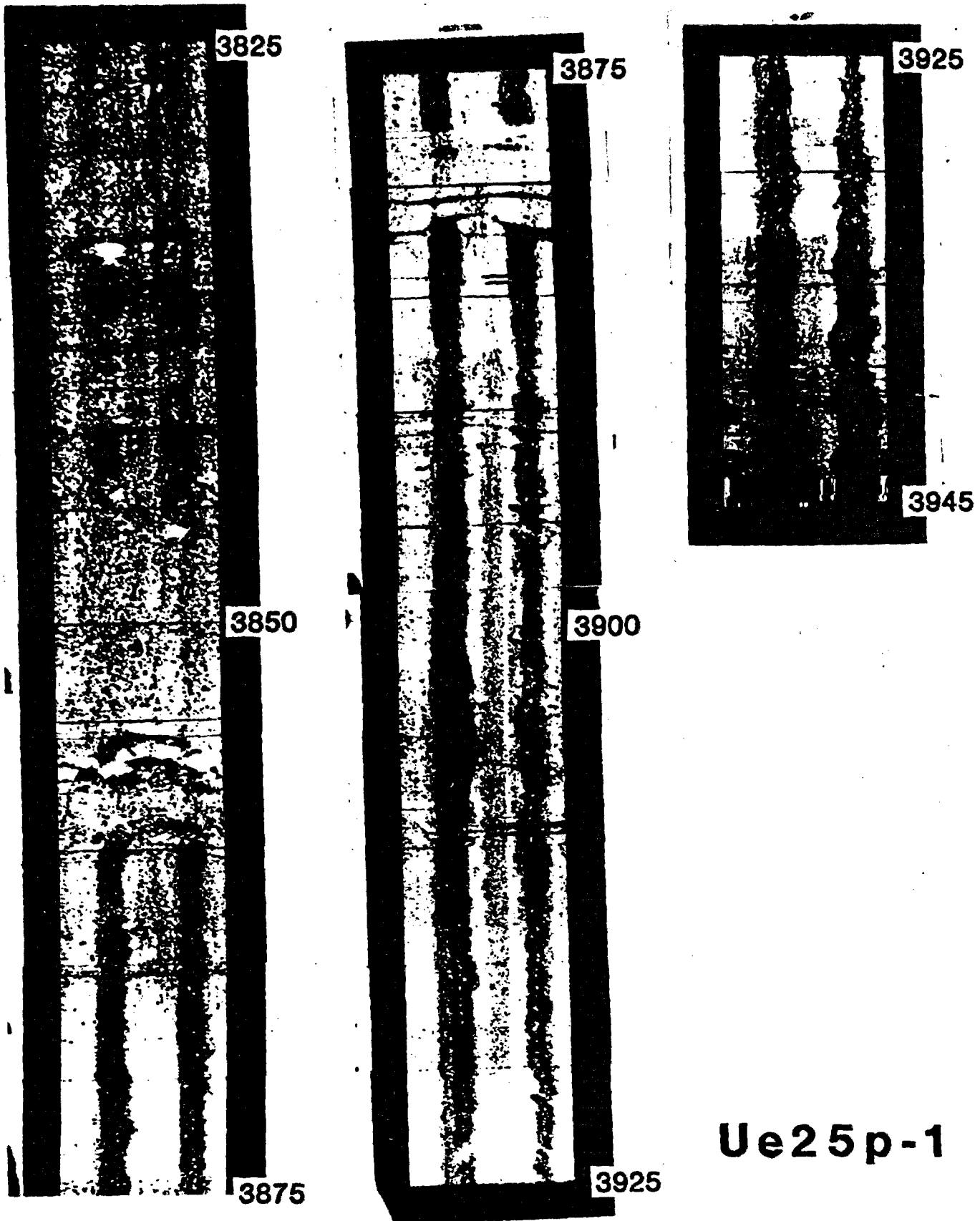


3780

3780

3800

3725



**Ue25 p-1**

## TELEVIEWER LOG DATA SHEET - Hole Ue-25p1 (Part II)

Date logged: July 17, 1983  
Tool no.: 1  
Surface panel no.: 1  
Zero depth at: top of casing, 1' above site grade Rezero: -3.1'  
Top of logged interval: 4,260' (bottom of liner in hole)  
Bottom of logged interval: 5,000' (nearing end of wireline)

Depth interval (ft)	Borehole gain	Blanking	TV Gain
4,255 - 4,275	7	038	232
4,275 - 4,340	6	038	232
4,340 - 5,000	8	038	232

Logged by: J. Svitek, J. Stock

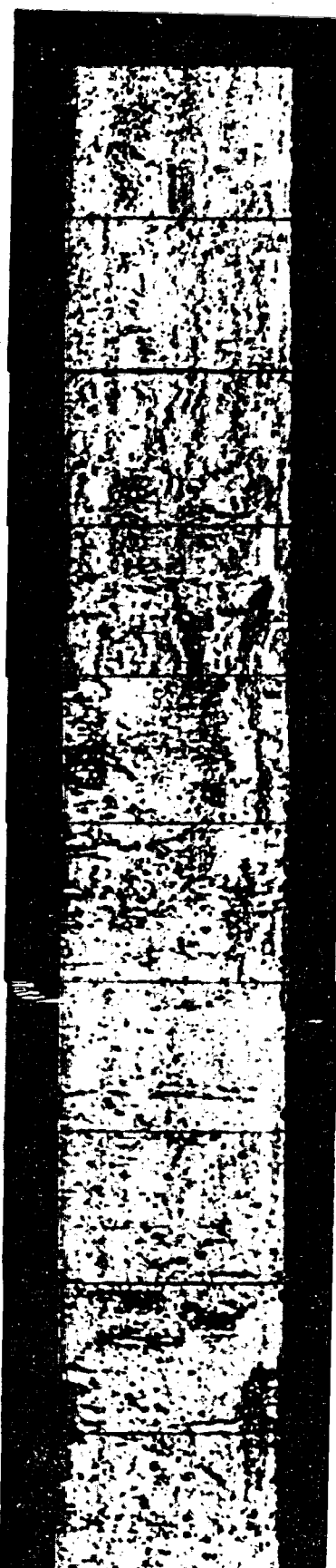
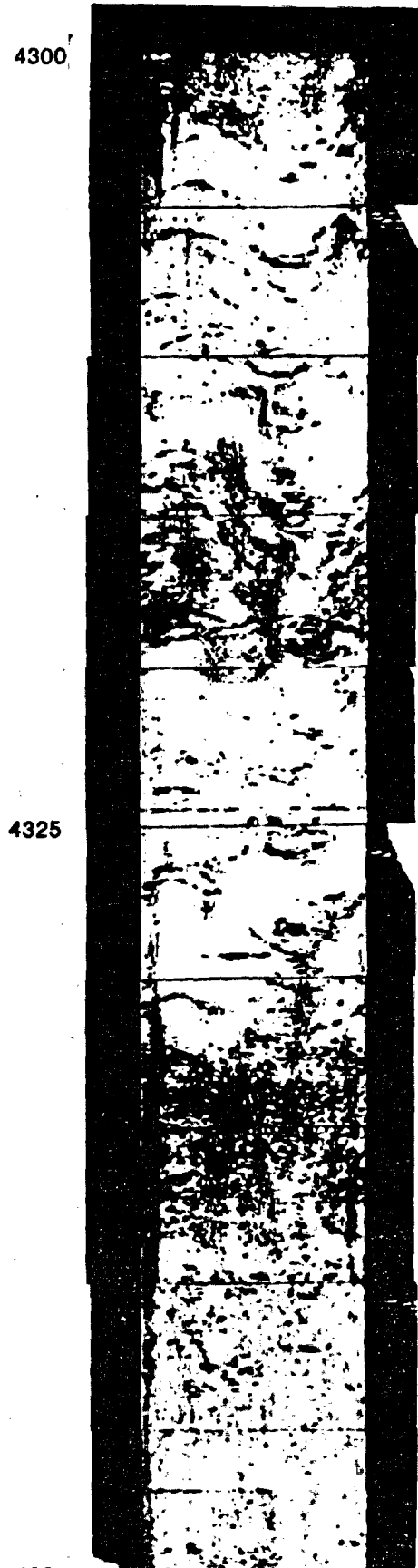
---

## TELEVIEWER LOG DATA SHEET - Hole Ue-25p1 (Part III)

Date logged: November 16, 1983  
Tool no.: 2  
Surface panel no.: 1  
Zero depth at: center of boot to top of casing Rezero: -3.9'  
Top of logged interval: 4,975' (match up and overlap 25' with previous log)  
Bottom of logged interval: 5,900' (hole filled to this depth)

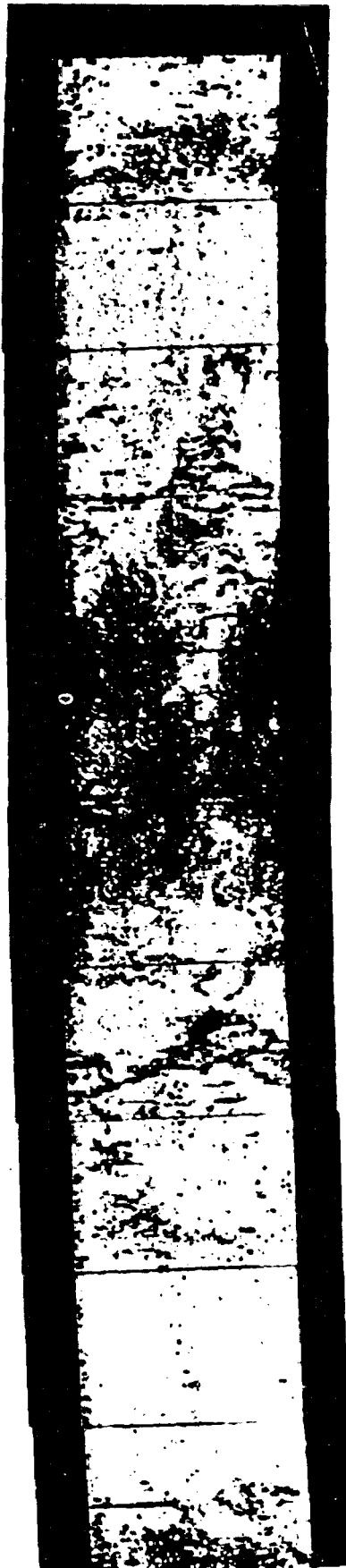
Depth interval (ft)	Borehole gain	Blanking	TV Gain
4,975 - 5,075	7	047	232
5,075 - 5,860	4	047	232
5,860 - 5,900	5	047	248

Logged by: J. Stock, L. Mastin, T. Denham



4350

4400



4450



4500



4425

4475

4525

4450

4500

4550

4550



4600



4650



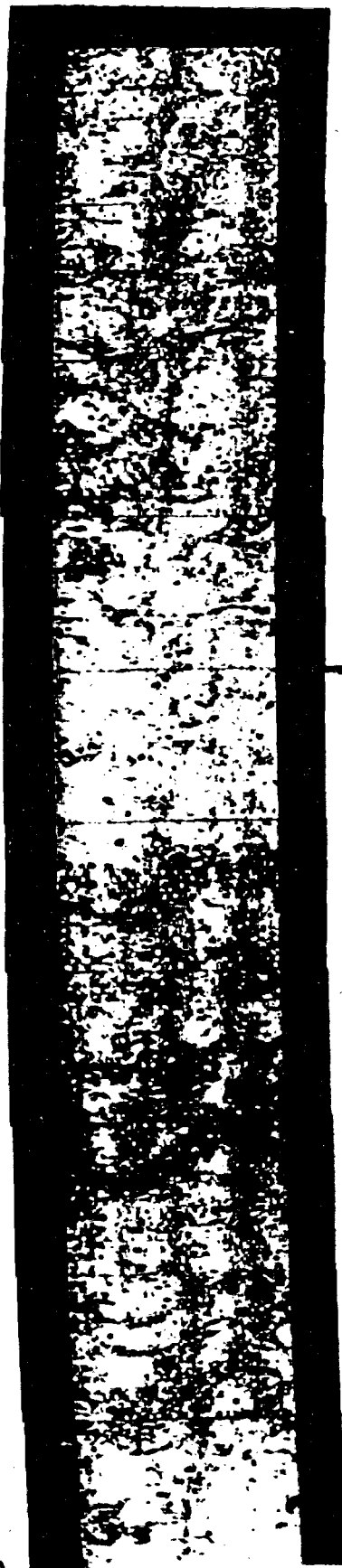
4575

4625

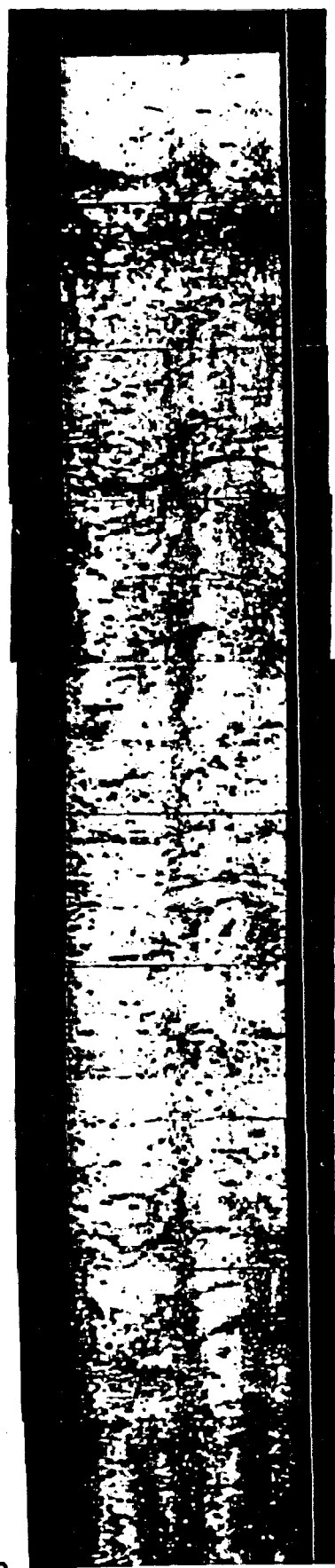
4675

4700

4700



4750



4800



4725

4775

4825

4750

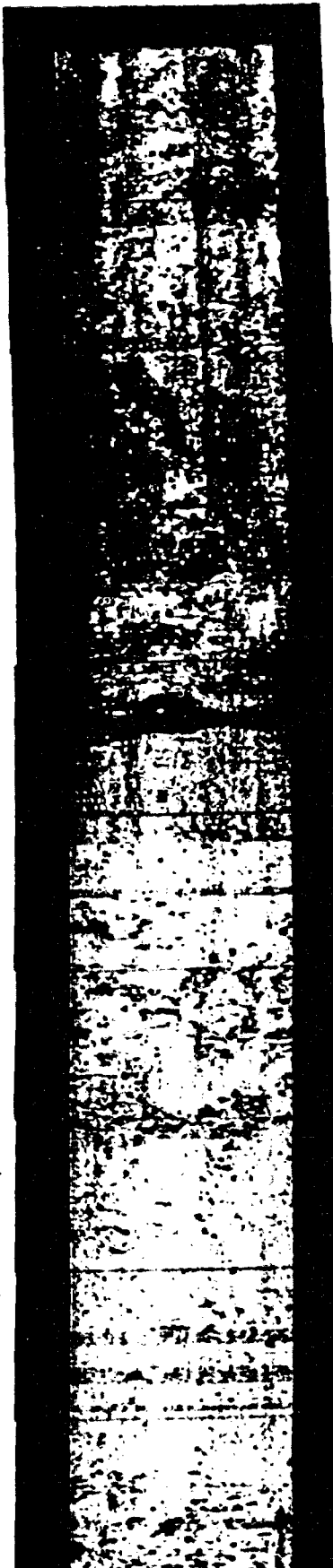
4800

4850

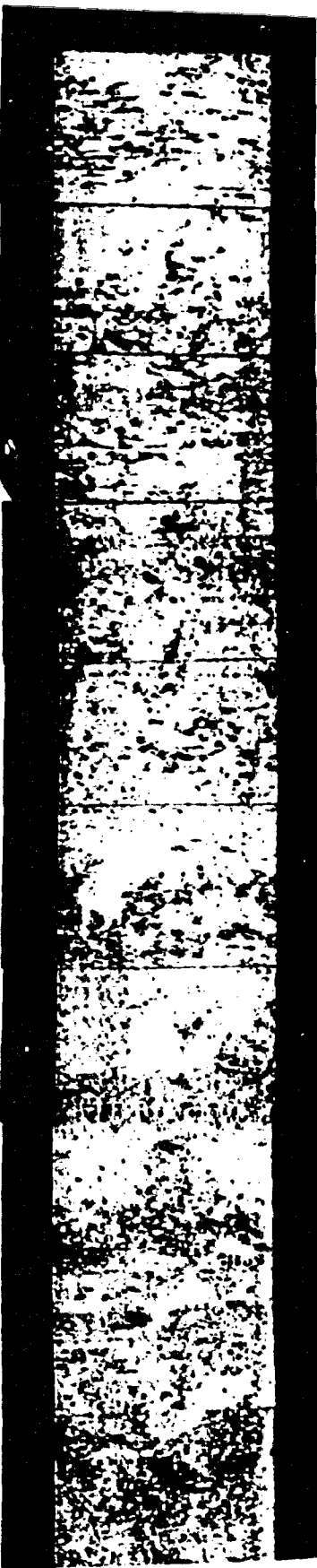
4850



4900



4950



4875

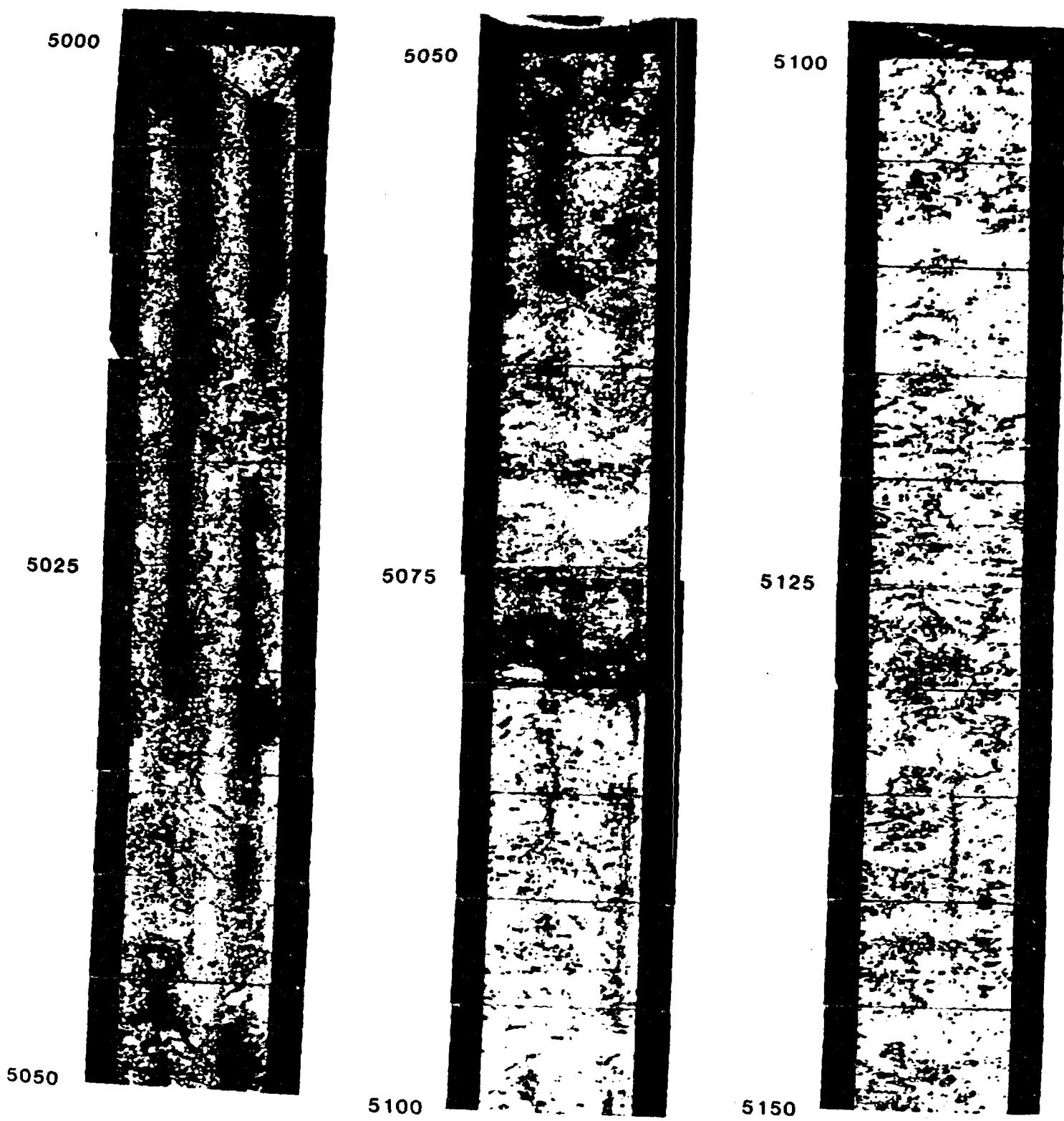
4925

4975

4900

4950

5000

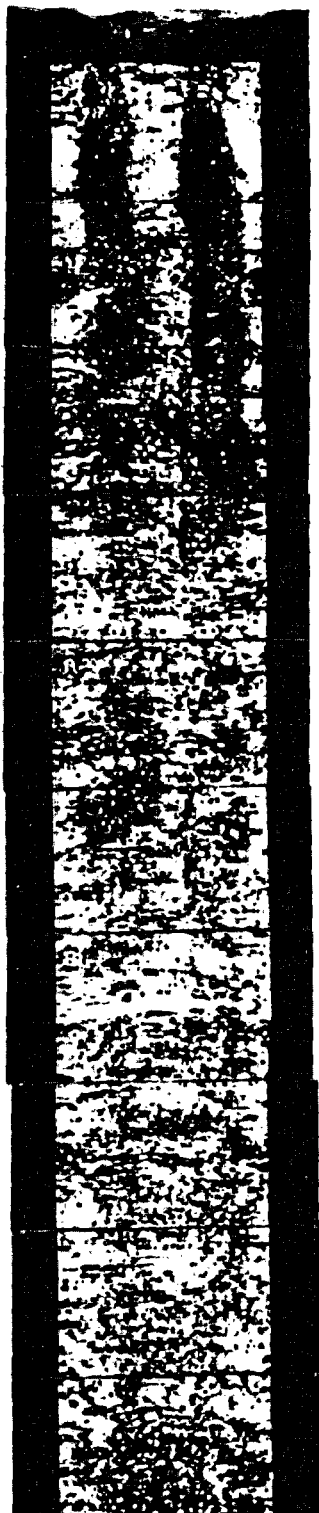


Ue25p- 1

5150



5200



5250



5175

5225

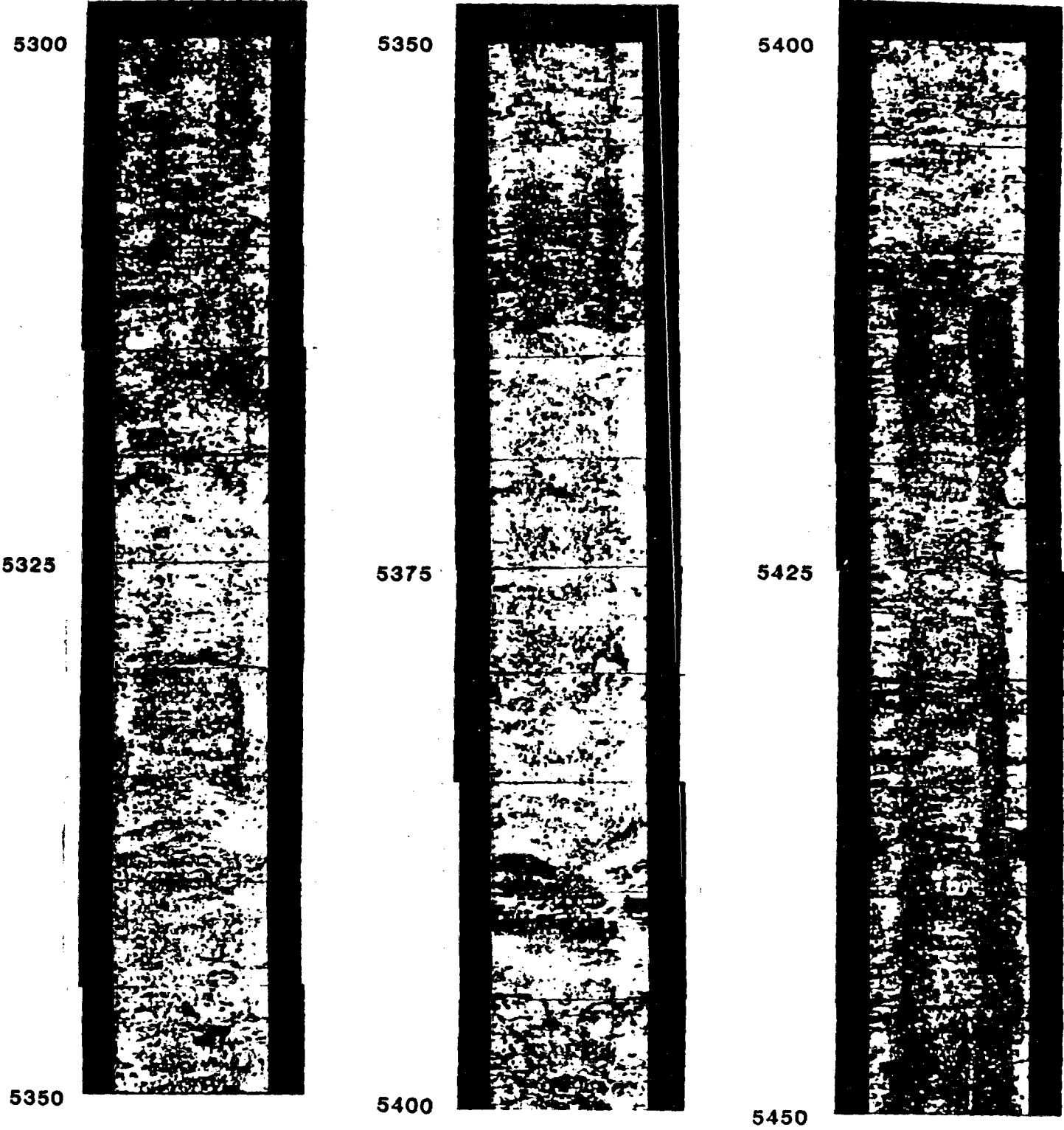
5275

5200

5250

5300

Ue25p- 1

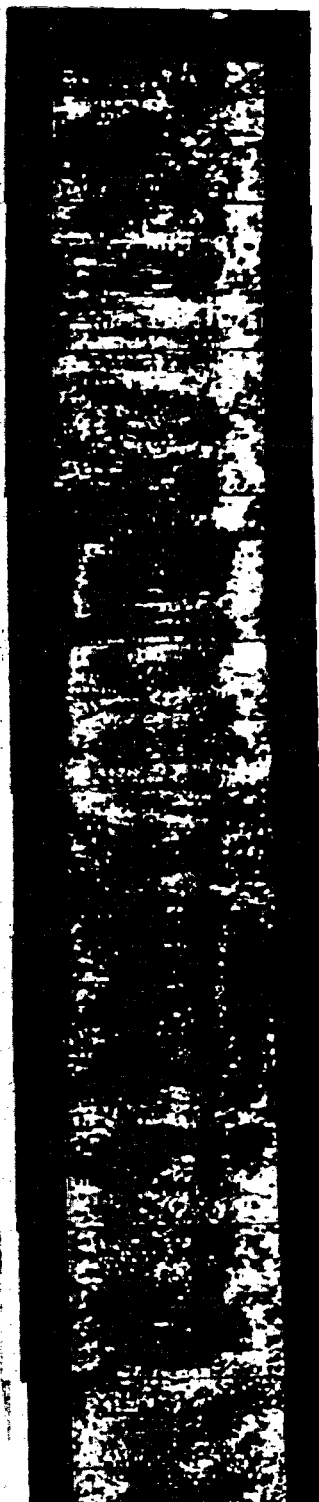


**Ue25p- 1**

5450



5500



5560



6475

6525

6575

5500

5550

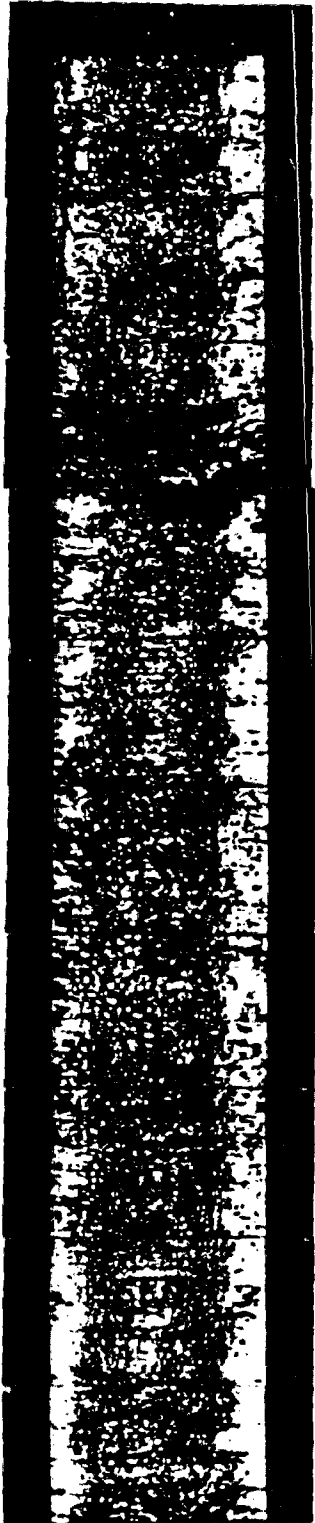
5600

Ue25p- 1

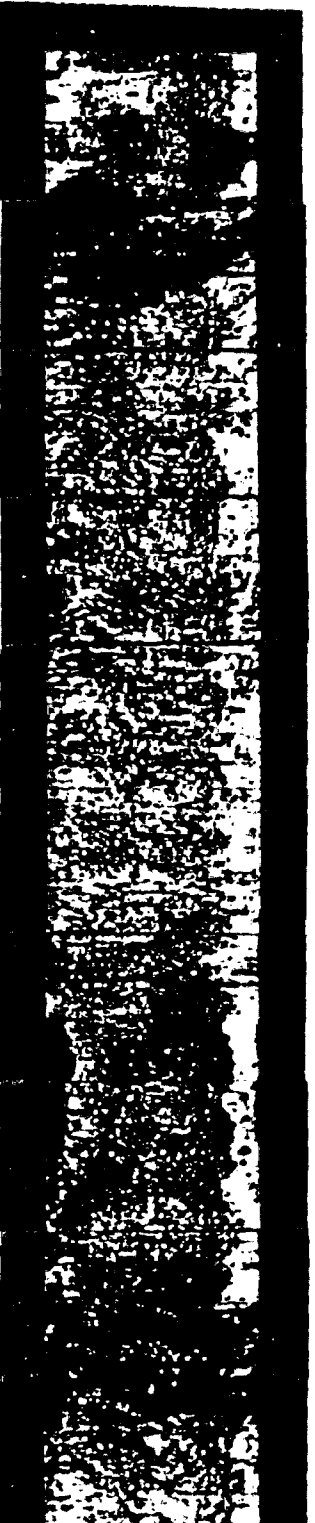
5600



5650



5700



5625

5675

5725

5650

5700

5750

**Ue25p- 1**

